NTNU – Trondheim
Norwegian University of
Science and Technology

Wave-to-Wire Model of the Wave Energy Converter Bolt2

Control and Power Extraction with an

All-Electric Power Take-Off System

Christian Mclisky Sandvik

Master of Energy and Environmental Engineering
Submission date: May 2012
Supervisor: Marta Molinas, ELKRAFT

Norwegian University of Science and Technology
Department of Electric Power Engineering

Problem Description

The aim of the master thesis will be to develop a detailed power take-off system for the wave energy converter Bolt2. The project will start with the design specification, selection and modelling of the electrical machine and the inverter to be used to drive the machine. The inverter modelling will assume a stiff DC bus with no energy storage, which implies that the grid connection issues will be omitted in this work. Once the power units are modelled in high detail, the hydrodynamic control strategies established for the WEC in the project part of this work (passive loading, complex conjugate control, intermediate control) will be implemented via simulations. In order to implement those strategies, a control system for the power electronic converter will be designed in order to drive the electrical machine to actuate the required instantaneous torques for extracting the maximum attainable power from the waves. The implementation of this control will be tested under irregular wave conditions.

Assignment given: 16 January 2012
Supervisor: Marta Molinas, NTNU
Co-Supervisor: Jonas Sjolte, Fred Olsen / NTNU

iv

Abstract

Fred Olsen is currently testing their latest wave energy converter outside of Falmouth Bay in England, preparing it for commercial exploitation at the Wavehub-project. Previous studies have shown that this device has potential for increased power extraction using reactive control, but so far these investigations have focused on the hydrodynamics of the device and on reducing the peak-to-average power ratio while omitting the effect of the electric power take-off system. This thesis shows the development of the hydrodynamic model of the device as well as a detailed model of the all-electric power take-off system consisting of a permanent magnet synchronous generator, inverter and DC-link. Vector control is used to control the permanent magnet synchronous generator, and field weakening control of the generator is applied in order allow over-speed operation.

Time domain wave-to-wire simulations are performed to evaluate the power take-off capabilities of the modelled wave energy converter with different control parameters. When tuned according to approximate complex conjugate control the accumulated average generator losses become large, giving a very low overall system efficiency. Optimal control with respect to electrical output power is found to be with low added mass, and when compared to pure passive loading a 1 % increase in annual energy production is achieved. The main factor that reduces the effect of reactive control is found to be the minimum 10 kN load-force constraint of the device, as this disables full oscillatory control. Example simulations on a device with different force constraint are performed which verifies this characteristic.

These results suggests that the Bolt2 has limited potential for increase in power extraction by implementing reactive control. The analysis in this thesis is nevertheless valuable, as it demonstrates how a wave-to-wire model can be used for power take-off investigations, annual energy production estimations and evaluations of different control techniques.

Sammendrag

Fred Olsen driver med pågående testing av sin nyeste bølgekraftomformer (WEC) ved Falmouth Bay utenfor kysten av England hvor målet er å gjøre den klar for kommersiell bruk ved Wavehub-prosjektet. Tidligere studier har vist til at WEC'en har potensiale for økt energiproduskjon ved å benytte reaktiv kontrol, men disse undersøkelsene har først og fremst sett på den hydrodynamiske modellen samt å redusere forholdet mellom maksimal og gjennomsnittlig effekt. Innflytelsen og begrensningene til det elektriske effektuttaket (PTO) har derimot ikke blitt inkludert. Denne masteroppgaven viser utviklingen av den hydrodynamiske modellen til bølgekraftomformeren samt en detaljert modell av den elektriske effektuttaket som består av permanent magnet synkrongenerator, omformerbro og likespenningsledd. For å styre generatoren benyttes vektorkontroll, og feltsvekkingkontroll nyttes for å kjøre generatoren over merkehastighet.

For å evaluere effektuttakevnen til den modellerte bølgekraftomformeren kjøres en rekke bølge-til-nett simuleringer med forskjellige kontrollparametere. Når kontrollparameterene tilnærmes optimal reaktiv kontroll viser det seg at det akkumuleres store generatortap som gir en veldig lav systemvirkningsgrad. Optimal kontroll med hensyn på levert elektrisk effekt viser seg derfor å være med lav tilført masse (*added mass*), og når dette sammenlignes med passiv last kontroll gir det en 1 % økning i årlig energiproduksjon. Hovedårsaken til den begrensede effekten av optimal kontroll viser seg å være kraftbegrensninger i effektuttaket som forhindrer dynamisk kontroll igjennom hele bølgeoscillasjonen. Simuleringner på tilsvarende bølgeomformermodeller med forskjellige kraftbegrensinger bekrefter dette.

Disse resulatene viser at omformeren har begrenset potensiale for økt energiproduskjon med innføring av reaktiv kontroll. Analysen i denne masteroppgaven er likefullt nyttig da den viser hvordan en bølge-til-nett modell kan utledes og brukes til effektuttakanalyser, energiproduksjonsestimater og evaluering av forskjellige kontrollstrategier.

Preface

This project is my master thesis and represents the final work in the Master course *Energy and Environmental Engineering - Electrical Energy Engineering* at the Norwegian University of Technology and Science.

A warm thanks to my supervisor Marta Molinas who has been very important in all stages of this project with enthusiastic guidance and encouragement. Especially I am thankful for being able to attend the inspiring and interesting workshops and conferences on renewable and wave energies which without Martas support would not have been possible. I also wish to thank my co-supervisor Jonas Sjolte for always having his door open for me giving support and advice.

x

Contents

List of Figures

List of Tables

Nomenclature

ζ	[m]	Wave Elevation
δ	[m]	Diraq Delta Function
η	[m]	Body Position
η_g	[-]	Gear ratio
ρ	[m]	Water Density
τ	[s]	Time Shift
ϕ	[rad]	Offset Angle
ϕ_L	[rad]	Load Angle
Ψ	[Wb]	Permanent Magnet Flux
ω	[rad]	Angular Frequency
ω_0	[rad]	Peak Frequency
$\mathbf{A}$	[-]	State-space System Matrix
$\mathbf{B}$	[-]	State-space System Matrix
B_L	[Nm/s]	Added Damping
C	[F]	Electric Capacitance
$\mathbf{D}$	[-]	State-space System Matrix
E	[V]	Source Voltage
e	[-]	Exponential
F_e	[N]	Excitation Force
F_L	[N]	Load Force
F_R	[N]	Radiation Force
f	[N]	Force
$\mathcal{F}$	[-]	Fourier Transform
G	[-]	Open Loop Gain
g	$[m/s^2]$	Gravity Acceleration
H	[m]	Wave Height
H_s	[m]	Significant Wave Height
$H_{F\zeta}$	[-]	Excitation Force Coefficient Transfer Function
$h_{ec\zeta}$	[-]	Excitation Force Coefficient Impulse Response
I/i	[A]	Electric Current
k	[-]	Radiation Force Impulse Response
L	[H]	Electric Inductance
M_L	[kg]	Added Mass
$M_{(\omega)}$	[-]	Closed Loop Gain
M / m	[kg]	Mass
m_r	[kg]	Added Mass
n_{scale}	[-]	Scaling Ratio
n_{pp}	[-]	Generator Pole-pairs

P	[W]	Power
R	$[Ohm]$	Electrical resistance
R_L	$[Ohm]$	Electrical Load resistance
R_r	[kg/s]	Radiation resistance
S	[-]	Hydrodynamic Stiffness
S_ω	[kg/s^2]	Wave energy spectrum
T	[s]	Wave period
T_0	[s]	Peak wave period
t	[s]	time
U / u	[V]	Voltage
V / v	[V]	Voltage
X	[Ohm]	Electrical reactance
z	[-]	State vector

Chapter 1

Introduction

1.1 Background

With increasing oil prices as well as focus on shifting the worlds energy-dependency towards renewable resources, wave energy is again given increased attention. It is estimated that when today's technology is fully matured, around 140 - 750 TWh per year will be commercially exploitable [1]. If all potential technology is realized this number can be greatly increased with some scenarios as large as 2000 TWh, corresponding to approximately 10 % of the worlds electricity consumption in 2008 [2]. One such technology is being developed by the Fred Olsen Wave Energy Project. Fred Olsen began research and development in wave energy in 2000, and has tested and built prototypes based on the point absorber concept. In early 2012 the latest prototype, *Bolt2Wavehub* or *Bolt2*, was deployed as a stand-alone system at Falmouth Bay, England. The next step is to make it commercially ready and launch it at Wavehub [3].

During the current deployment the performance of Bolt2 power take-off capabilities and control strategy is of great interest. In wave-energy, linear control of point absorbers is a well known subject [4], and for the Bolt2 concept Fred Olsen has focused on controlling the device through passive loading. However, initial investigations indicate that Bolt2 might have potential for increased power extraction using phase control or reactive control during calmer sea states [5] [6]. So far these investigations have focused on the hydrodynamical model of the Wave Energy Converter and on optimizing average power while reducing the peak- to average power ratio, and less attention has been paid to the limitations of the generator, switchgear and the rest of the power-take off system. The purpose of this study is therefore to develop a full wave-to-wire model of Bolt2 with an all-electric power take off system. This model is then used in order to evaluate the effect of different control strategies on the power take off capabilities of the WEC under different sea state conditions. Such a study is interesting in order to decide on an optimal

control strategy, as an increase in energy production can be important to the commercial potential of the project.

1.2 Description of the Investigated System

The Bolt2 concept is based on Fred Olsens previous experiences with point absorbers, and in particular Bolt which is still deployed outside of Riso in Norway. Bolt is made up of a single point absorber with a PTO which consist of a winch that is connected to the sea-floor. The generator is driven by this rope through a gear-box. Bolt also has an hydraulic spring system which acts as a energy storage system and maintains tension in the rope for the downwards movement of the device.

In contrast, Bolt2 has an all-electric power take-off system with no hydraulics. Instead an electric energy storage is used which is directly connected to the DC-link, and the tension in the rope is maintained by the generator. This means that the generator will have to act as a motor and wound in the rope on the downward movement of the device, meaning that some energy will have to be supplied to the system in this part of the oscillatory cycle. Another big difference between the two concepts is that Bolt2 consists of five point absorbers with individual power take-off systems connected together on a toroid shaped device and sharing a common DC-link. To concentrate the PTO's on a common platform has obvious economical advantages, but also from a power take-off point of view it is beneficial as such a larger device has the potential to utilize also the pitching motions of the sea.

For the purpose of this study it is beneficial to define a smaller boundary of the system. A single point absorber and inverter up to and including the DC-link can be considered a independent module, and is therefore the basis for the wave-to-wire model in this thesis. For further modelling the whole system, many such modules can then be connected together.

Figures 1.2 are taken from the test site where Bolt2 is now deployed. Figure 1.1 show an artistic impression of the Bolt2 wave energy system. More detailed descriptions and figures of the the PTO system is given in section 3

1.3 Structure of the Thesis

In **section 2** the modelling of an irregular sea and development of the hydrodynamic model of Bolt is treated. This has previously been treated in this authors specialization project [8] and conference proceedings [5], but a summary is provided. Additionally, the end of section 2 is dedicated to identification of optimal tuning frequencies to be used for linear control equations of WEC's.
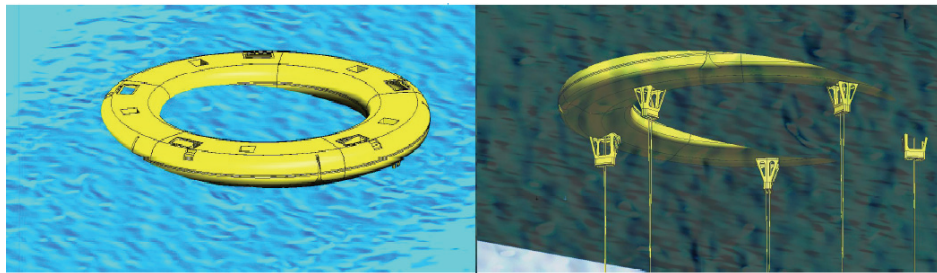
Figure 1.1: *Artistic impression of Bolt2 taken from J. Sjolte [7]*

Section 3 is regarding modelling of the all-electric power take off system of Bolt2, with main focus on vector control of a Permanent Magnet Synchronous Generator. It is shown that a simplified model of the Converter Bridge and DC-link gives a good performance, and a number of time-domain simulations are performed to verify that the PTO system performs in accordance with Fred Olsen experience.

In **section 4** a method to combine the hydrodynamic model of Bolt and model of the power-take off system for Bolt2 is described. A number of wave-to-wire simulations is performed using different control strategies, and an approach for developing a map of optimal control parameters for different sea states is demonstrated. Using this method, an estimation of annual energy production with and without reactive control is compared. At the end of this section some sensitivity analysis is performed and potential improvement for Bolt2 is discussed.

Evaluation of the methods, results and suggestions for further work is treated in ***Discussion* section** of the thesis. However, as this is also performed throughout the whole thesis, the *Discussions* section is kept relatively short.

Finally this thesis have an extensive **appendix** where all the Simulink Models used in the simulations are depicted. Also included is the paper *Time Domain Modelling of the Wave-to-Wire Energy Convert Bolt* based specialization project [8] which was presented during the proceedings of the 7'th International Conference on Ecological Vehicles and Renewable Energies in Monaco, spring 2012.
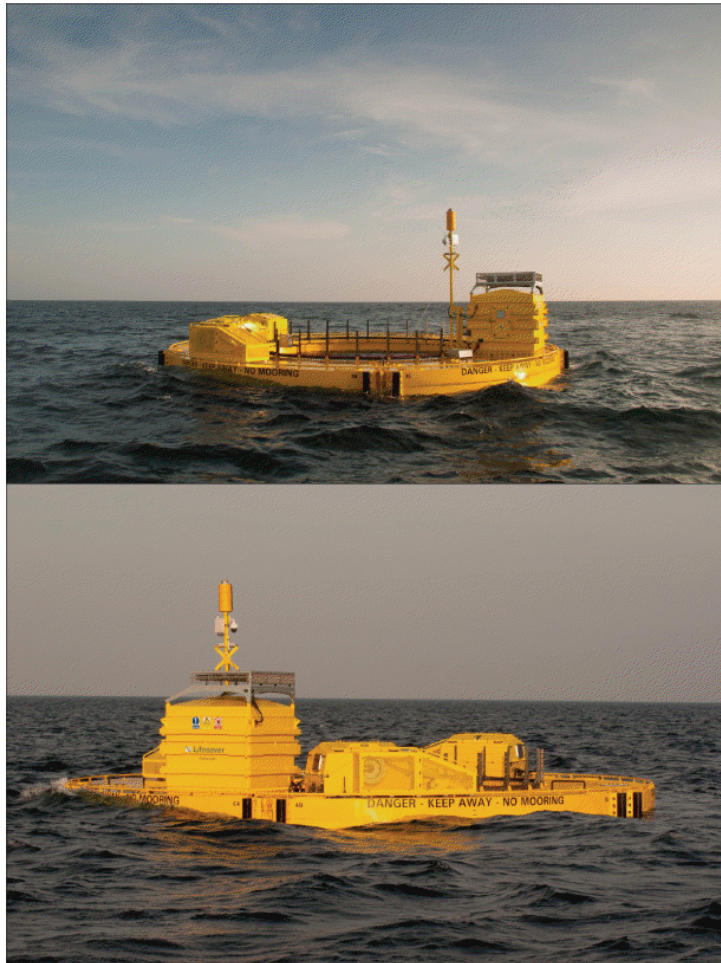
Figure 1.2: *Picture of Bolt2 taken at Falmouth Bay*

Chapter 2

Hydrodynamic Model

2.1   General

In the specialization-project *Wave-to-Wire Time Domain Model for the Wave Energy Convert Bolt* [8] and corresponding conference proceedings [5] the methodology for developing the hydrodynamic model for Bolt was treated in detail. As the implementation of this model is vital for the work of this thesis, a summary of the method and key results will be shown in this section. Similarly, linear control theory for wave energy will be summarized.

Finally, it is shown how tuning frequency for optimal control parameters are decided on. In the previous paper, the peak wave period and the peak excitation force period was used for this tuning, but simulations will show that this is indeed not the approach which gives optimal power extraction.

All hydrodynamic parameters used in the calculations are based on data obtained by Fred Olsen, and plots of these values are shown in the appendix together with the resultant state-space models.

2.2   Modelling the Hydrodynamics of Bolt

The hydrodynamic model of Bolt has the following input

- The sea state, represented by parameters significant height H_s and peak period T_p.

- Load force, F_L, often given by the load force parameters added damping B_L and added mass M_L.

The output of the model is the response of the device, where the velocity $\dot{\eta}$ and acceleration $\ddot{\eta}$ is the most interesting.

2.2.1 Wave Elevation Time-series

A common way to model the sea is by using an energy spectrum. There are various mathematical models that are used for defining such spectres, and the most widely known is the two-parameters Bretschneider spectra [9]. Its preferred analytical form is given by the following equation

$$S_{(\omega)} = \frac{5}{16} \; H_s^2 \; \frac{\omega_0^4}{\omega^5} \; e^{-\frac{5\omega_0^4}{4\omega^4}} \tag{2.1}$$

Here H_s is the significant height of the sea state and ω_0 is the peak frequency. Figures 2.1 and 2.2 show the Bretschneider spectra for varying values of significant height and peak frequencies.
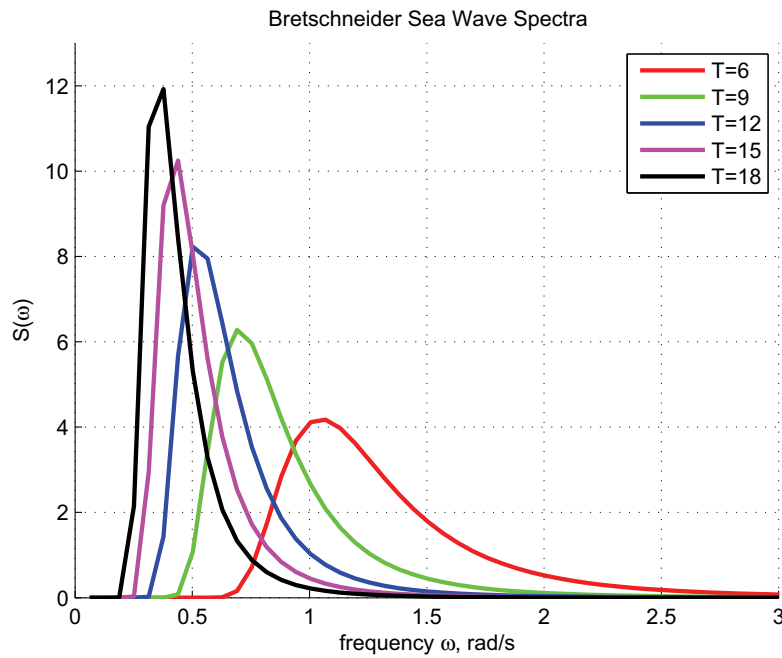
Figure 2.1: *Bretschneider spectra for different values of peak period T_p*

The time-domain wave elevation of an irregular ocean can be regarded as the superposition of different frequency sinusoidal waves. Thus the energy spectrum can be used to represent the sea by a large but finite amount of different frequency components, which is a fair approximation. The elevation due to each such wave can be expressed [10] by the following equations:

$$\zeta_n(t) = \sqrt{2S(\omega_n)d\omega} \sin\left(\omega_n t + \phi_n\right) \tag{2.2}$$

Where $d\omega$ is defined as

$$d\omega = \frac{2\pi}{T_{ser}} \tag{2.3}$$
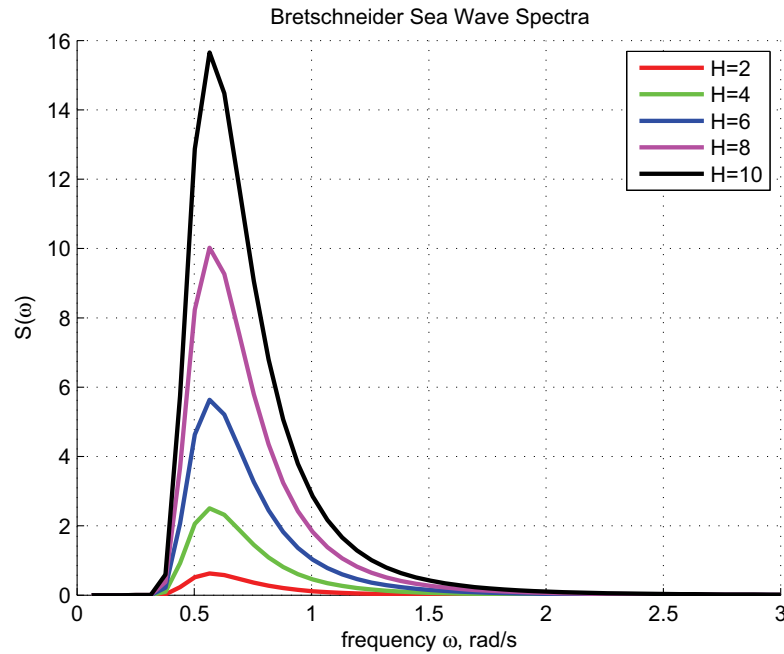
Figure 2.2: *Bretschneider spectra for different values of the significant height H_s*

and T_{ser} is the period of the time-series that are being analysed. By summing these waves a wave elevation time-series is created:

$$\zeta(t) = \sum_{n=1}^{N} \sqrt{2S(\omega_n)d\omega} \sin\left(\omega_n t + \phi_n\right) \tag{2.4}$$

Where ϕ_n is randomly generated offset angle for each wave component n.

For a time-series of 90 seconds, with a significant wave height of 7 meters and a peak period of 11 seconds, figure (2.3) is an example time-series.

2.2.2 Forces Acting on the System

The force balance for a buoy excited by an incoming wave is given by the following equation

$$M\ddot{\eta} = f_e(t) + f_s(t) + f_r(t) + f_m(t) \tag{2.5}$$

where η is the device position and M is the equivalent mass of the system corresponding to the mass of the WEC and added mass due the inertia of the power take-off system. Here f_e is the excitation force, f_r is the radiation force, f_m is the machinery force, or the force related to the power take-off system and f_s represents the hydrostatic force. In this model the mooring forces, viscous forces and environmental forces are disregarded.

Hydrostatic force

The hydrostatic force is the resultant force of gravitational forces and forces due acting on the buoy due to displaced water.

$$f_s = S\eta \tag{2.6}$$

Here S represents the hydrostatic stiffness, an η is the buoy displacement from equilibrium. Commonly the stiffness is considered a constant value and thus the force is proportional to device displacement [11].

Radiation Force

An oscillating device will create a diffraction wave, and the force acting on the device due to this wave is referred to as the radiation force. In the frequency domain it is typically expressed as

$$\hat{F}_R(\omega) = m_r(\omega)\ddot{\eta} + R_r(\omega)\dot{\eta} \tag{2.7}$$

where m_r is the added mass of the water oscillating with the device and R_r is the radiation resistance. As these parameters are frequency dependant the time domain expression of the radiation resistance becomes more complex [12]:
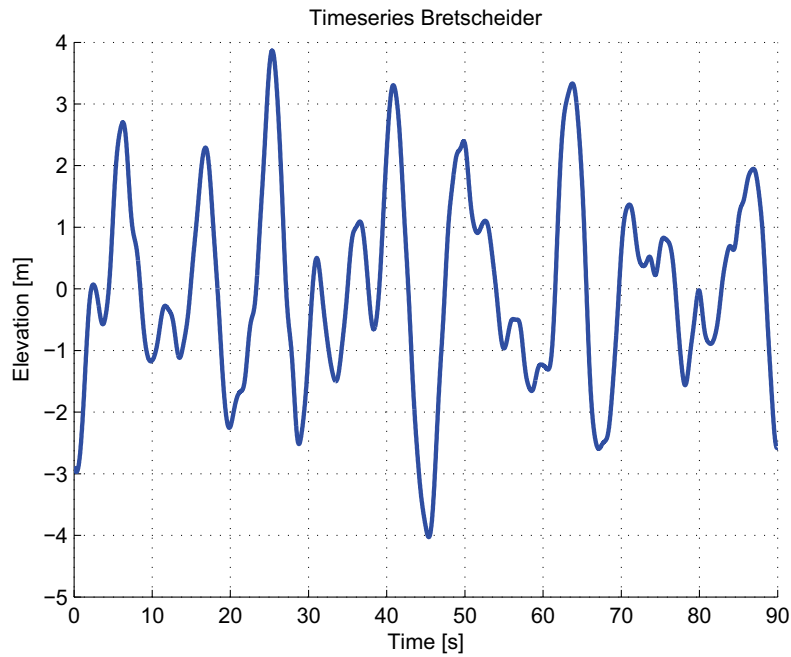
Figure 2.3: *Timerseries of a Bretschneider spectrum $H_s = 7$ and $T_p = 11s$*

$$F_r(t) = m_r(\infty)\ddot{\eta} + \int_0^t k(t-\tau)\dot{\eta}(\tau)d\tau \tag{2.8}$$

In the first term of this expression $m_r(\infty)$ is the added mass at infinite frequency and $\ddot{\eta}$ is the acceleration of the device. The second term is a convolution integral, where the convolution kernel k_t can be considered the radiation force impulse response. As discussed by Hals [11] a good approximation is to replace this convolution term by the state-space equivalent represented by equations (2.9) and (2.10).

$$F_r(t) = \mathbf{C}_k\mathbf{z}(t) + \mathbf{D}_k\dot{\eta}(t) \tag{2.9}$$

where the state vector z is given by

$$\dot{\mathbf{z}}(t) = \mathbf{A}_k\mathbf{z}(t) + \mathbf{B}_k\dot{\eta}(t) \tag{2.10}$$

Taghipoura, Pereza and Moan [13] show how *Realization Theory* can be used in order to identify the state-space parameters $\mathbf{A}_k$, $\mathbf{B}_k$, $\mathbf{C}_k$ and $\mathbf{D}_k$. By identifying the discrete radiation impulse response through inverse Fourier transform of $k(\omega)$ in equation (2.11), a state-space system with a corresponding impulse response is generated.

$$k(\omega) = i\omega\{m_r(\omega) - m_r(\infty)\delta(\omega)\} + R_r(\omega) \tag{2.11}$$

The values for radiation resistance and added mass of the device in frequency domain are known and supplied by Fred Olsen for a span of frequencies. This impulse response fitting is realized using the Matlab Robust Toolbox function *imp2ss* which is based on the Hankel Singular value decomposition proposed by Kung [14]. Using this a state-space system is generated, and a good representation of the radiation force is obtained. A more thorough explanation of how the radiation force is modelled for Bolt is given in the conference proceeding [5] in appendix F. The values for the state space parameters are given in appendix D.

Excitation Force

The force that the incident wave exerts on the WEC body is called the excitation force. It is given by the elevation of the sea ζ and the excitation force coefficient $H_{F\zeta}$.

$$F_{e,c}(\omega) = H_{F,\zeta}(\omega)\zeta(\omega) \tag{2.12}$$

This coefficient are known and supplied by Fred Olsen for a span of frequencies. Like for radiation force, the time domain expression of the excitation force becomes a convolution term [11].

$$F_{e,c}(t) = \int_0^t h_{F\zeta}(t - \tau_c)\zeta(\tau)d\tau \tag{2.13}$$

A state space representation of the convolution term is then found in the same manner as outlined for the radiation force; by impulse response fitting with the discrete excitation force impulse response extracted from the excitation force coefficient. The is outlined in detail in the specialization project [8].

Load force

The load force F_L, or machinery force, is the force applied to the system by the power take-off system. How much force, and how this force is applied greatly influences how much power is extracted from the WEC. Typically the load force is represented by a component proportional to the device velocity and one component proportional to the device acceleration.

$$F_L = B_L\dot{\eta} + M_L\ddot{\eta} \tag{2.14}$$

B_L is considered the machinery added damping while M_L is the machinery added mass. Input into the model is therefore either the load force or the load force parameters.

Simulink Model

Using equation (2.5) and the representations described in this section the hydrodynamic model becomes the following:

$$(M + m_r(\infty))\ddot{\eta} + \int_0^t k(t - \tau)\dot{\eta}d(\tau)\tau + S\eta$$
$$= \int_0^t h_{F\zeta}(t - \tau_c) + F_L(t) \tag{2.15}$$

Replacing the convolution terms by their state-space equivalents this equation can be illustrated graphically in the Simulink model seen in figure 2.4

2.3   Optimal Power Extraction - Linear Control Theory

By controlling the load force parameters, the power take-off of the WEC can be controlled. Linear control strategies are well established for wave energy converters [4] [15] [16]. The basis for these methods is the electric equivalent circuit of the mechanical model outlined
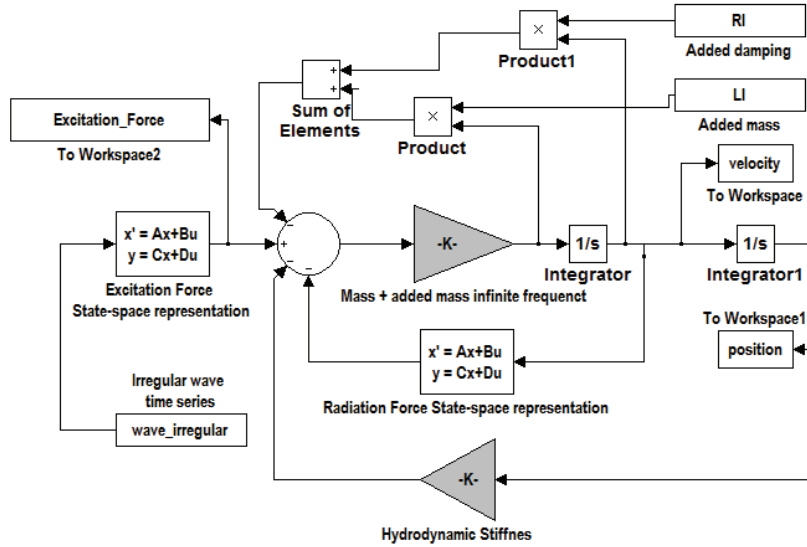
Figure 2.4: *Simulink model of the hydrodynamic model. The load force is represented by the load parameters as shown in equation (2.14)*

in equation (2.15). The relation between the mechanical and the electrical equivalents can be summarized in Table 2.1

Table 2.1: *Mechanical to electrical domain equivalents*

Mechanical Domain	Electrical Domain
Excitation force, F_e	Source Voltage, V_S
PTO Force, F_L	Load voltage, V_L
Velocity, $\dot{\eta}$	Electric current, i
Position, η	Electric charge, q
Damping, $B(\omega)$	Resistance, R
Mass, $M + m_r(\infty)$	Inductance, L
Stiffness, S	Inverse Capacitance, C^{-1}
Added damping, B_L	Load resistance, R_L
Added Mass, M_L	Load reactance, X_L

The electric equivalent circuit is shown in figure 2.5. A few points need to be mentioned about linear control of wave energy converters

- The electrical equivalent circuit is only only valid for sinusoidal input.

- In order to apply linear control on an irregular sea input, a dominant frequency, or *tuning frequency*, needs to be determined.

- This representing frequency can then be treated as a sinusoidal input into the linear control.
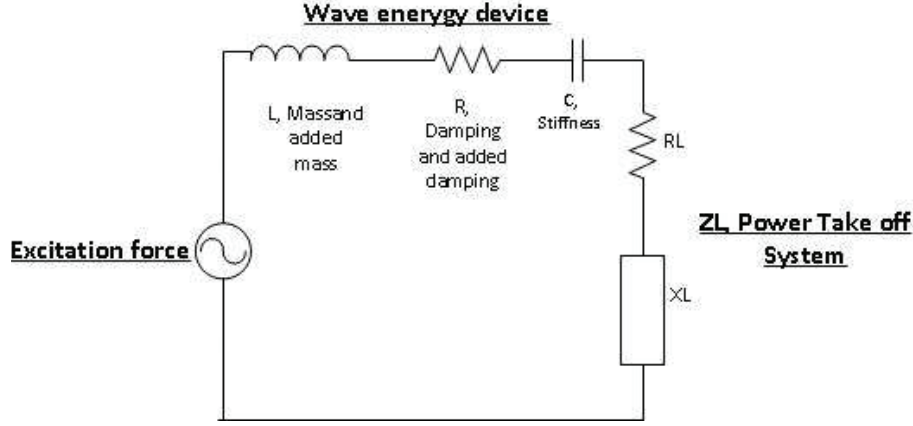
Figure 2.5: *Electrical equivalent of the point absorber WEC*

From the electric circuit in figure 2.5 an expression for the current I can be deduced as a function of the source voltage E.

$$I = \frac{E}{\sqrt{(R + R_L)^2 + \left((L + L_L)\omega - \frac{1}{\omega C}\right)^2}} \tag{2.16}$$

From this the load voltage V_L and average output power can then expressed

$$V_L = I\sqrt{R_L^2 + (\omega L_L)^2} = \frac{E\sqrt{R_L^2 + (\omega L_L)^2}}{\sqrt{(R + R_L)^2 \left((L + L_L)\omega - \frac{1}{\omega C}\right)^2}} \tag{2.17}$$

$$P_L = R_L I^2 = \frac{E^2 R_L}{(R + R_L)^2 + \left((L + L_L)\omega - \frac{1}{\omega C}\right)^2} \tag{2.18}$$

Using these equations, the given frequency ω and excitation force E, one can decide on control parameters for optimal average power extraction. Typically one distinguishes between passive loaded control, in which the load voltage is in phase with the current, and reactive control in which the load voltage also has a component in phase with the source voltage E [4].

Passive Loading

The simplest form of control is passive loading. As explained, this is obtained by keeping the load voltage V_L in phase with the current I. This is obtained by having a purely resistive load, keeping $X_L = 0$ in the electric equivalent circuit in figure 2.5. From electric circuit analysis we then know that maximum output power is achieved by tuning R_L as seen in equation (2.19):

$$R_L = \sqrt{R^2 + \left(\omega L - \frac{1}{\omega C}\right)^2} \tag{2.19}$$

A characteristic of passive loading is that the power flow is always positive. This of course since the load force and current are in phase, the product is always positive.

Complex Conjugate Control

For a given frequency one can obtain maximum power extraction by applying complex conjugate control [4]. From electric circuit analysis one knows that maximum power extraction is achieved by applying a resonance condition. This is achieved by tuning the load parameters as seen in equations (2.20) and (2.21).

$$R_L = R \tag{2.20}$$

$$L_L = -\left(\omega L - \frac{1}{\omega C}\right) \tag{2.21}$$

What signifies complex conjugate control is that current is in phase with the source voltage. Mechanically, this means that the device velocity is in phase with the excitation force. This is important to note, as one can use this property to verify whether optimal power extraction is achieved.

Even though complex conjugate control gives the most mechanical power extraction, some important drawbacks of this control method needs to be mentioned.

- In contrast to passive loading, the power flow of complex conjugate control is both ways. This is becuase the current is not in phase with the load voltage. Thus the generator and power electronics need to deal with the challenge of a bi-directed power flow.

- Complex conjugate control is characterized by large peaks in instantaneous power and a high peak-to-average power ratio. This leads to large overrating of the generator and power electronic equipment with respect to the average power. [16].

- Another problem with complex conjugate control is that it will lead to high load voltages at low currents. Mechanically this means that one will have high load force even at low device velocities. Under such conditions the generator efficiency is typically low.
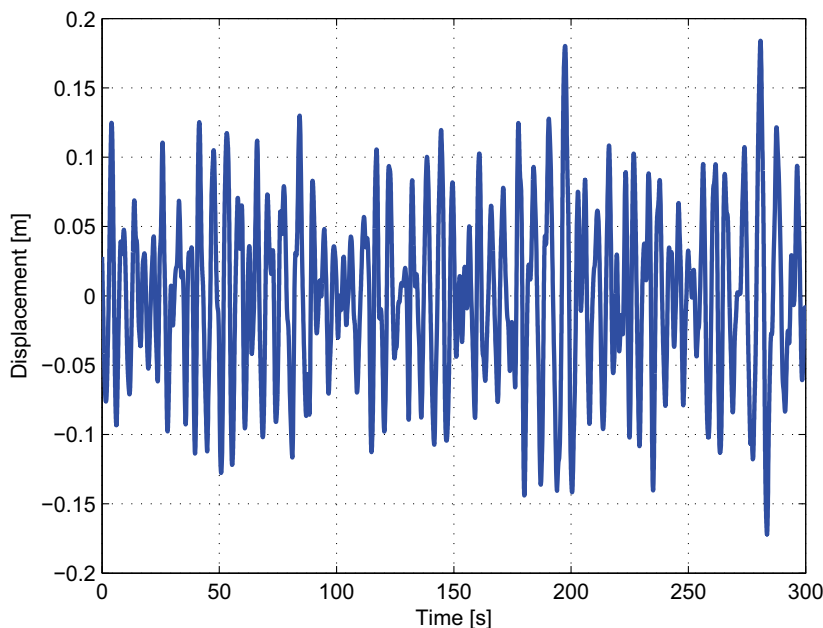
Figure 2.6: *Irregular wave of significant height $H_s = 0.25$ and peak period $T_p = 6.5$.*

Intermediate Control

Due to these known problems of complex conjugate control, the truly optimal control parameters may also be in-between passive control and complex conjugate control. This is sometimes referred to as *Intermediate Control*. In [17] E. Tedeschi and M. Molinas shows a control strategy which optimizes average power under a peak power constraint. In the specialization project [8] a control strategy based on this algorithm was developed and it showed potential. Another approach is to introduce also a force constraint on the system and optimize average power under this condition.

Intermediate control in its analytical form will not be treated in this thesis, but as will be shown in later sections, is in practice found to be a interesting approach to controlling the Bolt wave energy system.

2.3.1   Hydrodynamic Model Simulations

It is interesting to investigate how the power take-off of the hydrodynamic model is under different control strategies. For this purpose simulations will be performed within the hydrodynamical model of Bolt under passive loading and complex conjugate control. An irregular wave input is designed with an significant height of 0.25 meters and a peak period of 6.5 seconds. The input wave into the simulations can be seen in figure 2.6.
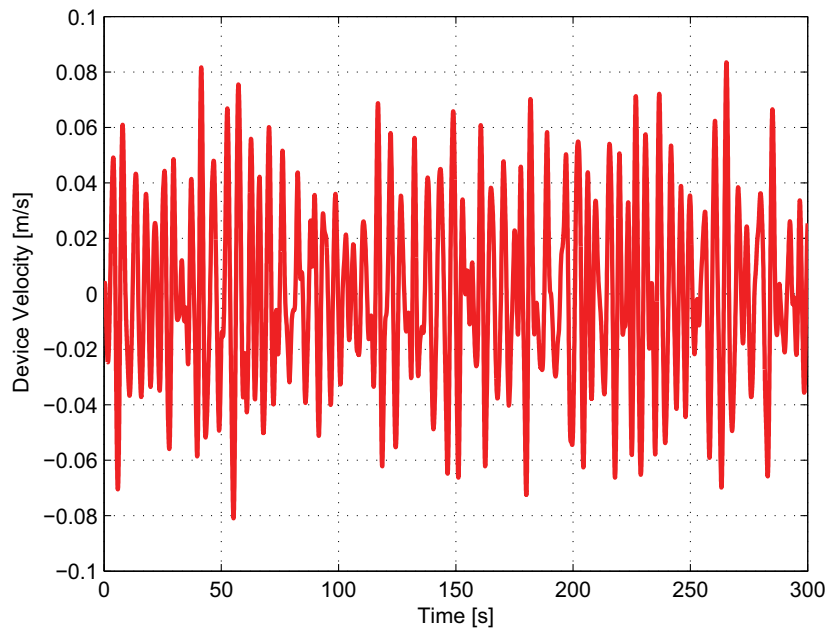
Figure 2.7: *Device velocity when passively loaded with $R_L = 178\ 000$*

Simulation - Passive loaded system

The load parameter when passively loaded is calculated according to equation (2.19). The tuning frequency for this initial simulations is chosen to be the peak frequency of the sea state, though as it will be shown later this is far from the optimal tuning frequency.

$$R_L = \sqrt{9165^2 + \left(\omega(5000 + 40\ 000) - \tfrac{197\ 430}{\omega}\right)^2}$$

where ω is given by

$$\omega = \tfrac{1}{7}\tfrac{2\pi}{180} = 0.898$$

This gives a damping of $178\ \frac{kN}{m/s}$, meaning $R_L = 178\ 000$. Figure 2.7 show the device velocity when this damping is applied. Figure 2.8 show the instantaneous and average power for the device when passively loaded. The average extracted power is 0.456 kW, and the peak power in this simulations is 3.2 kW giving a peak-to-average ratio of 7.

Complex Conjugate Control

Again, using that the tuning frequency is based on the peak period of the sea state, the complex conjugate control parameters can be calculated according to equations (2.20) and (2.21).
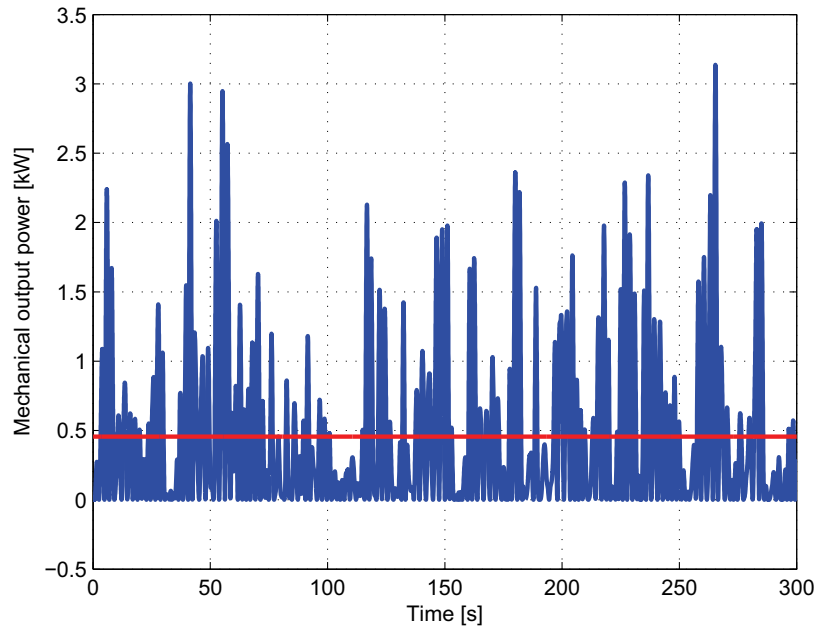
Figure 2.8: *Device mechanical extracted power when passively loaded with $R_L = 178\ 000$. Average power is 0.456 kW*

$$R_L = 9165$$

$$X_L = \omega(5000 + 40\ 000) + \frac{194\ 330}{\omega} = 178\ 670$$

Applying the irregular wave seen in figure 2.6 the velocity and mechanical extracted power is seen in figures 2.9 and 2.10.

As seen from this simulation, by applying complex conjugate control the power extraction can be significantly increased compared to passive loading. In this case the average power is increased by over 50 %. However, one does also observe a significant increase in peak to power ratio for complex conjugate control.

For sinusoidal input complex conjugate control shows even more potential for Bolt [6], meaning that if a improved tuning is performed the power extraction will increase further. Some sort of predictive control can be considered, where the load is tuned on a wave-to-wave basis. But this is not straight forward, especially there are challenges with reaching steady-state oscillation on a wave-to-wave time-frame. However, as the following section will show, it is much potential for increased power extraction by choosing an optimal tuning frequency.
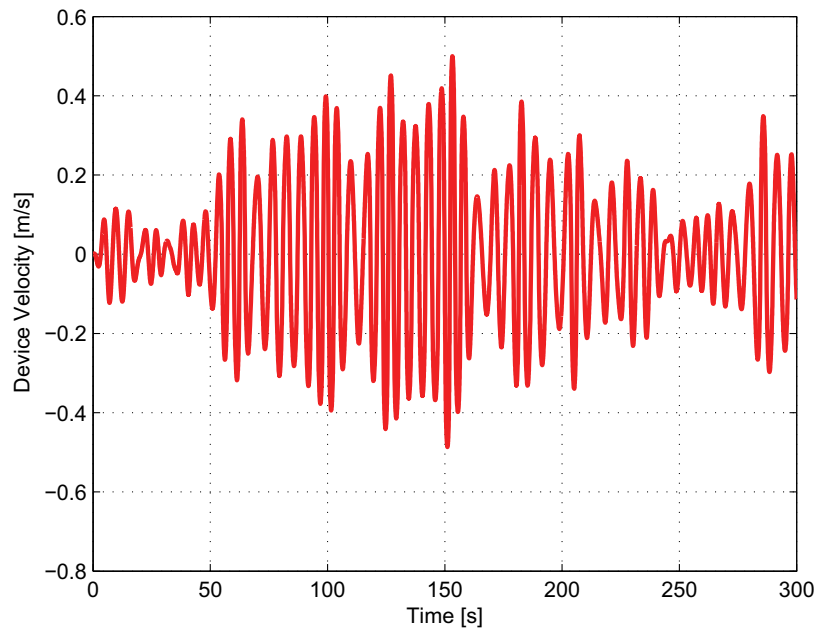
Figure 2.9: *Device velocity when load tuned to approximate complex conjugate control with* $R_L = 9000$ *and* $L_L = 178\ 670$
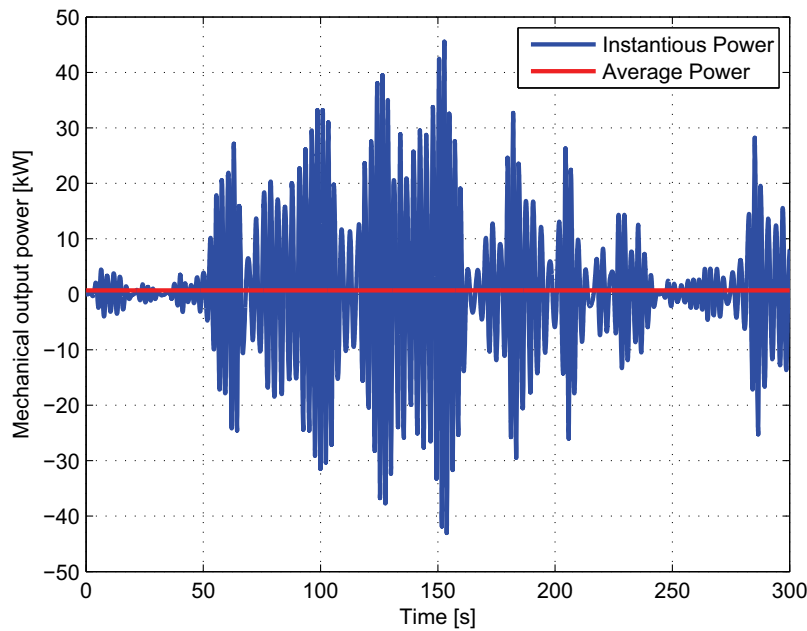
Figure 2.10: *Device mechanical extracted power when load tuned to approximate complex conjugate control with* $R_L = 9000$ *and* $L_L = 178\ 670$. *Average power is 0.697 kW*

2.4 Optimal Tuning Frequency of a WEC

In the specialization project [8] the tuning frequency was decided based on the peak frequency of the sea spectra. The tuning angular frequency ω_0 was calculated by equation
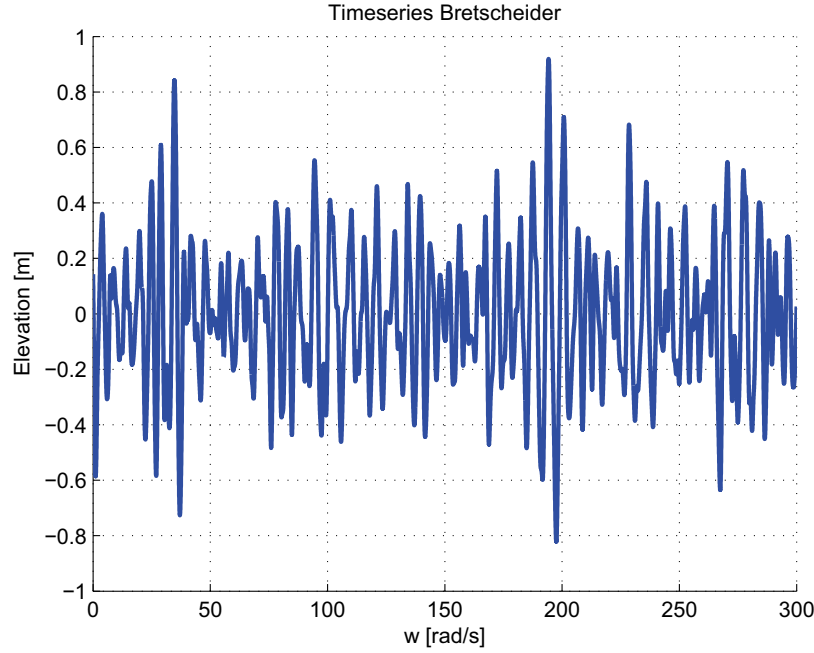
Figure 2.11: *Irregular wave time-series of peak period 6.5 seconds. This time-series has 123 zero-crossings in 300 seconds*

$$\omega_0 = \frac{2\pi}{180T_p} \tag{2.22}$$

However, it was noted that a better approach would be to tune it instead to the dominant frequency of the excitation force. As the excitation force is a function of the wave elevation and the excitation force coefficient as seen in equation (2.12), it is not explicit that the dominant frequencies of these two will be similar enough to allow such an simplification.

2.4.1   Identifying the Dominant Frequency of the Excitation Force

The best way in which to evaluate which is the dominant frequency of the excitation force is to make a fast Fourier transform of the excitation force signal. As this is challenging in real time, a simplified approach can be to evaluate the number of zero-crossings and use a rule-of-thumb factor of 1.3 to approximate the dominant frequency. To verify the validity of this approach, an irregular wave time-series of 300 seconds is simulated as seen in in figure 2.11 From the number of zero-crossings and simulation time, the average period of the signal can be determined as seen in equation (2.23).

$$T_{wave} = \frac{2T_{signal}}{n_{zerocrossing}} = \frac{2 \times 300}{123} = 4.878s \tag{2.23}$$

The dominant frequency of the signal can then be approximated by an factor of 1.3
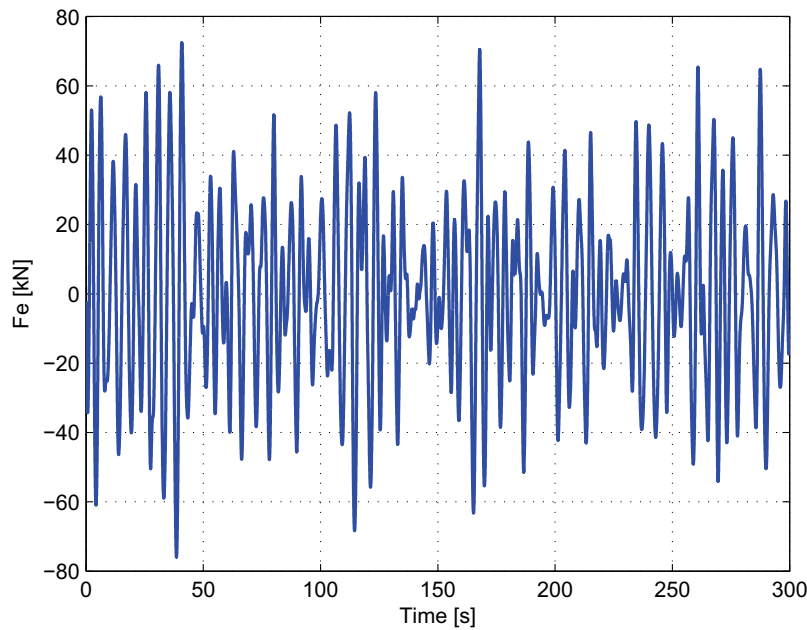
Figure 2.12: *Excitation for time-series corresponding to the irregular wave in figure 2.11. This time-series has 134 zero-crossings in 300 seconds*

$$T_{dominant} = 1.3 \, T_{wave} = 6.34s \tag{2.24}$$

Which is within the expected variance of a 300 second time-series with $T_P = 6.5$ seconds as input. It is now interesting to analyse the force excited on the wave energy converter, or excitation force F_e, by this input irregular wave time-series. In figure 2.12 this excitation force time-series is shown.

Interestingly, this has more zero-crossings than the input wave elevation time-series, meaning frequency of the excitation force is higher than the wave elevation. Solving in similar manner as shown for the input wave, the period of the excitation force is found to be 5.82 seconds.

The observation that the force excited on the device is not in phase with the wave elevation is important to note. As the difference is quite considerable, one would expect there is significant difference in extracted power when tuning the control parameters for the two different periods. As explained in section 2.3, optimal power is extracted when device velocity is in phase with the excitation force, and thus tuning for the correct period is important.

Table 2.2: *Average power extraction for a wave of significant height H_s of 1.5 meters and peak period T_P of 6 seconds. Results are shown for a 300 second long irregular wave input*

Damping R_L [kNs/m]	149	85	82.5	80	77.5	75
Average Power [kW]	5.933	6.67	9.74	9.75	9.778	9.745

2.4.2   Simulation Identification of Optimal Tuning Frequency

It has been shown that tuning the load parameters according to the dominant wave frequency will not give the optimal tuning frequency as the excitation force has a higher dominant frequency than the sea state. What remains to be determined is whether the dominant frequency of the excitation force is the optimal tuning frequency to input into equations (2.20) and (2.21). In order to investigate this, the following approach is undertaken:

- A number of 300 second long irregular wave elevation time-series is simulated with different peak periods T_P. For each of the defined peak periods at least 5 such time-series are generated in order to get average values.

- For each of the generated time-series, a passive loaded WEC system is manually tuned in order to find optimal power extraction.

- The tuning is done according to equation (2.19). By varying the tuning frequency the parameters $R(\omega)$ and $L(\omega)$ vary, and so will the calculated added damping R_L.

- Once this is performed, an optimal tuning frequency can be addressed to a peak sea state frequency.

Table 2.5 summarizes these simulations. For each wave peak period T_p the average power extraction using the T_p as the tuning frequency is calculated. Also, using a iterative approach the optimal damping for each simulation is calculated. An example of this is summarized in Table 2.2. Simulations for each sea state is performed 5 times, as exemplified in Table 2.3.

In Table 2.4 the results for all the different sea states can be seen. Both the values for the optimal damping when tuned for the peak frequency of the sea state and the damping which gives maximum average power is listed. This can then be used to determine an optimal tuning frequency for each sea state. In Table 2.5 an optimal tuning period is attributed to each sea state peak period.

Table 2.3: *Table showing optimal damping coefficient R_L with corresponding average extracted power for 5 300 second long irregular wave input simulations. $T_p = 7$ seconds, and $H_s = 1.5$.*

	$R_{L,opt}[kNs/m]$	P_{avg}
Simulation 1	75.0	9.62
Simulation 2	75.0	9.32
Simulation 3	80.0	9.43
Simulation 4	75.0	9.52
Simulation 5	77.5	9.78

Table 2.4: *Table listing peak period of the sea, damping parameters when tuned for peak period of the sea state R_{lin}, and damping parameters which gives maximum extracted average power*

Peak period T_p	R_{lin}	R_{opt}
2.40	27.8	27.5
3.90	69.8	45.0
5.10	112.0	65.0
6.00	144.0	77.5
7.00	181.0	90.0
9.05	216.0	97.5
10.15	253.0	105.0
11.00	290.0	115.0
2.40	319.0	120.0

Table 2.5: *Table listing peak period of the sea and corresponding optimal tuning period.*

Peak period T_p	Tuning period T_{opt}
2.40	2.40
3.90	3.00
5.10	3.80
6.00	4.10
7.00	4.50
9.05	4.80
10.15	5.05
11.00	5.10

Table 2.5 can also be illustrated with the plot seen in figure 2.13. Notably, for sea states with large periods there is greater difference between tuning frequency and wave dominant frequency. In Table 2.2 it was shown that a 50% increase in average power extraction was observed. For sea states with larger peak periods and thus a larger difference in tuning frequency even greater increase in power take-off can be expected.

2.4.3   Remarks about Tuning Frequency

Finally, it has been shown that in order to maximize the mechanical power extraction using linear control equations, the chosen tuning frequency is of great importance. Simulations show that in contrast to a monochromatic input (sinusoidal regular wave-input), when a irregular time-series wave are considered the excitation force has a higher dominant frequency than the sea state.

But in fact, the optimal tuning frequency in terms of maximum extracted power is also higher than the dominant frequency of the excitation force. The reason for this attribute is interesting to investigate analytically, but for this thesis a practical approach has been applied in which the optimal tuning frequency is determined accoring to the simulation experiences seen in Table 2.5.
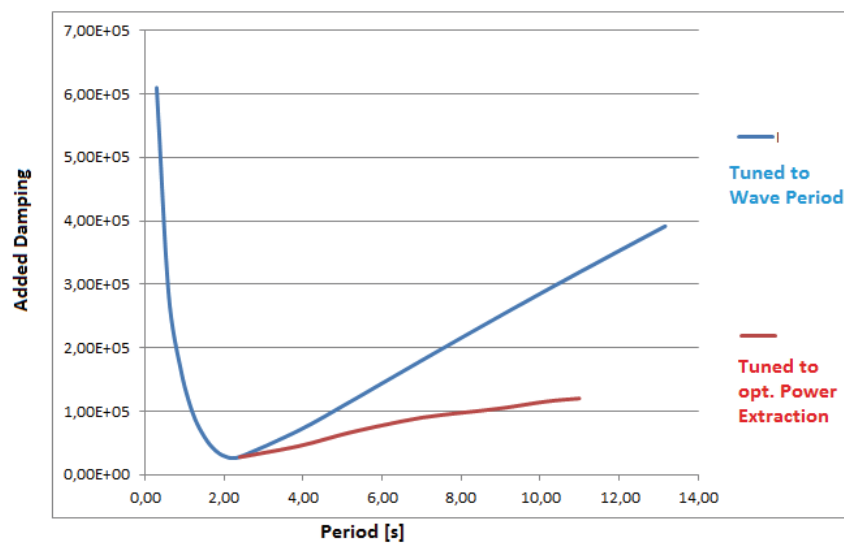
Figure 2.13: *Plot showing damping R_L as a function of wave period. Both values for damping tuned for peak period of the sea state (blue)*

Chapter 3

Electric Power Take Off System

3.1   The Bolt2 Electric Power Take Off System

The Bolt2 power take off system (PTO), which is the basis for the model developed in this thesis, uses an all-electric solution. The stand-alone system currently deployed outside the coast of England consists of the following components [7]:

- Permanent Magnet Synchronous Generator

- Inverter

- Capacitor Bank

- DC-link Charger

- Battery Charger

- Brake Charger and Dump Resistor

In the Toroid Bolt2 concept, all the point absorbers are coupled on a common DC link, as seen for point absorbers 1-5 in figure 3.1. The point absorber with the generator and inverter is considered a complete system which only need to connect to a DC link to function. The scope of this thesis is defined to model one such module and to consider the DC link as a constant voltage of 600 V. The electric system considered in this thesis is therefore as shown in figure 3.2.

The main specifications of the PTO as defined by Fred Olsen are shown in Table 3.1

In order to develop a model for this system a few assumptions have to be defined:

- Classical equations [18] can be used to model the PM generator.

- For longer time domain simulations the losses in the converter bridge can be neglected or approximated through an average value in order to reduce simulation time.

- The DC link can be considered constant.

As the detailed characteristics for the generator and converter module is not available, the modelling has to be approached by using a general description of these and manipulate the model so that it performs in accordance with real testing experiences of the Bolt2
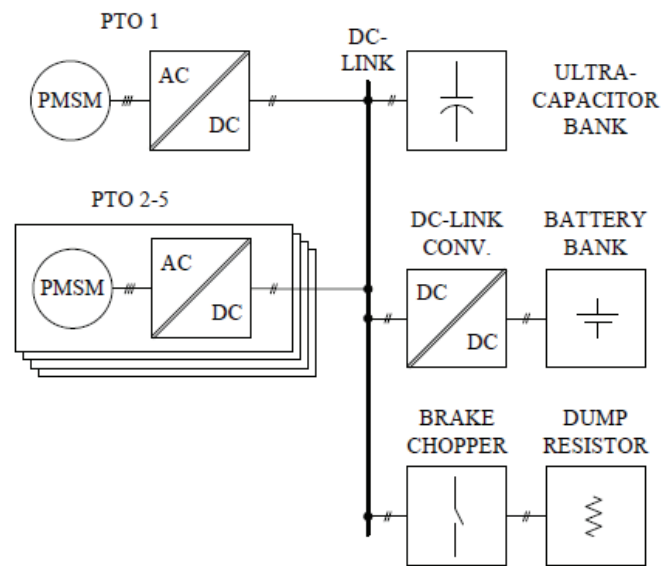
Figure 3.1: *Current topology of the stand-alone system for Bolt2. Figure taken from [7]*
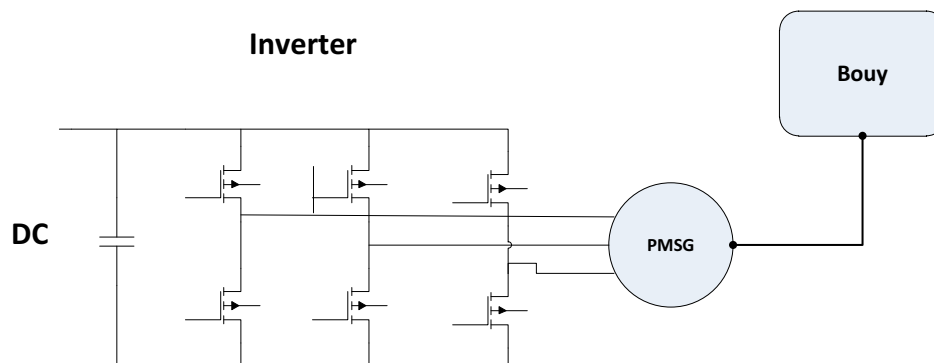
Figure 3.2: *Plot of PTO up to DC-link.*

Table 3.1: *Bolt2 PTO characteristics*

Property	Value	-
Nominal speed Generator	400	[rpm]
Maximum Force Generator	100	[kN]
Minimum Force Generator	20	[kN]
DC-link voltage	600	[V]

PTO-system.

3.2 Pulse-Width Modulation and Converter Bridge

A full model of the PWM-controlled Converter Block has been made in Simulink environment in order to perform some study into how the system behaves in detail under different conditions.

3.2.1 Detailed PWM Controlled Converter Bridge Simulink Block

In figure 3.3 the Simulink model of the converter bridge is depicted. Input into this block is the reference voltage in the dq-frame which is the output of the current controller. This reference signal is then transformed into the abc-reference frame and normalized as seen in equation (3.1).

$$V'_{ref,abc} = \frac{V_{ref,abc}}{V_{DC}} \tag{3.1}$$

This signal is then compared to the internal carrier signal of the PWM generator and pulses are generated. A more detailed explanation of the PWM is shown in appendix B. The generated pulses are then fed into the gate of the converter bridge which control the switching of the IGBT's. The output voltage should then correspond to the reference
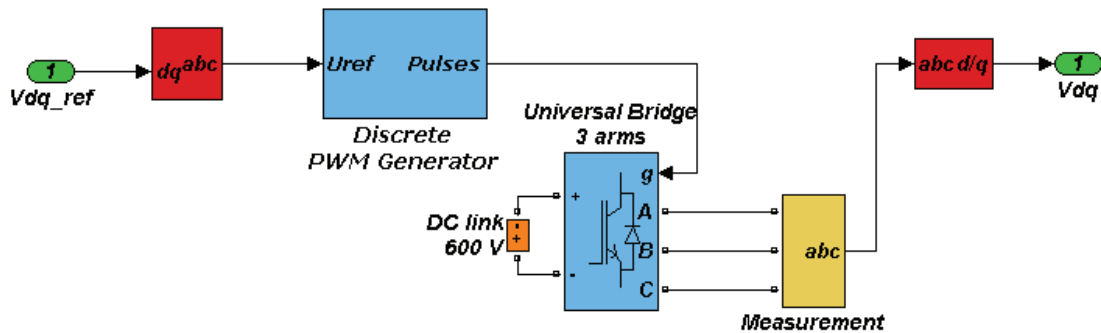
Figure 3.3: *Simulink Model of PWM and Converter Bridge.*
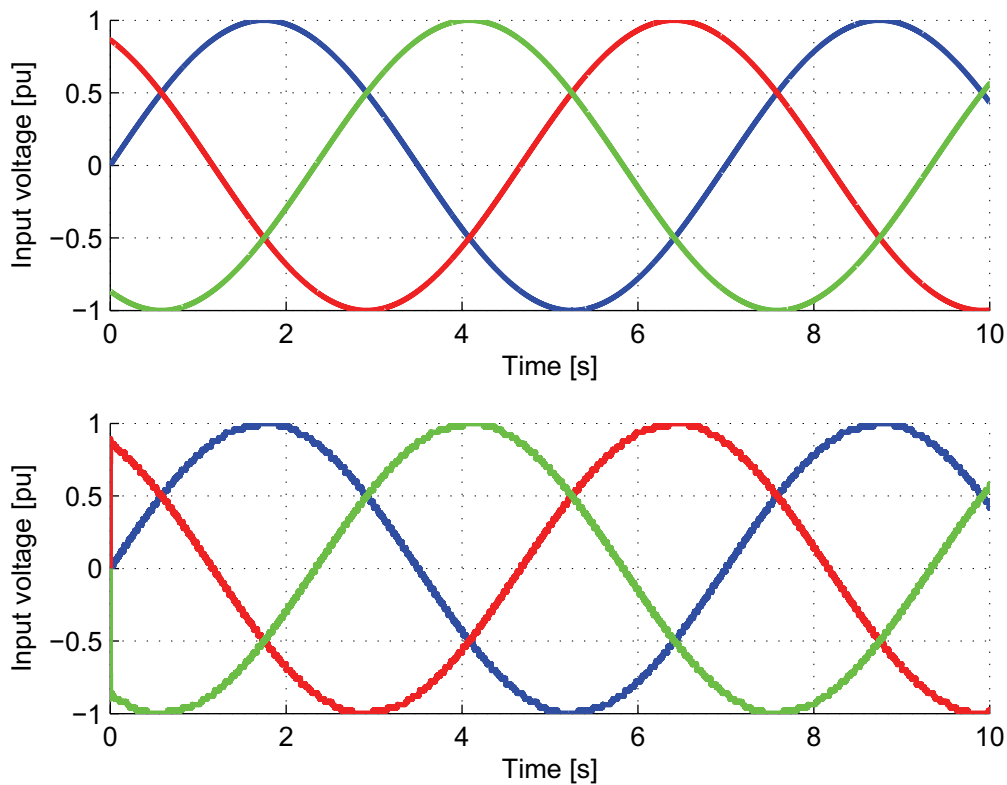
Figure 3.4: *Input reference voltage in abc-reference frame (upper) and filtered output voltage of the converter bridge (lower).*

value input if these do not exceed the DC-link maximum. An example simulation show how the detailed Simulink system behaves. In figure 3.4 the input reference voltage is shown along with the filtered output voltage. The generated pulse signal is seen in figure 3.5.

It is interesting to note what happens when the reference voltage exceeds the limit of the DC-link in the system. In figure 3.6 the reference voltage goes above the 1 pu limit, and it is seen that the output voltage is not able to follow this and is saturated at the value of the DC-link voltage. This can also be seen by the over-modulation [19] of the gate signal in figure 3.7. How this effects the rest of the system will be discussed and analysed in the following section.
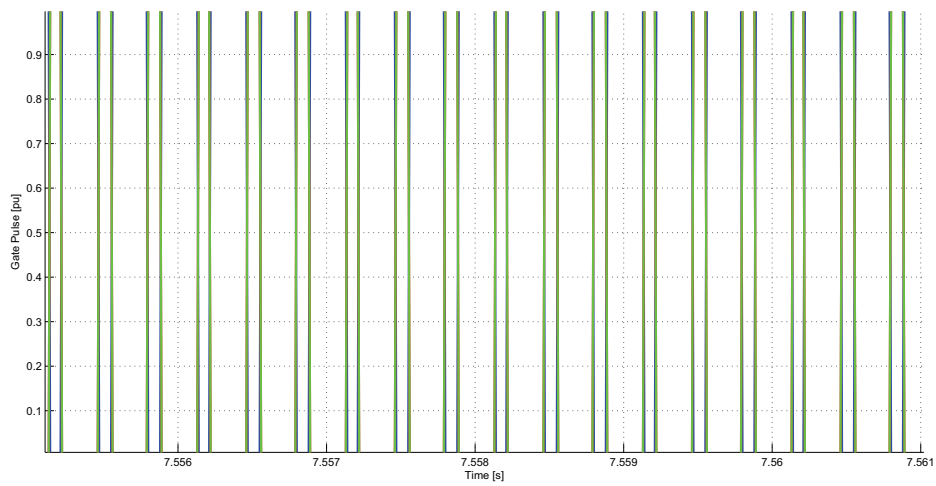
Figure 3.5: *Generated pulse signal which is input into the converter bridge.*
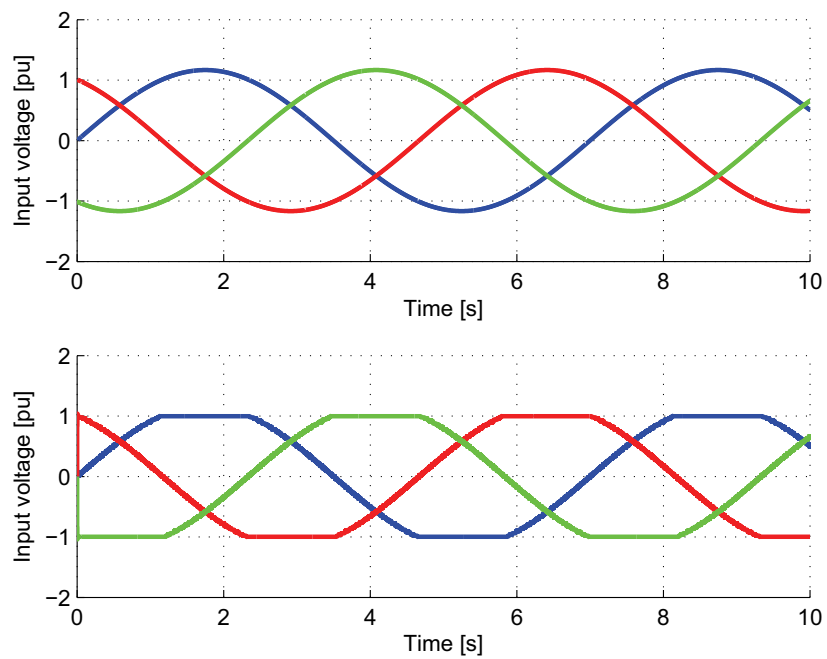
Figure 3.6: *Input reference voltage in abc-reference frame (upper) and filtered output voltage of the converter bridge (lower) when reference voltage exceed maximum DC link value.*
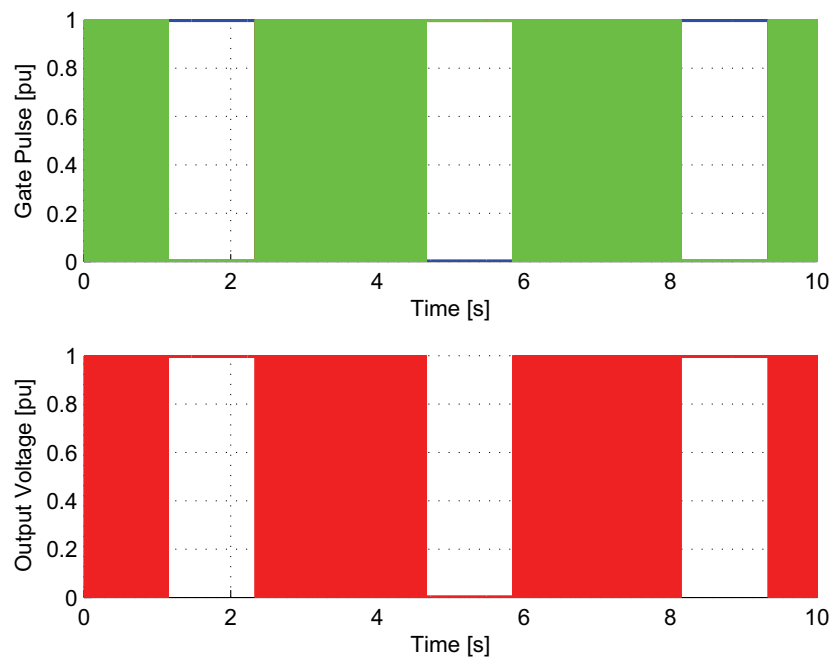
Figure 3.7: *Generated pulse signal (upper) and output unfiltered voltage (lower) when reference voltage exceeds maximum DC link value. Over-modulation occurs as is seen by the period of non-switching.*

3.2.2 Simplified PWM Controlled Converter Bridge Simulink Block

As will be discussed in section 3.3.3 the PWM and converter-bridge block can be considered to have a time constant equal to unity in the comparably slow wave energy system. This means that simulations are run where PWM and Converter bridge are represented by a 1-to-1 block in the simulink system. This implies that the applied voltage by the converter is considered to follow the reference voltage perfectly and instantly. An approach like this has some great advantages:

- Simulation time is significantly reduced. Even for low switching frequencies in the converter bridge, the simulation time becomes tenfold times longer than with a ideal block solution.

- No filters is needed in the system in order to evaluate voltage measurements, as the harmonic distortion due to the high frequency switching is not present.

For the sake of the simulations and investigations that are being performed in this thesis there are two important attributes to consider for the converter bridge. One is the maximum value of the voltage, which is set by the constant value of the DC-link, and the other are the losses that occur in the converter. The first condition is easily handled by applying maximum limitation on the output signal, and can be handled without high frequency switching. The losses are harder to evaluate, especially since not enough key data are known for the converter bridge used in the Bolt2 concept. However, in general terms, these losses tend to be very small compared to generator losses.

Based on these observations a simplified solution for the PWM and converter bridge Simulink block is shown in figure 3.8. This is a simple 1-to-1 block except that it enforces a saturation for voltages with absolute values larger than the DC-link value. As this Simulink block uses logic operators and summation instead of switches the simulation time is also kept low.
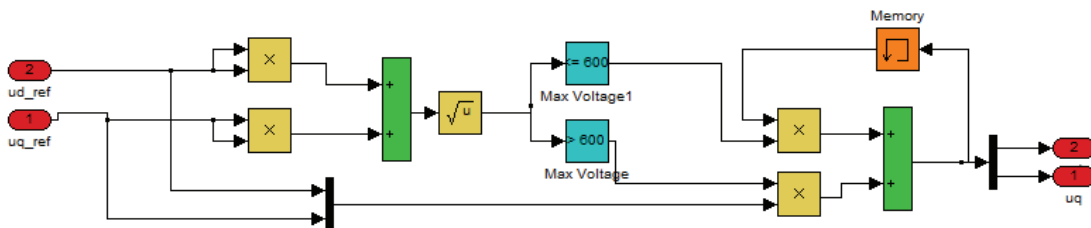
Figure 3.8: *Simulink model of simplified PWM and converter bridge*

3.3   Modelling and Control of a Permanent Magnet Synchronous Generator

3.3.1   General

The transformation from mechanical to electrical energy is done by a Permanent Magnet Synchronous Generator (PMSG). The PMSG has been given growing attention for a various number of applications due to its favourable characteristics: high efficiency, high power density and high torque-to-inertia ratio [20]. As the rotor field is excited by permanent magnets there are no rotor copper losses, and as there are no need for brushes or slip rings the PMSG is significantly smaller in size than a conventional synchronous machine.

One can distinguish between two classes of PMSG, the surface mounted and the interior mounted permanent magnet machine. As the name suggest, the difference lies the placement of the permanent magnets. Figure 3.9 shows an example 4 pole Surface Mounted PMSG. The d-axis is defined as through the center of the magnetic pole, while the q-axis is perpendicular (90 electric degrees) on the d-axis. Notably, for a surface mounted generator the inductance in both these axis are the same [18], as the permanent magnetic material can be considered to have a relative permeability near unity. In this model of the Bolt2 PTO, the generator is considered to be a 28 pole-pair surface-mounted PMSG. The generator characteristics which are used for the model is defined in Table 3.2.

Table 3.2: *Generator characteristics*

Property	Value	-
Number of poles, n_p	28	[]
Torque Constant, k_T	10.8	[Nm/A]
Winding Resistance, R	0.038	[ρ]
Inductance, L	1.4	[mH]
Inertia, J_{gen}	1.31	[kgm^2]
Max Current, I_{max}	240	[A]

3.3.2   PMSG Equations

For given voltages v_q and u_d on the generator terminals, the current equations [18] for the PMSG is commonly expressed as:

$$\frac{di_d}{dt} = -\frac{R_S}{L_d}i_d + \omega_e\frac{L_q}{L_d}i_q + \frac{1}{L_d}u_d \tag{3.2}$$
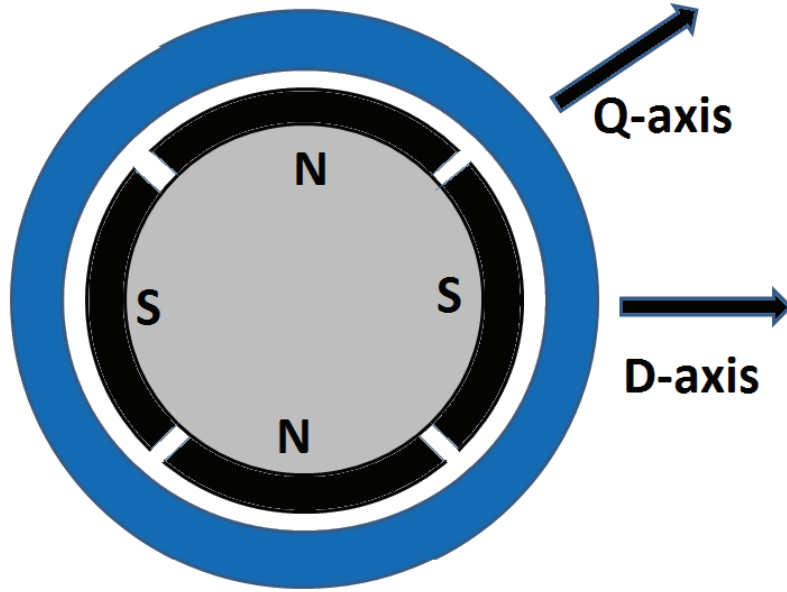
Figure 3.9: *Figure of 4-pole Surface Mounted PMSG*

$$\frac{di_q}{dt} = -\frac{R_S}{L_q}i_q - \omega_e\left(\frac{L_d}{L_q}i_d + \frac{\Psi_{PM}}{L_q}\right) + \frac{1}{L_d}u_q \tag{3.3}$$

Here ω_e is the electric angular frequency of the generator, i_d and i_q are the d- and q-axis current, while R_s and $L_{d/q}$ is the stator resistance and inductance is defined in table 3.2. For a surface mounted PMSG, the inductance in the d- and q-axis can be considered equal. The equations can therefore be simplified to

$$\frac{di_d}{dt} = -\frac{R_S}{L}i_d + \omega_e i_q + \frac{1}{L}u_d \tag{3.4}$$

$$\frac{di_q}{dt} = -\frac{R_S}{L}i_q - \omega_e\left(i_d + \frac{\Psi_{PM}}{L}\right) + \frac{1}{L}u_q \tag{3.5}$$

In figures 3.11 and 3.10 the electrical equivalent circuits for the generator is showed in the dq-reference frame.

The electromagnetic torque of the generator is expressed as a function of the permanent magnet flux linkage Ψ_{PM} and q-axis current i_q.

$$T_e = \frac{3}{2}n_{pp}\Psi_{PM}i_q \tag{3.6}$$

This equation can also be used in order to determine the permanent magnetic flux Ψ_{PM}
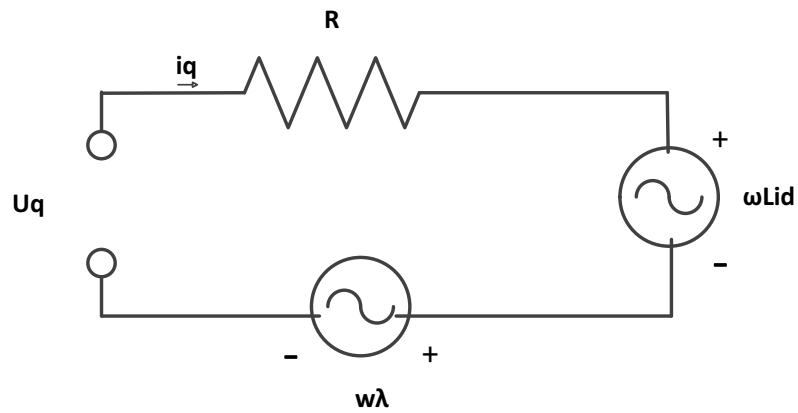
Figure 3.10: *The Q-axis electric equivalent of a surface mounted PMSG.*
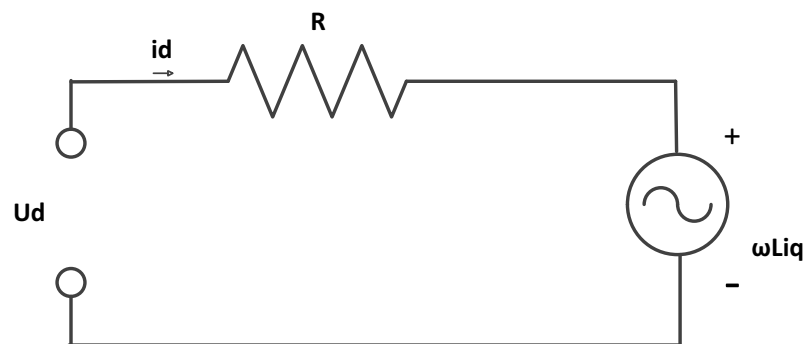
Figure 3.11: *The D-axis electric equivalent of a surface mounted PMSG.*

of the generator. As shown in Table 3.2 the torque constant of the generator is 10.8. Using that $\frac{M_n}{I_n} = 10.8$ and that $n_p = 28$ the permanent magnetic flux of the PMSG is approximated to be 0.257 Wb.

A model of a generator based on the above equations is a good approximations within
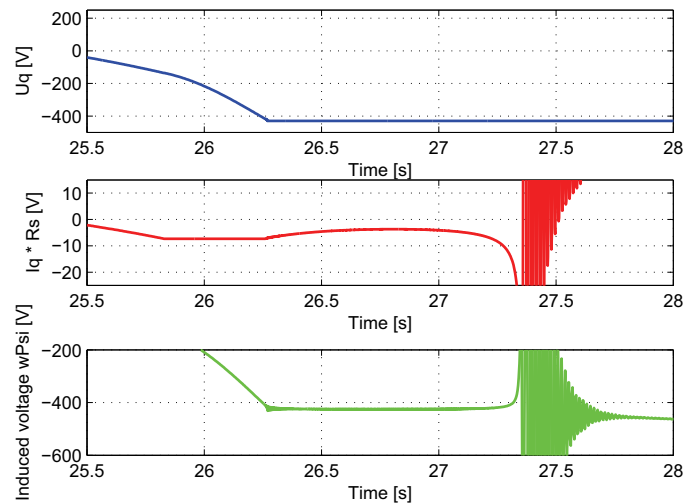
Figure 3.12: *System response to uncontrolled voltage saturation. Top plot show the q-axis voltage from the output of the converter bridge U_q, the second plot show the voltage over the stator resistance $R_s i_q$ and the bottom plot show the induced voltage $\omega \Psi_{PM}$*

the rated areas of operation. Given a stator voltage and shaft speed, a current will be generated. One important limitation to be aware of however is what happens in over-speed operation. As seen in the electrical equivalent in figures 3.11 and 3.10, the induced voltage is a function of generator speed and permanent magnetic flux. In this model the stator voltage is limited by the DC-link in the converter bridge. This is represented by the PWM and converter bridge block in the Simulink model seen in figure 3.19. If the total reference voltage input into this block is above the maximum voltage V_{max}, then the output value is saturated. This means that the voltages u_d and u_q in figures 3.11 and 3.10 reaches a maximum value. If the speed and induced voltage increases further, one will observe a decreasing q-axis current and a decreasing torque. When the induced voltage due to speed and field strength becomes equal to the maximum voltage U, then the q-axis current becomes zero and the generator is not able to supply any torque. We are in highly unstable mode of operation. In figure 3.12 the q-axis voltage responses for the system is shown when the voltage limit is reached.

As seen, when uncontrolled this leads to unstable conditions and a breakdown. Physically, the response seen in this model is not possible, as clearly seen in the generators very large post-fault values for torque in figure 3.13. However, for the purpose of this model it is sufficient to note that if the maximum induced voltage limit is not controlled the generator becomes highly unstable.
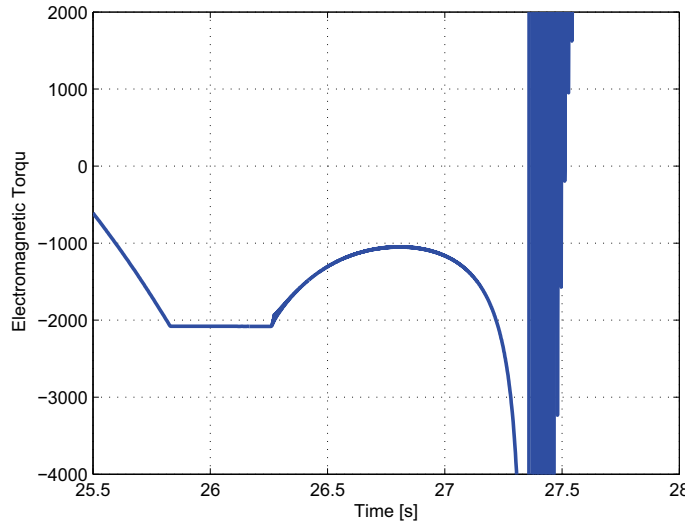
Figure 3.13: *System response to uncontrolled voltage saturation. Plot is of electromagnetic torque of the generator.*

3.3.3   Current Control

Current control is needed to make sure the actual current follows the wanted current reference values. As is known from dq reference analysis [18] there is a cross coupling between the q- and the d-axis in equations (3.4) and (3.5). This can be avoided by feed-forward technique, defining that a reference voltage $v_d = u_d + \omega_e L i_q$ and $v_q = u_q - \omega_e L i_d - e_q$. This gives two independent first order equations in the dq frame as follows

$$v_d = R_s i_d + L_s \frac{di_d}{dt} \tag{3.7}$$

$$v_q = R_s i_q + L_s \frac{di_q}{dt} \tag{3.8}$$

The transfer functions from i to v can therefore be written as

$$\frac{i(s)}{u(s)} = \frac{\frac{1}{R_s}}{1 + \frac{L_s}{R_s}s} \tag{3.9}$$

These current loops are controlled using PI regulators. Figure 3.14 show the block diagram with the PI-controller, PWM and converter bridge included. The transfer block of the PWM and converter bridge is set to be unity, as this is a fair simplification for the comparably slow wave energy converter system.

$$G_{OL} = K_p \frac{1 + T_i s}{T_i s} \frac{\frac{1}{R_s}}{1 + \frac{L_s}{R_s}s} \tag{3.10}$$

The parameters of these PI regulators are tuned according to the modulus optimum [21],
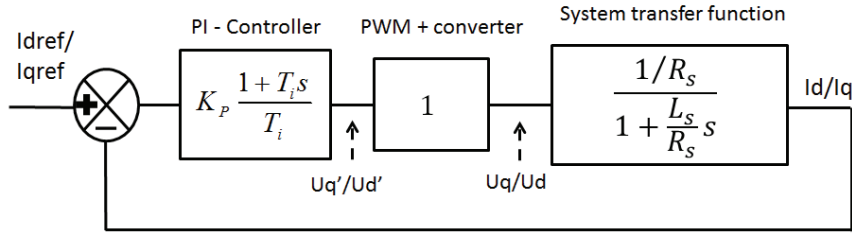
Figure 3.14: *Block diagram of current control loop. Notably the PWM + converter block is represented by a unity gain.*
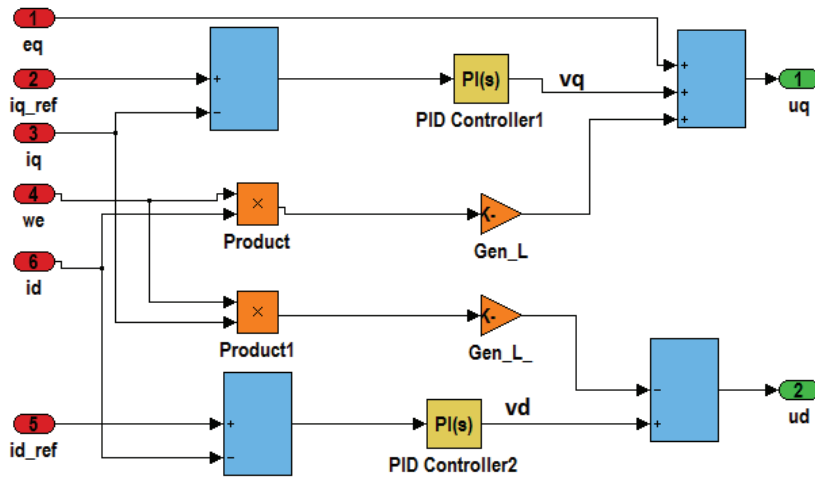
Figure 3.15: *Current Control implemented in Simulink*

cancelling out the electrical time constant $T_i = \frac{L_s}{R_s}$. This gives the following open-loop transfer function:

$$G_{OL} = K_p \frac{1 + T_i s}{T_i s} \frac{\frac{1}{R_s}}{1 + \frac{L_s}{R_s} s} = K_p \frac{\frac{1}{R_s}}{\frac{L_s}{R_s} s} = K_p \frac{1}{L_s s} \qquad (3.11)$$

Determining the gain K_p is done through evaluating the term for the closed loop transfer function. As one want to have a closed loop transfer function gain equal to unity, a value for K_p can be approximated.

$$M(\omega) = \frac{G_{OL}}{1 + G_{OL}} = \frac{K_p}{L_s j\omega + K_p} = 1 \qquad (3.12)$$

In order for this equality to hold, then $K_p >> L_s \omega$. As the value for $L_s = 1.4$ mH and $\omega_{e,max} < n_{max} \frac{2\pi}{60} n_{pp} \approx 5000$ it is considered that $K_p = 25$ is sufficiently large for all operation areas. In figure 3.15 the current control with de-coupling and PI controllers is shown implemented in a Simulink block called *Current Control*

3.3.4   Torque Control

In wave energy large fluctuations in speed is to be expected and consequently a large overrating of the generator will be needed for it not to operate above rated speed. Thus a more practical approach is to allow over-speed operation. In order to extend the operation speed to above rated speed it is necessary to weaken the magnetic field [22]. As one cannot directly control the field produced by the permanent magnets, controlling the flux is not as easy as for conventional double excited electrical machines. Under rated conditions the d-axis current is kept at zero in order to s low as possible current under constant torque operation. However, in order to weaken the resultant magnetic field a negative d-axis current is needed. This is called *field weakening control*, and is a well known subject for PM-machines [18].

Saturation Points

There are several constraints in the PTO system. Limiting data include maximum torque or force on generator and gear equipment, maximum current in the generator, maximum voltage of the DC-link and maximum speed of the generator and the inverter. When the speed increases the first saturation point that occur is due to the maximum torque of the generator. As the electromagnetic torque is proportional to the q-axis current, this can be enforced by maintaining the reference value for this current at a constant value. The minimum force constraint of the system is controlled in the same way, but with a minimum reference q-axis current.

The next saturation point occurs when the maximum power of the generator is produced. In other words, the maximum induced voltage of the generator has been reached. For further increase in speed, the induced voltage will have to be kept constant. By entering the constant power region, the control aims to keep both current and voltage constant. The voltage and current limits can be plotted together in the dq-axis. This is done by implementing the current and voltage limitations seen in the following equations:

$$i_d^2 + i_q^2 \leq i_{max}^2 \tag{3.13}$$

$$v_d^2 + v_q^2 \leq u_{max}^2 \tag{3.14}$$

Next, the steady-state equations for (3.4) and (3.5) can be expressed as:

$$v_d = R_s i_d - \omega_e L i_q \tag{3.15}$$

$$v_q = R_s i_q + \omega_e (L i_d + \Psi_{PM}) \tag{3.16}$$

Using these expressions, the voltage boundary as a function of electric speed can be expressed in terms of i_d and i_q. Substituting equation (3.15) and (3.16) into (3.14) one get the following expression:

$$\left(i_d + \frac{\omega_e^2 L \Psi_{PM}}{R_s^2 + \omega_e^2 L^2}\right)^2 + \left(i_q + \frac{\omega_e R_s \Psi_{PM}}{R_s^2 + \omega_e^2 L^2}\right)^2 \leq \frac{V_{max}^2}{R_s^2 + \omega_e^2 L^2} \tag{3.17}$$

Figure 3.16 show these boundaries plotted together in a current-axis reference system. Here the blue circles marks the maximum voltage boundaries plotted for varying generator speeds. The green circle marks the maximum current boundary of the PTO-system. In order to maximise the power extraction, one wants to maintain as high torque as possible, meaning keeping the q-axis current at its maximum and the d-axis current at zero. This corresponds to the uppermost point of the maximum current circle. As the generator speed increases, the voltage limitation circles enforces the optimal point to move leftwards along the maximum current circle, maintaining as large a value as possible for the q-axis current. This becomes the optimal trajectory for the current operation points [23].

Determining reference values

In order to make sure that the limiting data are not exceeded proper control needs to be implemented. For low generator speeds, which means operation below rated condition,
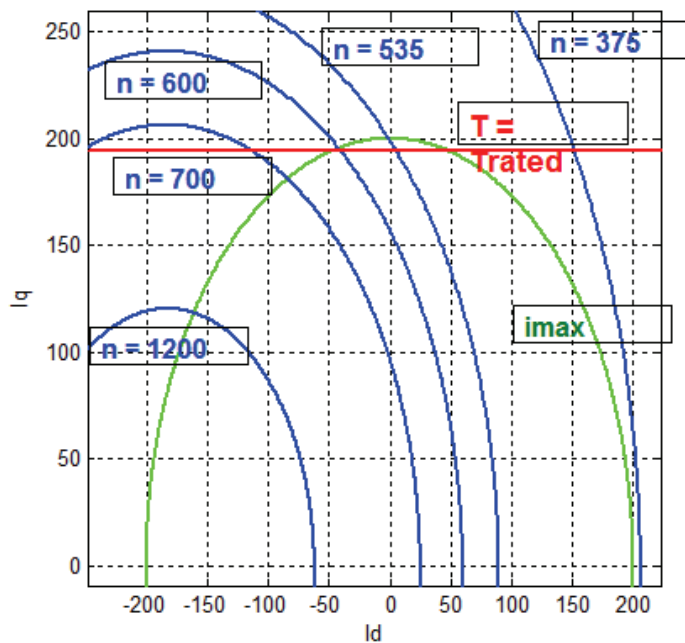
Figure 3.16: *Generator voltage and current boundaries of operation. Green circle represents the maximum current boundary, blue circles represent the maximum voltage boundary for different generator speeds. X-axis is i_d current, y-axis is i_q current.*

the main focus will be to maximize power extraction. For now this is considered to be done by maintaining a constant damping B_r, which gives a linear increase in torque as the speed increases. However, torque-control is required to saturate the load-force at its maximum value as well as to implement the field weakening control reference current-values. Initially the torque control method over the whole range of operation speeds is thought to function as described in figure 3.17

The input into the torque-control flowchart in figure 3.17 is the i_q reference current and the generator speed ω_e. The reference current is obtained from the reference torque as follows

$$i_{q,ref} = \frac{T_{e,ref}}{\frac{3}{2}n_{pp}\Psi_{PM}} \tag{3.18}$$

The reference torque is calculated from the mechanical model of the wave energy converter:

$$T_{e,ref} = \frac{1}{\rho_g}\left(B\dot{\eta} + M_L\ddot{\eta}\right) \tag{3.19}$$

where ρ_g is the total gear ratio, B is the added damping and M_L is the added mass. The generator speed is also calculated from the mechanical model, and is given as:

$$\omega_e = n_{pp}\rho_g\dot{\eta} \tag{3.20}$$
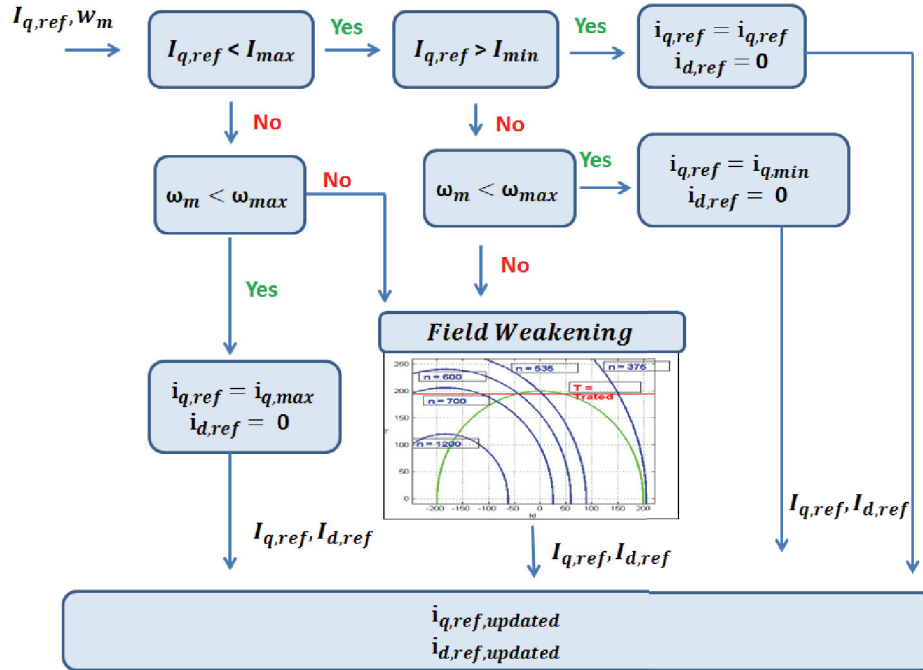
Figure 3.17: *Flowchart representing the idea behind the torque control determination of the reference currents.*

The speed in which field weakening begins, $\omega_{max} = \omega_{fw}$, corresponding to the point in which a maximum voltage curve crosses the $i_q = i_{max}$ point in figure 3.16, can be expressed [23] by the generator characteristics as the following

$$\omega_{fw} = \frac{-2R_s I_{max} \Psi_{PM} + \sqrt{(2R_s I_{max} \Psi_{PM})^2 - 4(\Psi_{PM}^2 + LI_{max}^2)(R_s^2 I_{max}^2 - V_{max}^2)}}{2(\Psi_{PM}^2 + L^2 I_{max}^2)} \quad (3.21)$$

Reference Currents under Field Weakening

The reference current calculations are based on the equations from the robust field weakening control strategy described by Ching-Tsai Pan and Jenn-Horng Liaw [23]. Combining equations (3.13) and (3.17) one can express the voltage constraint solely as a function of speed and the d-axis current:

$$\left(i_{d,ref} + \frac{\omega_e^2 L \Psi_{PM}}{R_s^2 + \omega_e^2 L^2}\right)^2 + \left(\pm\sqrt{I_{max}^2 - I_{d,ref}^2} + \frac{\omega_e^2 R \Psi_{PM}}{R_s^2 + \omega_e^2 L^2}\right)^2 \leq \frac{V_{max}^2}{R_s^2 + \omega_e^2 L^2} \quad (3.22)$$

Rearranging (3.22) in order to get an expression for the d-axis current gives the following equation:

$$i_{d1,2,ref} = \frac{-b \pm \sqrt{b^2 - 4ac}}{2a} \quad (3.23)$$

where

$$a = 4\left(i_{d,center}^2 + i_{q,center}^2\right)$$

$$b = 4i_{d,center}\left(\frac{V_{max}^2}{R_s^2 + \omega_e^2 L^2} - (I_{max}^2 + i_{d,center}^2 + i_{q,center}^2)\right)$$

$$c = \left((I_{max}^2 + i_{d,center}^2 + i_{q,center}^2) - \left(\frac{V_{max}^2}{R_s^2 + \omega_e^2 L^2}\right)\right)^2 - 4i_{q,center}^2 I_{max}^2$$

The values $i_{d,center}$ and $i_{q,center}$ represent the coordinates of the center of the voltage constraint circle expressed by equation (3.17).

$$i_{d,center} = -\frac{\omega_e^2 L \Psi_{PM}}{R_s^2 + \omega_e^2 L^2}$$

$$i_{q,center} = -\frac{\omega_e R_s \Psi_{PM}}{R_s^2 + \omega_e^2 L^2}$$

As the determinant $b^2 - 4ac$ is positive for all velocities in the field weakening region,
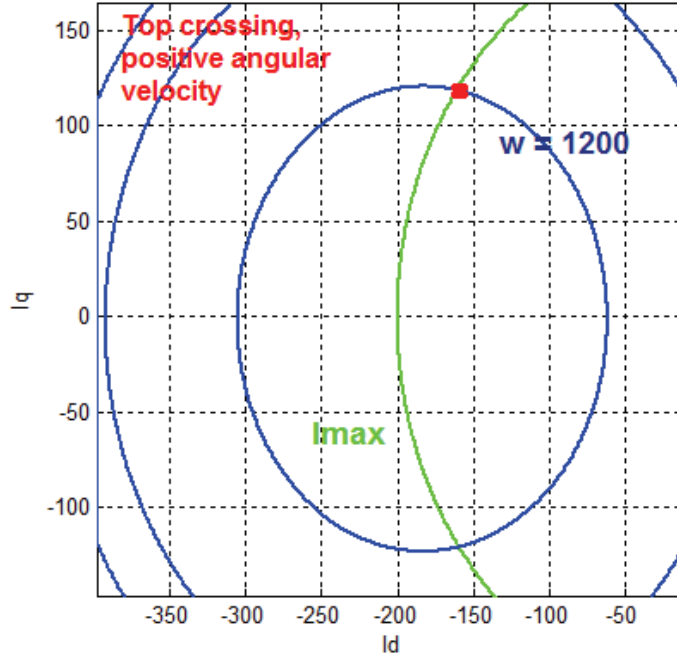
Figure 3.18: *Current and voltage boundary plots showing a point marked for a given positive angular velocity.*

this algorithm should not have problems with imaginary values. Solving these second order equations yield two solutions for the d-axis current, corresponding to the two points where the maximum voltage circle crosses the maximum current circle. The top crossing, giving a positive value for i_q represents the case with a positive generator speed, meaning a positive input electromagnetic torque reference. The lower crossing gives the current values for the corresponding speed of negative value.

This means that a final selection of the d-axis reference current can be chosen

$$i_{d,ref} = \frac{-b + \sqrt{b^2 - 4ac}}{2a} \ if \ w_e > 0 \tag{3.24}$$

$$i_{d,ref} = \frac{-b - \sqrt{b^2 - 4ac}}{2a} \ if \ w_e \leq 0 \tag{3.25}$$

The q-axis reference current can then be updated and is given as:

$$i_{q,ref} = \sqrt{i_{max}^2 - i_{d,ref}^2} \tag{3.26}$$

3.3.5 Verification in Simulink

Using the equations (3.4) and (3.5) to represent the PMSG and the torque control outlined in the flowchart in figure 3.17, the Simulink system in figure 3.19 represents the whole wave-to-wire model. In order to verify that the control strategy functions as wanted some initial simulations with passive loading is performed. In figure 3.20 the wave elevation time series is shown as well as the corresponding speed on the generator. In figure 3.21 one can see that the torque is effectually saturated at its peak value of approximately 2600 Nm. Also one sees that the q-axis current is saturated at 240 A, which has been set as the peak current for this initial simulation and corresponds to the a maximum induced electromagnetic force of 100 kN. The times when the control goes into to field weakening mode can be recognized by the negative peaks in d-axis current.

These figures indicate that the model performs as expected. When the generator speed increases above the rated value the control goes into field weakening mode. When this happens, one also sees the characteristic 'dip' in torque as shown in figure 3.22

Finally, it is interesting to verify that the 3-phase voltages and current does not exceed their maximum values. Figure 3.23 show how the maximum current and voltage respectively are for the simulation.
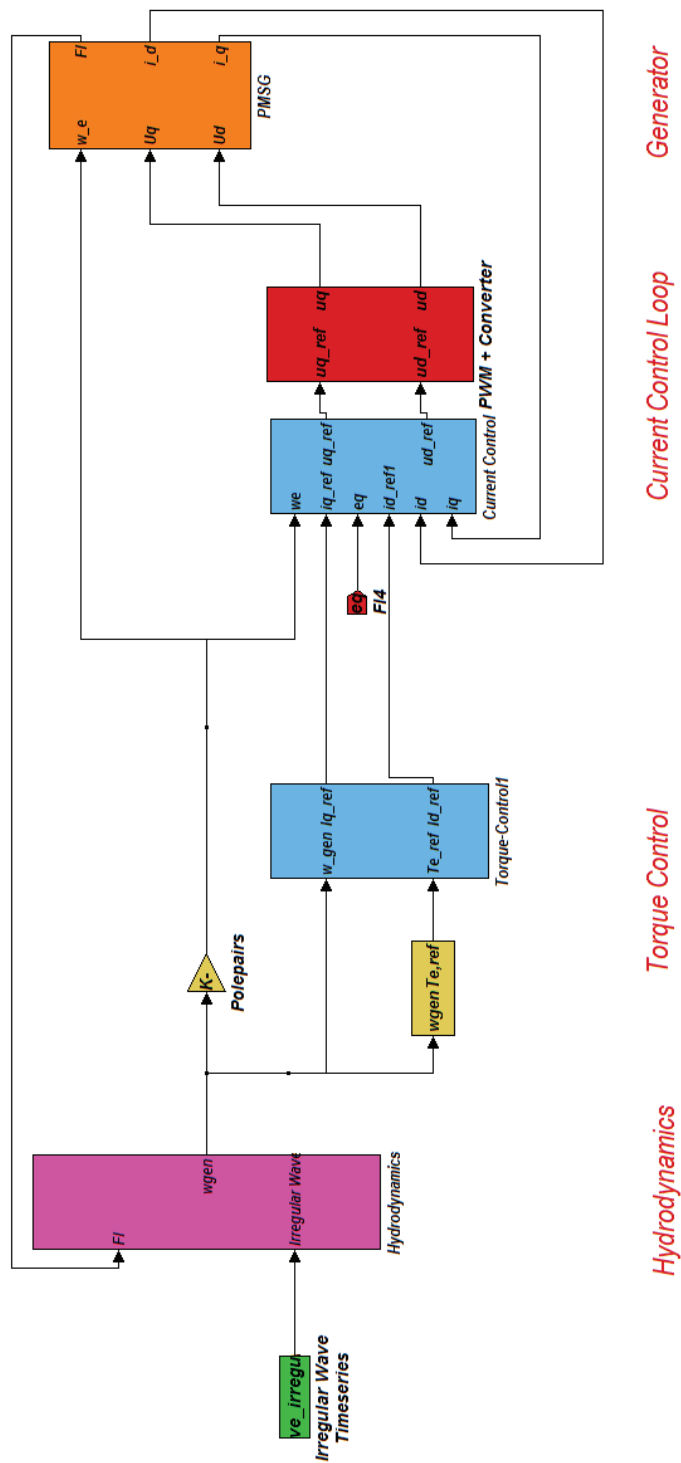
Figure 3.19: *Simulink model representing the wave to wire model with the implemented torque control and current control.*
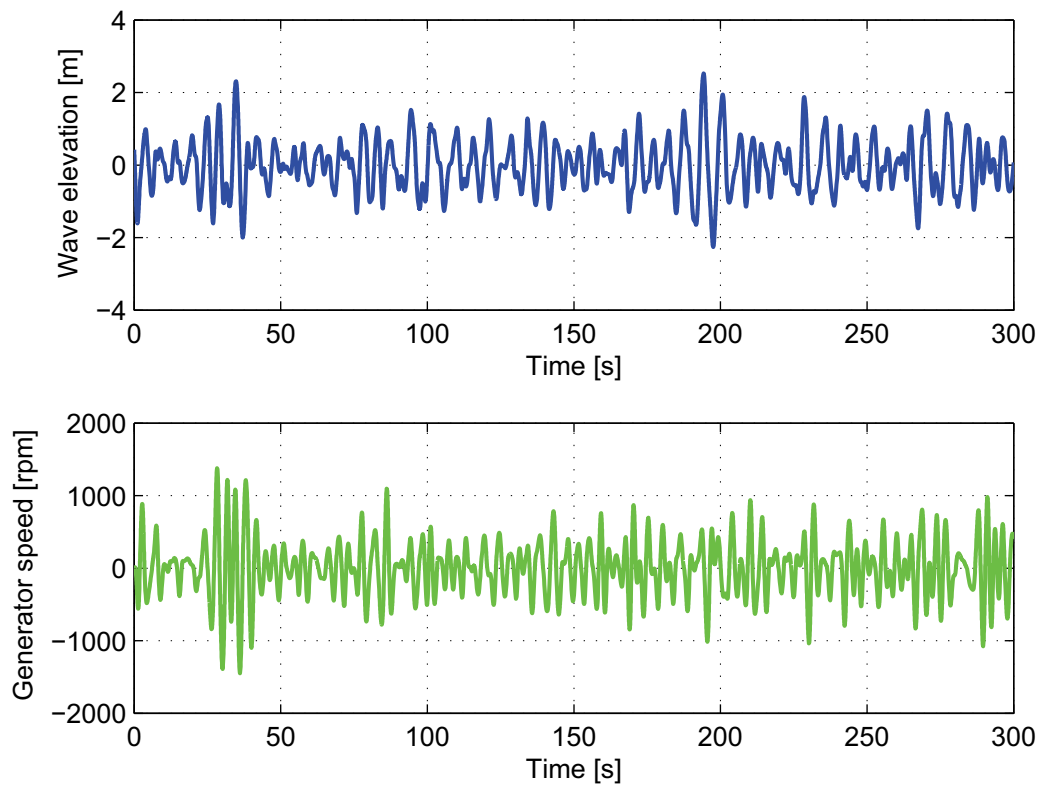
Figure 3.20: *Wave elevation and generator speed for a 300 second timeseries simulation with irregular wave input. Hs = 2.75 m, Tp = 6.5 s*
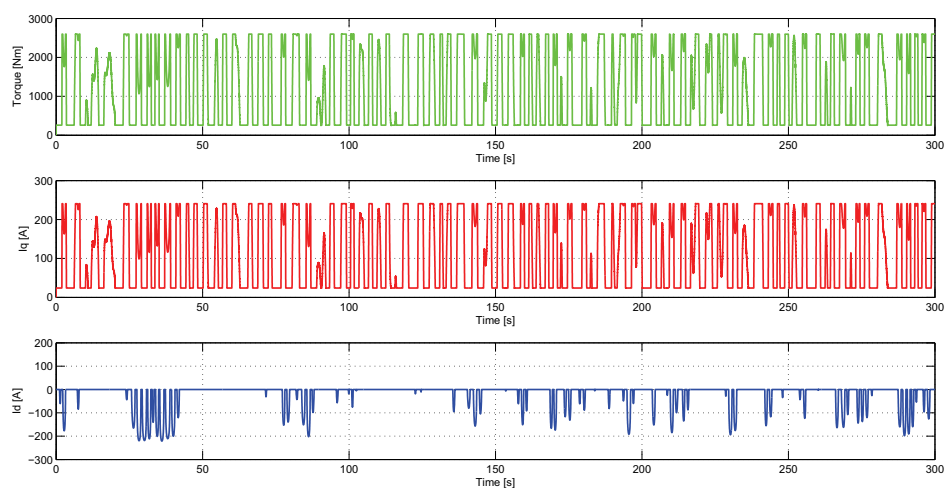
Figure 3.21: *Electromagnetic torque, q-axis current and d-axis current for a 300 second time-series simulation with irregular wave input. Hs = 2.75 m, Tp = 6.5 s*
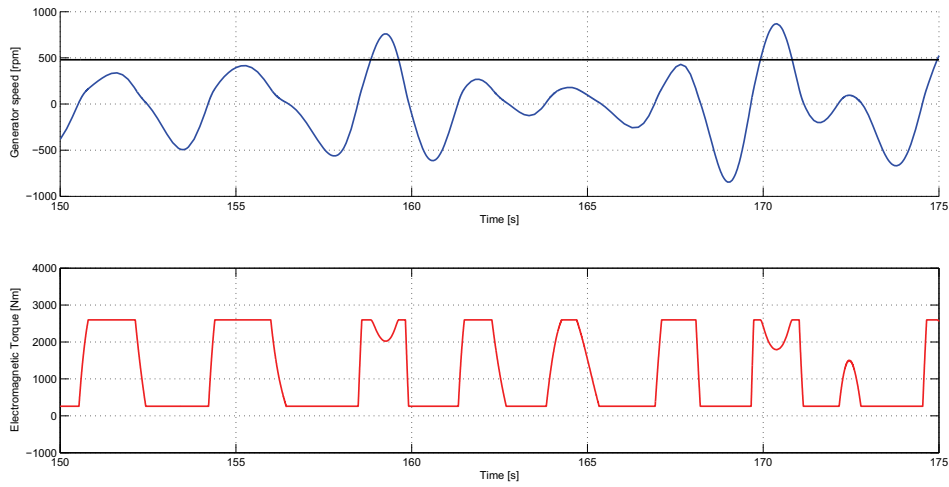
Figure 3.22: *Generator speed and electromagnetic torque. When $\omega_g > \omega_{rated}$ (black line) field weakening begins and torque decreases.*
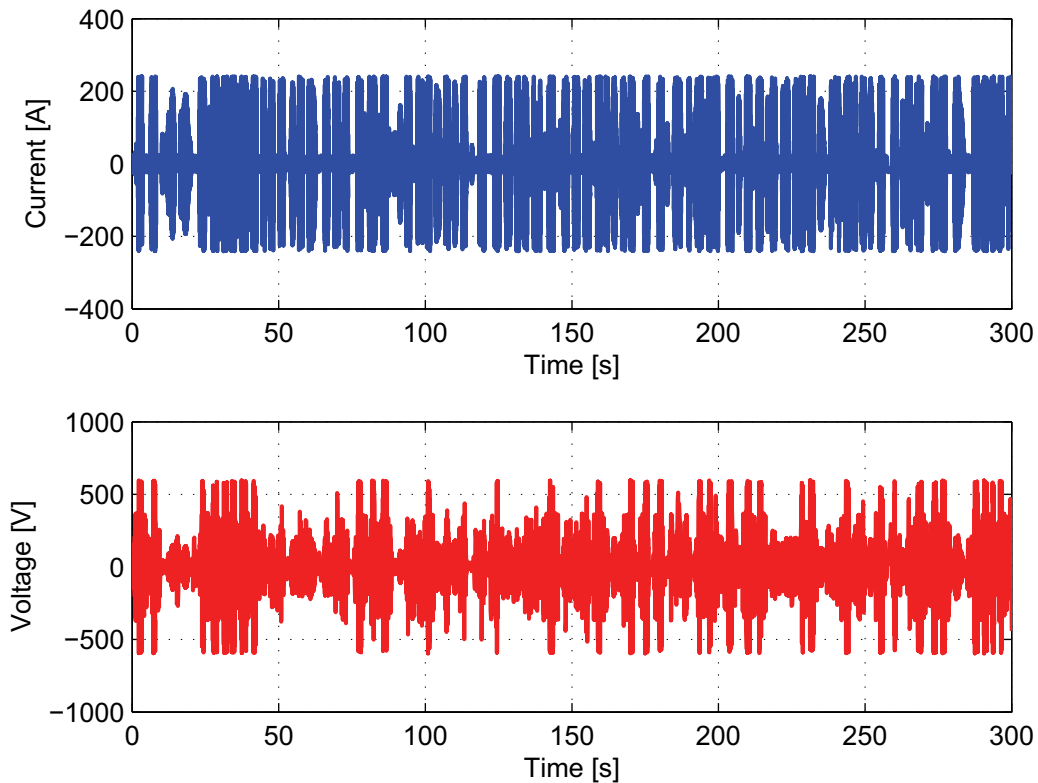
Figure 3.23: *ABC voltage and current for a 300 second simulation with irregular wave input. Hs = 2.75 and Tp = 6.5 s.*

Chapter 4

Wave-to-Wire Modelling

4.1 General

In the specialization project [8] a wave-to-wire model of Bolt was described with the PTO-system being represented by an applied force. In this thesis it is defined as a model which has as input an irregular wave and outputs electric power to the DC-link. Arguably, a complete wave-to-wire model should include also integration with other WECs, the DC/AC converter and a model of the land-cable. Such an extension of the model should be considered for further studies.

4.2 Combining the Hydrodynamic and Electric PTO models

A main problem for this model of the Bolt2 wave energy converter is that the hydro-dynamical model is built on measurements and data for Bolt while the generator and inverter is based on Bolt2 PTO characteristics. A method to combine these in a suitable way is necessary in order to properly model the wave energy converter in detail. Key differences for the two systems is the hydrodynamics of the buoy as well as the size of the generator. The maximum force applied to the rope in Bolt was 40 kN [24] while it is 100 kN for Bolt2 [7]. An important question is therefore if the hydrodynamics of Bolt can be used together with the generator from Bolt2, and if not, how to improve the model.

According to the Fred Olsen experiences from Bolt2 optimal damping with respect to both hydrodynamics and generator efficiency the damping should be approximately $300 \frac{kN}{m/s}$ for all sea states. The reason for this is that it is the generator efficiency that limits the damping, as the optimal damping of the hydrodynamical model is higher than this. To observe a similar trend in the model is therefore an important verification that it performs as wanted. When simulating with the two models directly, such an behaviour

does not occur as. This means that some up-scaling / downscaling is necessary.

4.2.1   Scaling the Models

In order to match the models, three approaches is considered.

- Scaling the hydrodynamic parameters

- Scaling the generator ratings

- Scaling the forces between the two models

Ideally, a up-scaling of the hydrodynamical model should be performed by tuning the hydrodynamical parameters in such a way that the whole system is identical to Bolt2. This however is non-trivial, as the radiation and excitation forces can not be verified to behave proportional to an increase in load force.

The next approach is to scale down the generator model by enforcing a saturation on 40 kN. In this way one gets a match between proper speed and torque saturation, and one can use the original hydrodynamic parameters. The main drawback of this is that the generator efficiency and other generator characteristics that is supplied by the manufacturer will not be valid for a down-scaled version.

What is then considered to be the best approach is keep the two systems as they are but to introduce a scaling ratio

$$n_{scale} = \frac{F_{max,Bolt}}{F_{max,Bolt2}} = \frac{4}{10}$$

in the intersection of these two models. As the load parameters R_L and L_L are tuned for the hydrodynamic parameters, these have to be scaled by a ratio of $\frac{1}{n_{scale}}$ in the generator model. Similarly the load force applied by the generator to the hydrodynamic model is scaled by a factor of n_{scale}. Figure 4.1 shows how this is implemented in the Simulink system.

The drawback of this approach is that the power observed in the mechanical model is not the same as in the electrical model. Also there is difficult to say if the sea-state input in the hydrodynamic model is the same experienced in the electrical model. This means that classification of the electrical output in terms of significant height and peak period needs to be done with relative values. Despite of this, this relatively easy method fulfils the main purpose of matching generators torque-saturation speed at optimal damping with the results obtained by Fred Olsen.
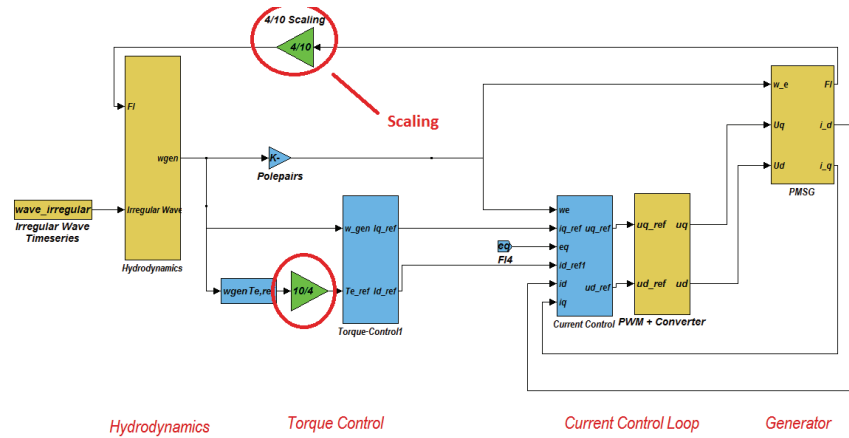
Figure 4.1: *Simulink model with the scaling factor of n_{scale} implemented.*
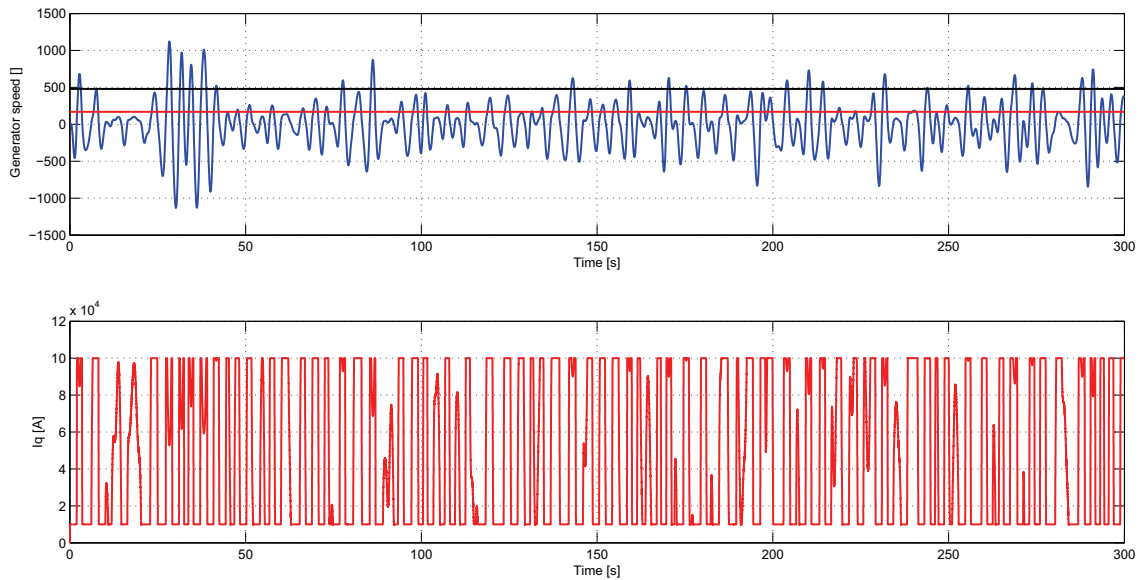
Figure 4.2: *Plot of generator speed in RPM (Top) generator electromagnetic torque in Nm(Bottom). In the speed figure the torque-saturation speed (red) and field-weakening speed (black) is marked.*

4.2.2 Torque Saturation in Scaled Model

The load parameters for these initial simulations are tuned according to the hydrodynamic parameters of Bolt and linear theory as showed in section 2. The scaling of force is undertaken as shown in figure 4.1. For now only a passive loaded system is considered.

The speed-torque measurement shown in figure 4.2 show that the torque-saturation speed is now reduced from the results seen in the unscaled simulations. It is now a better match with the experiences of Bolt2, which operates with a saturation speed of 0.27 m/s [100 rpm].

Table 4.1: *Table showing simulink model Force, Power, Losses and Efficiency as a function of speed*

Speed [m/s]	Force [kN]	Power [kW]	Losses [kW]	Efficiency [%]
0.1	30	3	0.7	76.7
0.3	90	27	6.29	76.7
0.337	100	34.1	7.76	76.7
0.5	100	50	7.76	84.5
0.75	100	75	7.76	89.7
1.25	100	125	7.76	93.8
2	7.75	155	7.76	95.0
3	5.17	155	7.76	95.0

4.3   Generator Efficiency - Determining Losses in the Generator and Power Take Off System

The generator efficiency is very important in determining the optimal control strategy for the WEC, especially if one is to consider complex conjugate or intermediate control.

4.3.1   Determining Losses in PMSG Simulink Model

The losses that occur in the Simulink model of the PMSG is due to the resistance R seen in the electric equiavlent circuit shown in figures 3.10 and 3.11. As the q-axis current is proportional to the torque, the following observations can be made about the stator-copper losses in this model.

- When torque increases, losses increase.

- When torque reaches saturation, the maximum losses are reached as well. A further increase in speed will not increase the losses of the system.

- As speed increases, the power increases while the losses are constant. The efficiency of the generator is therefore increasing.

- When the maximum power saturation point is reached, a constant efficiency is observed for increasing speed as both losses and power are constant.

This means that in the model, a high speed-high torque operation is more favourable than a low speed - high torque operation. This corresponds to the efficiency plot shown in the paper by J. Sjolte [7]. In order to evaluate if this model can be used directly to evaluate the losses a similar figure as shown by this paper is made. In table 4.1 the calculations that are the basis for this is shown.
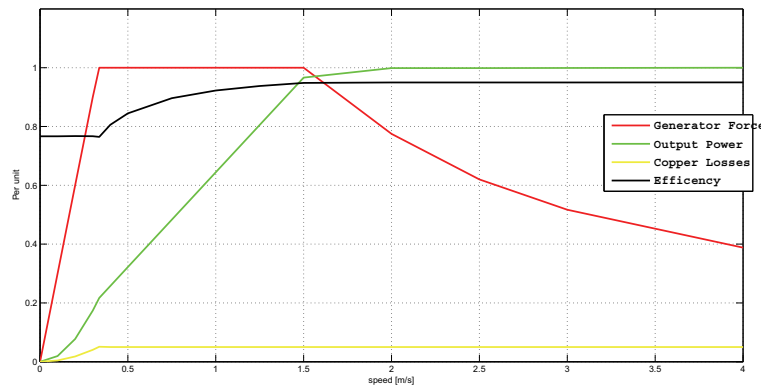
Figure 4.3: *Plot showing the Simulink PMSG-model -force, power, losses and efficiency for varying speed with $B_L = 30kNs/m$. Compared to efficiency plot by J. Sjolte in [7] the efficiency is higher for all speeds.*

One can conclude from these data that by using only the stator winding resistance to evaluate the losses gives a fair but ultimately wanting result. Throughout, the losses calculated are small compared to measurements. This can give large errors when deciding on control strategies, as especially the low-speed operation areas are of interest in this investigation. The reason for why the efficiency of the PMSG-model are not similar to the documentation provided by Fred Olsen are partly because losses such as magnetic losses and friction losses are not accounted for in this model. A more detailed analysis is needed in order to include this in the model as well.

Another factor that adds to the difference between the Simulink model efficiency and Fred Olsen measurements due to losses in the PWM and converter bridge. In the simulink model this is treated as a 1:1 ideal block, with no losses. This is a fair approach as the losses in such a topology are relatively small, but in order to get a more accurate model the converter losses as a function of speed should also be considered.

4.3.2   Approximating the Generator Losses Externally

As the generator and converter is not known in detail, it has been shown that it is hard to make an accurate model of the losses in the system. However, from the manufacturer of the generator and converter module, the efficiency at a number of operation points have been supplied to Fred Olsen. This has been used by Jonas Sjolte in order to develop an polynomial expression for the module losses as a function of generator torque and speed.

$$P_{loss} = a_1 M^4 + a_2 M^2 + a_3 |N| + a_4 N^2 + a_5 |N||M| + a_6 |N|M^2 \qquad (4.1)$$

It is this function that was used to develop figure 4.4. The coefficients a_1 to a_6 are known through Fred Olsen, but will not be given in this thesis for confidentiality reasons. By
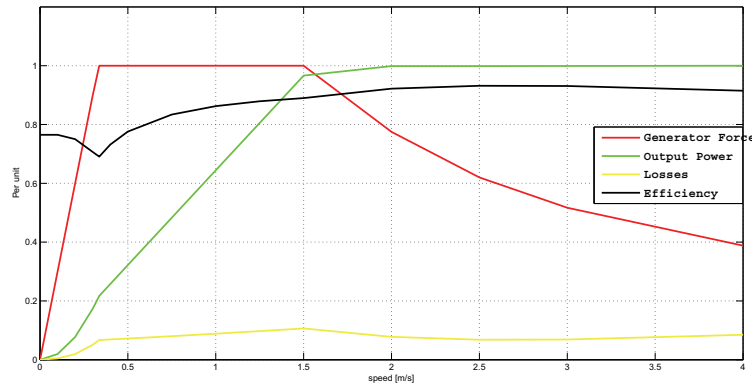
Figure 4.4: *Plot showing the Simulink PMSG-model -force, power, losses and efficiency for varying speed with $B_L = 30kNs/m$. The losses are calculated by equation (4.1), and results therefore agree with the efficiency plot by Sjolte in [7] has a max efficiency of approximately 93 % at 2.5 m/s.*

using equation (4.1) to determine the instantaneous losses, the efficiency of the whole system is accurately defined for operation below rated speed. For over-speed operation it is considered that using the maximum value for the electromagnetic torque gives a fair approximation of the generator efficiency. When applying this approach to determine the losses, the losses due to the winding resistance R_S in the Simulink PMSG-model needs to be neglected. The methodology can be summed up by the following points

- D- and q-axis voltage and generator speed is input into PMSG model as described by equations 3.2 and 3.3.

- When calculating the current in the model using the PMSG equations 3.2 and 3.3 the R_S terms are left out. This means that the PMSG currents are equal to reference currents, and the electrical output P_{el} power is the same as the mechanical input power.

- The losses P_{loss} are calculated according to equation (4.1) where the moment is calculated from equation 3.6.

- A updated electrical output power P'_{el} is calculated by deducting P_{loss} from P_{el}

In similar manner as in figure 4.3 the force, power and losses of the generator is now plotted as a function of speed. The result is seen in figure 4.4.
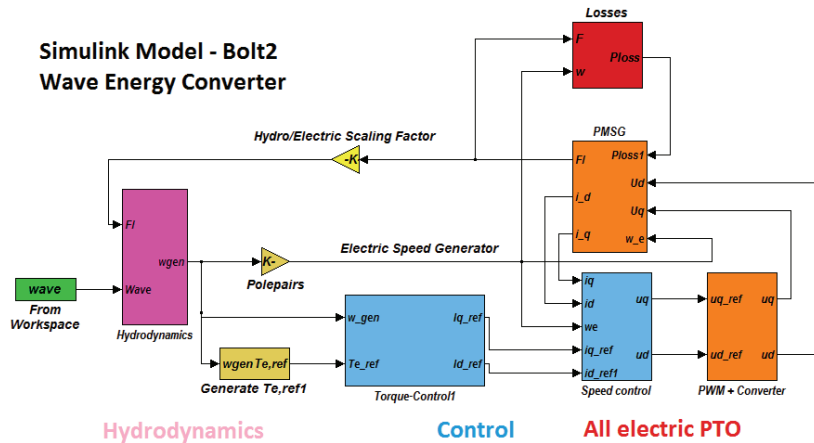
Figure 4.5: *Simulink system showing the Bolt hydrodynamics, Bolt2 all-electric PTO, control loops and loss approximation model.*

4.4 Model verification - Identifying Main Characteristics of Bolt2 Operation under Passive Loading

The hydrodynamical- and electrical PTO model have both been separately verified to perform as expected, and a methodology for determining the instantaneous losses has been decided on. Now the hydrodynamic model, electric PTO and loss approximation model can be combined as seen in figure 4.5.

4.4.1 Simulation results for a passive loaded system

An initial test for the full wave-to-wire model is to verify that the generator efficiency is the limiting factor for a passive loaded system. According to testing experiences from Fred Olsen, the operation point which gives the most output power is under-damped with respect to mechanical power extraction optimum as seen in figure 4.6. For this purpose a series of 300 seconds long simulations with sea state parameters significant height H_s and peak period T_p are performed. For each such simulated sea state the load parameters are varied and using iterative methods the optimal parameters are identified for both mechanical extracted power and output electrical power.

Simulations results for $H_s = 0.5$ meters and $T_p = 6.5$

For a sea state peak period of 6.5 seconds the optimal load parameters according to equation (2.19) is $R_L = 180kNs/m$. As shown in section 2.4, the optimal tuning frequency for a sea state of 6.5 seconds is in fact 4.3 seconds. This gives a theoretical optimal damping of $88.7kNs/m$. It is reason to suspect however that this method will not give
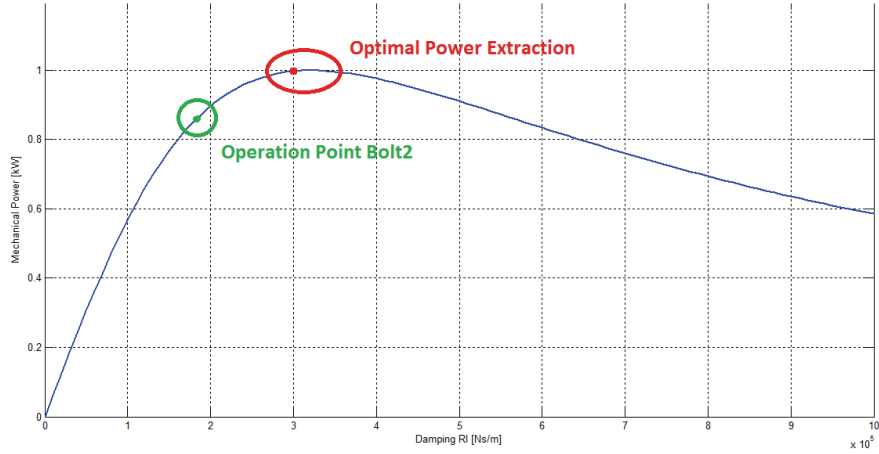
Figure 4.6: *Plot showing average extracted mechanical power as a function of the load damping R_L*

maximum power take off, as the force limitation of the generator is very different than what was used in the hydrodynamic model. Therefore, in addition to these two load parameters, an iterative method will be used in order to determine the damping which gives maximum output electrical power. In Table 4.2 the main results for this sea state can be seen.

The main points of these simulations are ass follows:

- It is shown that the damping $R_L = 240kNs/m$ which gives maximum mechanical power, is not the damping which gives maximum output electrical power. It is damping $R_L = 140kNs/m$ which gives the optimal electrical output power of 1.328 kW.

Table 4.2: *Simulation results for a passively loaded system of input $H_s = 0.5$ meters and $T_p = 6.5$ seconds for different damping parameters R_L. Optimal mechanical average power extraction is with $R_L = 90kNs/m$ and optimal electrical average power output is observed with a damping of $R_L = 77.4kNs/m$.*

Damping R_L [kNs/m]	$P_{mech}[kW]$	P_{loss} [kW]	P_{el} [kW]	Efficiency [%]
60	1.330	0.421	0.909	68.35
80	1.670	0.532	1.138	68.14
100	1.926	0.658	1.268	65.84
120	2.122	0.795	1.327	62.54
140	2.265	0.937	1.328	58.63
180	2.443	1.205	1.238	50.68
200	2.492	1.320	1.172	47.02
220	2.525	1.425	1.100	43.56
240	2.547	1.520	1.027	40.32
260	2.53	1.600	0.930	36.76

- These results indicate that the generator efficiency is limiting the optimal power extraction, which is the similar experiences observed by Fred Olsen.

- Notably, the damping which gives optimal mechanical power is not corresponding to the damping found in section 2. This is due to the minimum force constraint of the generator, meaning that in practice the control strategy is not passive loading. This means that the linear control theory cannot be directly applied.

- Also it it is interesting to note the low efficiency of the system, which does not correspond to the efficiency plot seen in Table 4.1. This has to do with the bidectional power flow, where the losses contribute to lower amplitude of electric power in the positive cycle, and larger amplitude in the the negative cycle. This gives an overall low system efficiency.

Simulations results for $H_s = 1.5$ meters and $T_p = 6.5$

For a simulation where input is a sea state of significant height $H_s = 1.5$ meters the results can be seen in Table 4.3. Again the damping-value R_L for optimal mechanical power and the damping-value for electrical output power is different, and the generator efficiency limits the optimal power extraction.

4.4.2 Evaluation of Simulation Results

The simulations show that the Simulink model performs in accordance with the experiences of Fred Olsen. In particular, the following points serve to verify the model.

- Optimal operation from an electrical output power point of view is found to be under-damped compared to optimal extraction of mechanical power.

- System efficiency is low directly compared to generator efficiency seen in Table 4.1. Especially for the sea states of low significant height the system efficiency becomes

Table 4.3: *Simulation results for a passively loaded system of input $H_s = 1.5$ meters and $T_p = 6.5$ seconds for different damping parameters R_L.*

Damping R_L [kNs/m]	P_{mech}[kW]	P_{loss} [kW]	P_{el} [kW]	Efficiency [%]
100	14.75	3.46	11.29	76.54
120	15.08	3.72	11.36	75.33
140	15.30	3.92	11.38	74.38
160	15.46	4.08	11.38	73.61
180	15.50	4.2	11.30	72.91
200	15.47	4.29	11.18	72.27

very low. This is due to the bidirectional power flow, and the high accumulated
average losses due to this.

- The electrical output power for these simulations appears to be comparable with
  Fred Olsen test measurements from similar sea states.

A key observation to be made from these simulation is the mentioned inconsistency be-
tween the optimal damping found from theory in hydrodynamic section, and the damping
which gives optimal power when also the generator limitations and efficiency into account.
This means that the equations from wave energy control theory explained in section 2 is
of limited use for Bolt2 with the current PTO-system. However, it is shown in appendix C
that when a symmetrical power take off system is used, the tuning of control parameters
according to linear control gives a very good match.

Also the observation that the damping gives optimal power extraction is not the same
that gives optimal electrical output is interesting. When that is said, it is recognized that
difference is electrical output power between these two cases is not very large. In Table
4.2 there is a 3% decrease in average extracted power, and for larger sea states it is lower
than this. This means that the generator allows the system to operate sufficiently close to
optimal operation for passive loading. By increasing the generator torque rating further
the final percentage of extracted power might be utilized, but it is probable that this is
is not worth the increased costs of high generator ratings.

4.5   Wave-to-Wire Modelling - Comparing Passive Load-ing and Reactive Control

In section 2.3 one saw that the mechanical power output when applying complex conjugate
control was increased by 50% for a sea state of significant height 0.25 meters. Simulations
in the specialization project [8] show similar results. To further investigate this potential
full wave-to-wire simulations will be performed where the limitations and efficiency of the
all-electric power take off system is also included. Due to the force limits of the system
complex conjugate control is not achievable. However, when the control is being referred
to as 'complex conjugate' it is meant that the load parameters are being tuned according
to complex conjugate control equations in the non-saturated mode of operation.

4.5.1   Simulation Results for a Passive Loaded System with an Input Sea-state of $H_s = 0.5$ and $T_p = 6.5$

The load coefficient is calculated according to equation 2.19 and the tuning frequency for
this equation is decided according to Table 2.5 to be 4.2 seconds. This gives the damping
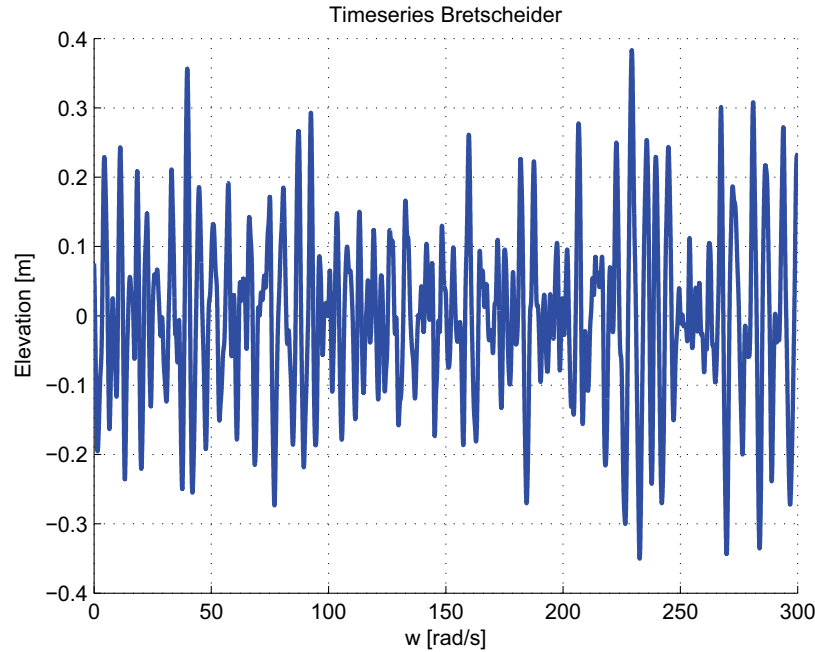
Figure 4.7: *Plot showing input wave elevation time series.* $H_s = 0.5$ *and* $T_p = 6.5$

$R_L = 90\,\text{kNs/m}$. The results seen in the previous section regarding the generator efficiency effect on optimal damping in neglected for these simulations.

In figure 4.7 the input wave elevation can be seen. In figure 4.8 the corresponding generator speed is plotted. Notably the generator speed is well below the torque saturation speed for the whole simulation time. The d-axis current, q-axis current and generator torque is shown in figure 4.9, and in accordance with the generator speed plot these plots show that torque saturation does not occur for this simulation. The constant zero d-axis current also indicate that field weakening does not occur. The mechanical extracted power, generator losses and output electrical power can be seen in figure 4.10 and 4.11.

The average extracted mechanical power for this simulation is found to be 1.75 kW, and the generator losses are 0.56 kW. This gives and average efficiency of 66.85 % and an electrical output power of 1.17 kW.
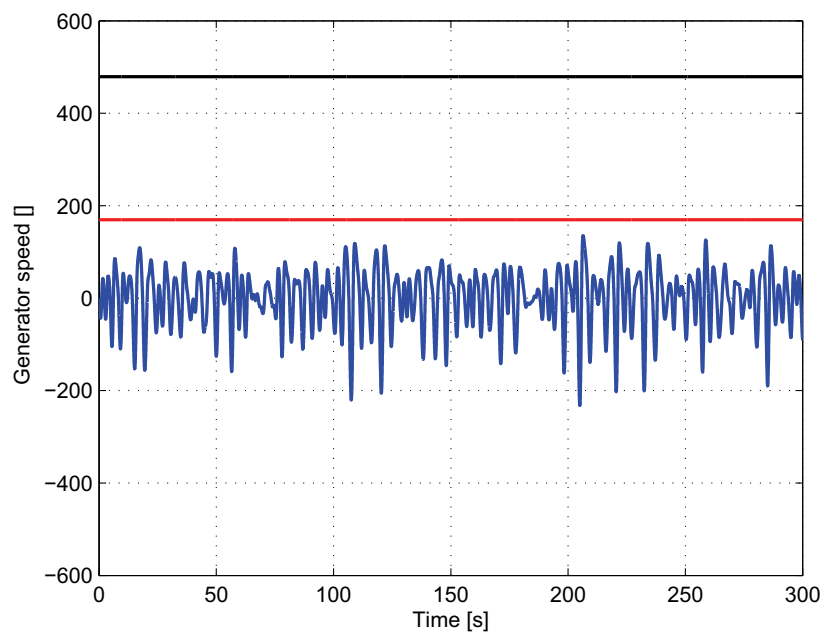
Figure 4.8: *Generator speed for an input the input wave elevation shown in figure 4.7. Red line indicates torque saturation speed, black line indicated field weakening speed. System is passively loaded.*
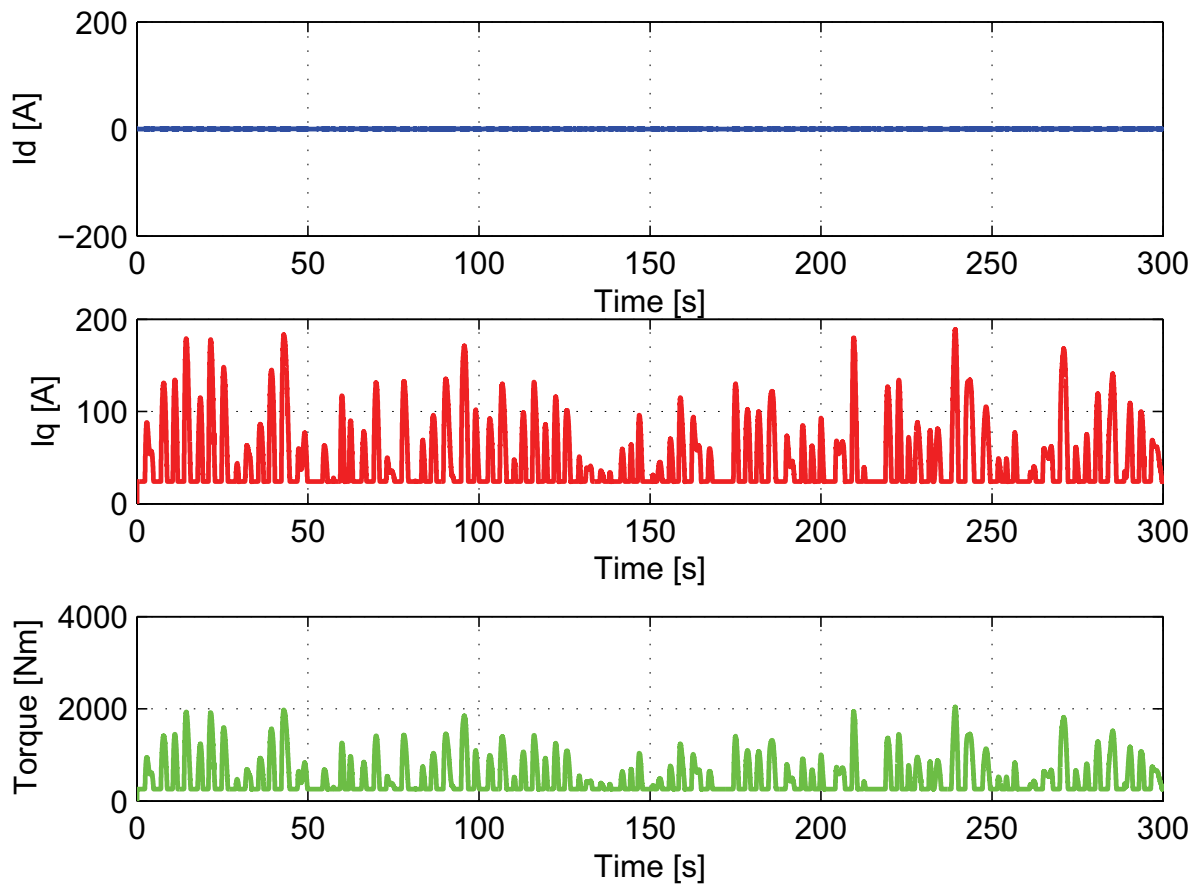
Figure 4.9: *D-axis current (top), q-axis current (middle) and generator torque (bottom). System is passively loaded.*
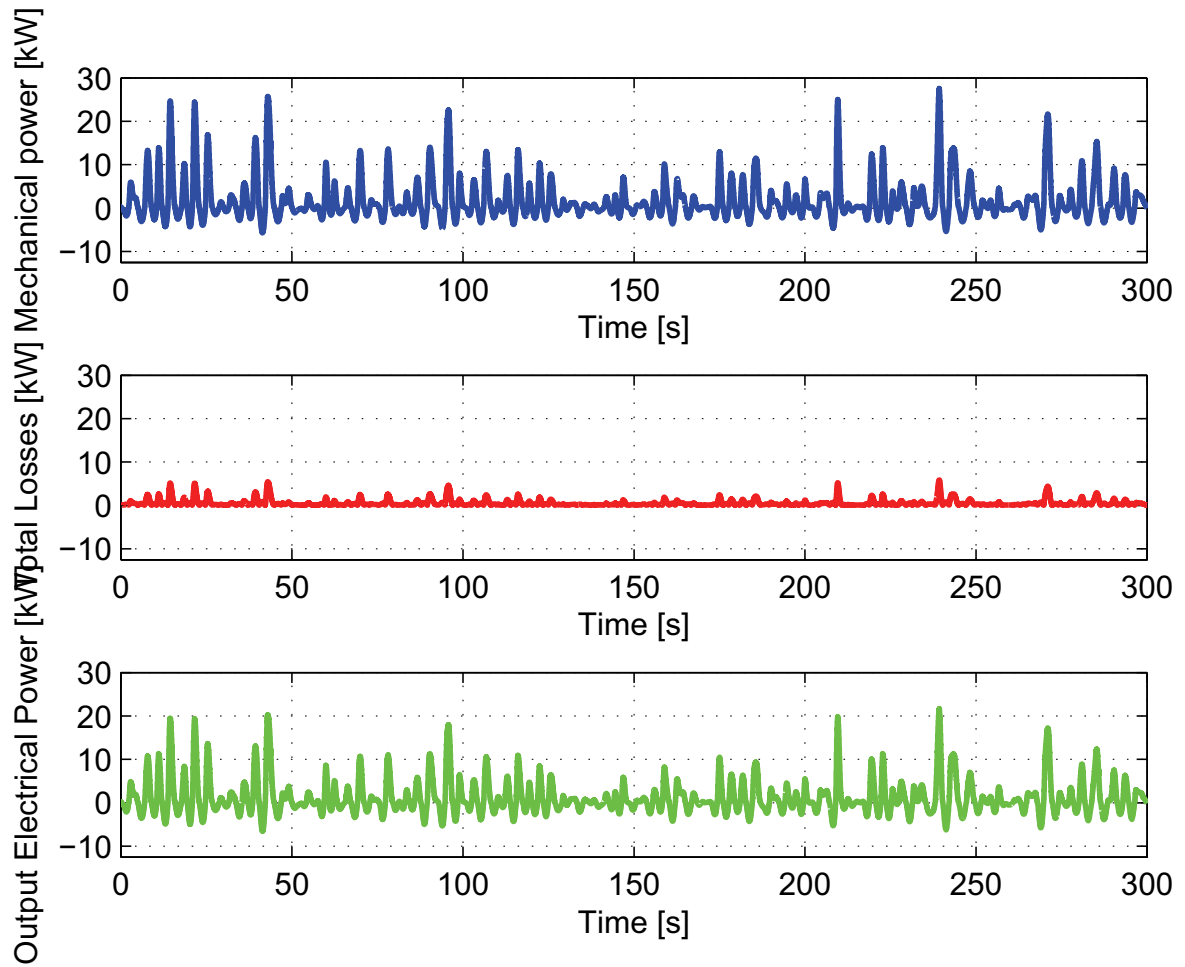
Figure 4.10: *Mechanical extracted power (top), generator losses (middle) and electrical output power (bottom). System is passively loaded.*
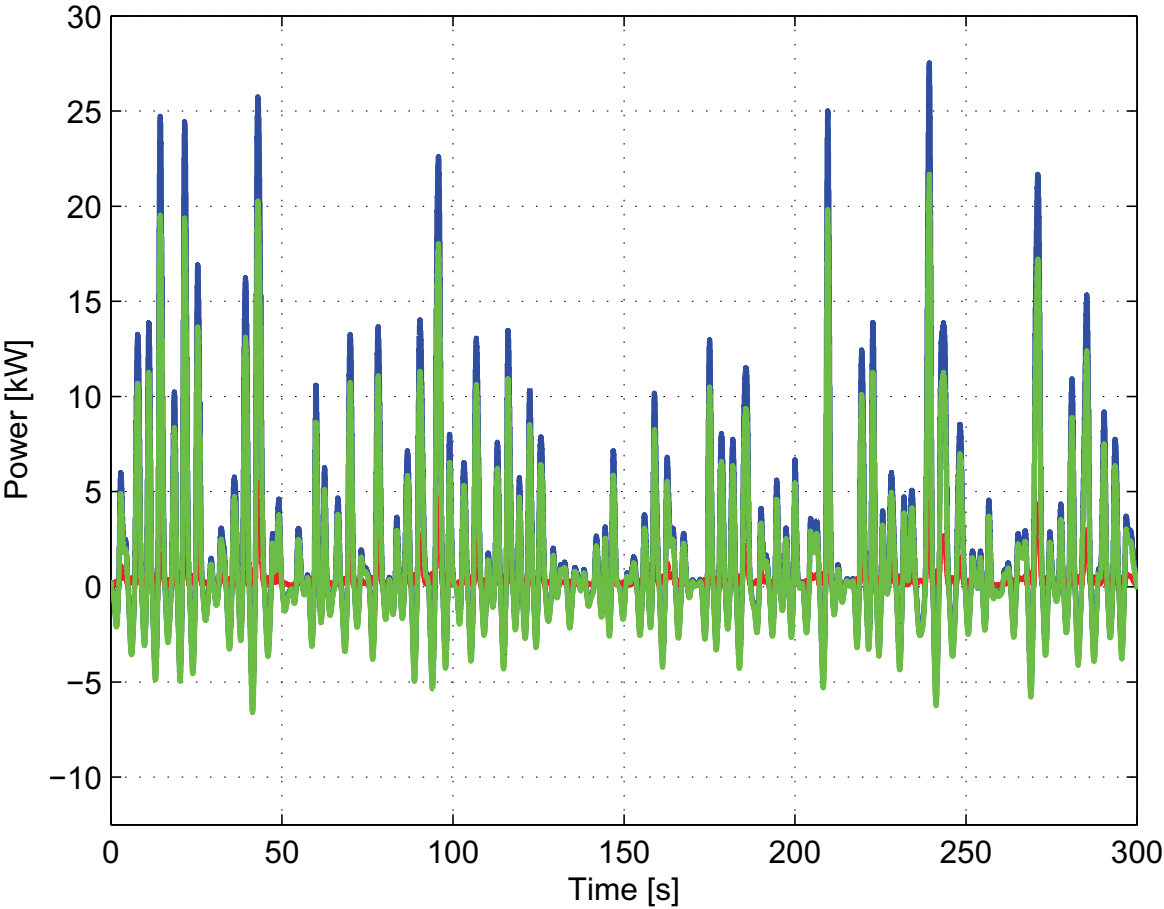
Figure 4.11: *Mechanical extracted power (blue), generator losses (red) and electrical output power (green). System is passively loaded.*

4.5.2 Simulation Results for a Reactive Controlled System with an Input Sea-state of $H_s = 0.5$ and $T_p = 6.5$

Now a wave-to-wire simulation is performed for a similar wave elevation input as seen in figure 4.7. The load parameters is tuned according to equations (2.20) and (2.21) when torque is non-saturated, and the tuning frequency is determined according to Table 2.5. This gives an damping $R_L = 22.1\ kNs/m$ and a added mass of $L_L = 84.4$ tons. The generator speed for such an controlled system can be seen in figure 4.12, and as expected the generator speed is significantly increased when compared to the reference case of passive loading as seen in figure 4.8. When generator speed increases above 190.5 RPM the q-axis current and the torque saturates, as is seen for in figure 4.13. In figure 4.14 the generator speed and torque is plotted in the same normalized figure, and figure 4.14 shows this for a smaller time-frame. In contrast to the passively loaded system, the torque is not in phase with the generator speed.
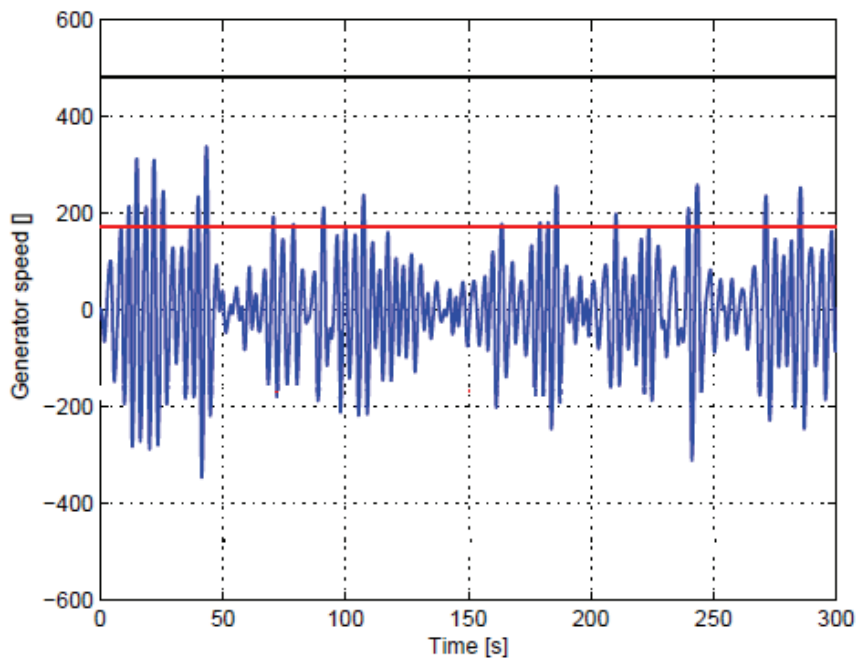
Figure 4.12: *Generator speed for an input the input wave elevation shown in figure 4.7. Red line indicates torque saturation speed, black line indicated field weakening speed. System is reactively controlled.*
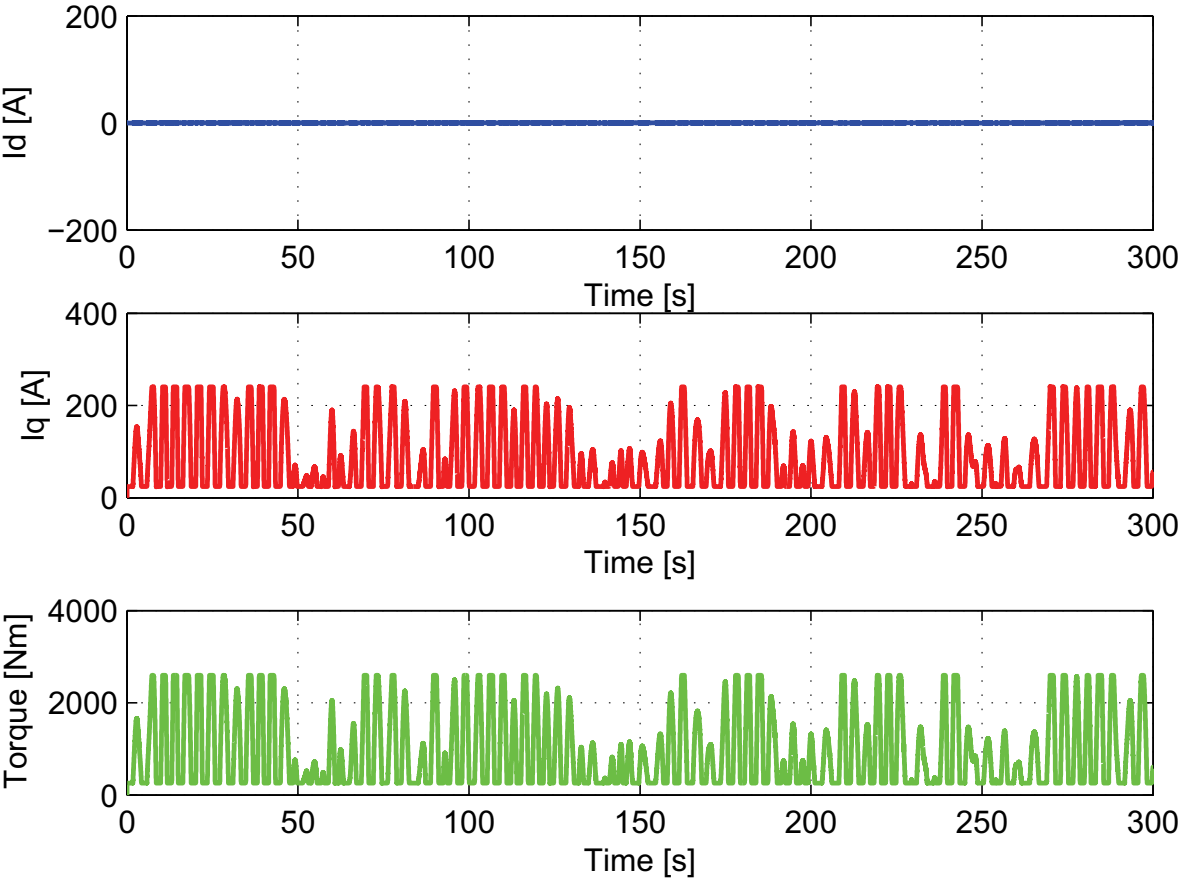
Figure 4.13: *D-axis current (top), q-axis current (middle) and generator torque (bottom). System is reactively controlled.*
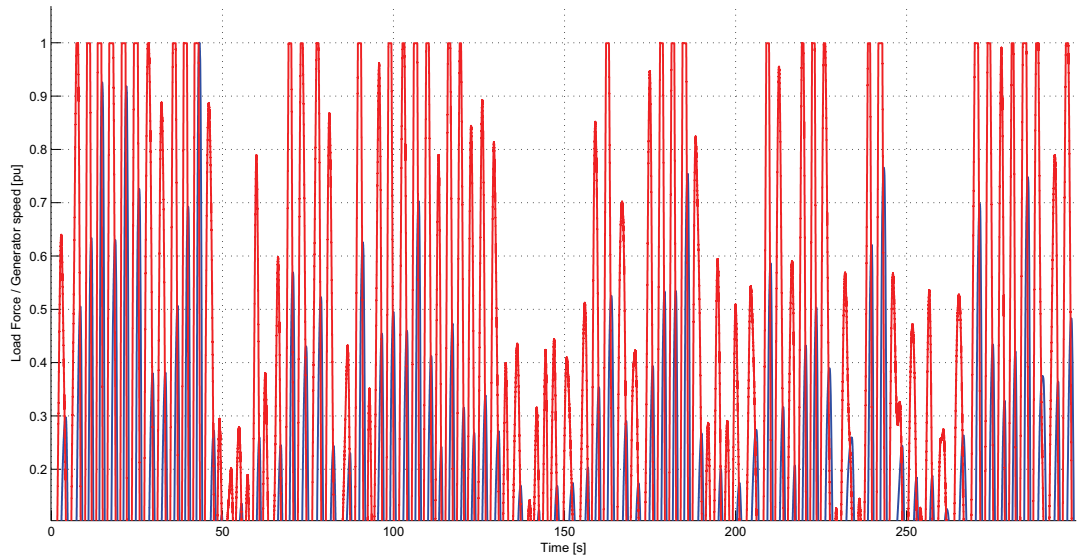
Figure 4.14: *Generator speed (blue) and generator force (red) plotted together and normalized. System is reactively controlled.*
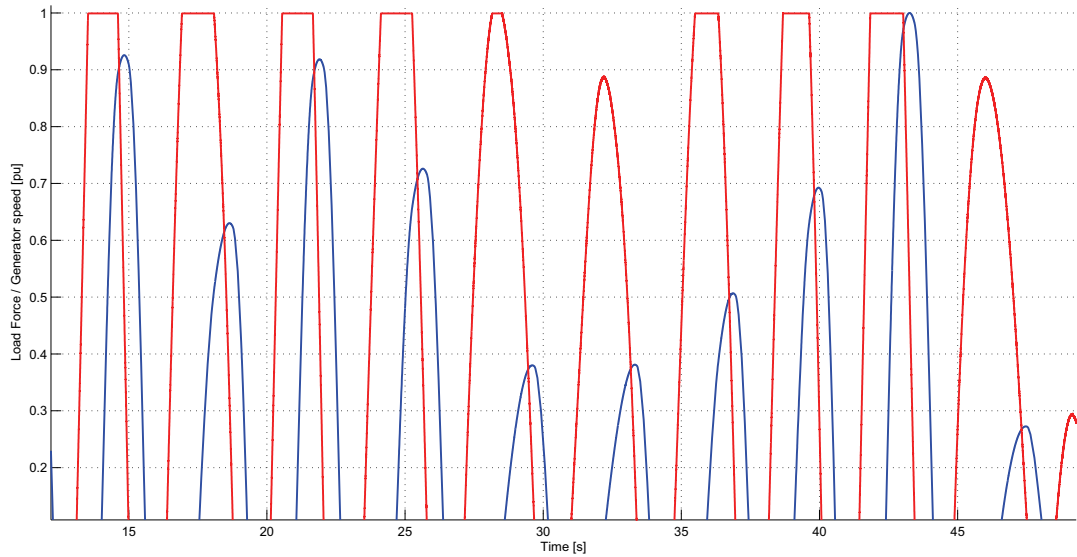
Figure 4.15: *Zoomed in plot of generator speed (blue) and generator force (red) plotted together and normalized. System is reactively controlled.*

From linear control analysis one knows that when a reactive component is added to the applied force one will observe a large negative power-flow. This can also be understood from the plot of generator speed and force as seen in figure 4.15 where there is a phase difference between these two values. When dealing with the the switching direction of the power flow, it is important to evaluate the losses in the correct way. In the Simulink model, the absolute value of the losses is calculated. The electrical output power is then found by the following equation

$$P_{el,out} = P_{mech} - |P_{loss}|$$

This means that the electrical power will have lower magnitude than the mechanical power in the positive power sequence, but larger magnitude than the mechanical power when it is negative. The time domain plots for these values are seen in figures 4.16 and 4.17. Figure 4.18 show in more detailed how these powers compare to each other between 135 and 145 seconds.

It is important to keep in mind the fact that loss does not behave bidirectional, and that the accumulated average of the losses can become even bigger than the average extracted mechanical power. The performed simulation is an example of this; the average extracted mechanical power is 2.57 kW while the average losses are 2.72 kW. This means that the average output electrical power is $-0.15 kW$, and the permanent magnet machine performs in average as a motor, supplying power from the grid to the wave energy converter.

4.5.3 Comments Regarding Passive Loading and Reactive Control

The key result from these simulations is that when taking generator losses into account, reactive control close to complex conjugate control performs very badly. In fact, average delivered power to the grid is negative, meaning an average power flows from the grid to the WEC.

In order to understand why such conditions occur, one has to recognize a few key characteristics about complex conjugate control. In order to achieve complex conjugate control, the machinery which supplies the load force not only receives energy but also have to return some energy. This we recognize by the increased bi-directional power flow. This results in high peaks of received power, and slightly lower peaks in returned power. On average, the power is therefore positive. However, as J. Falnes comments on [4] this calls for an energy conversion efficiency preferably close to unity. This is not the case for the Bolt2 generator, and the consequence is that the accumulated average power becomes significant. In general one can say that a large peak-to-average power ratio gives also
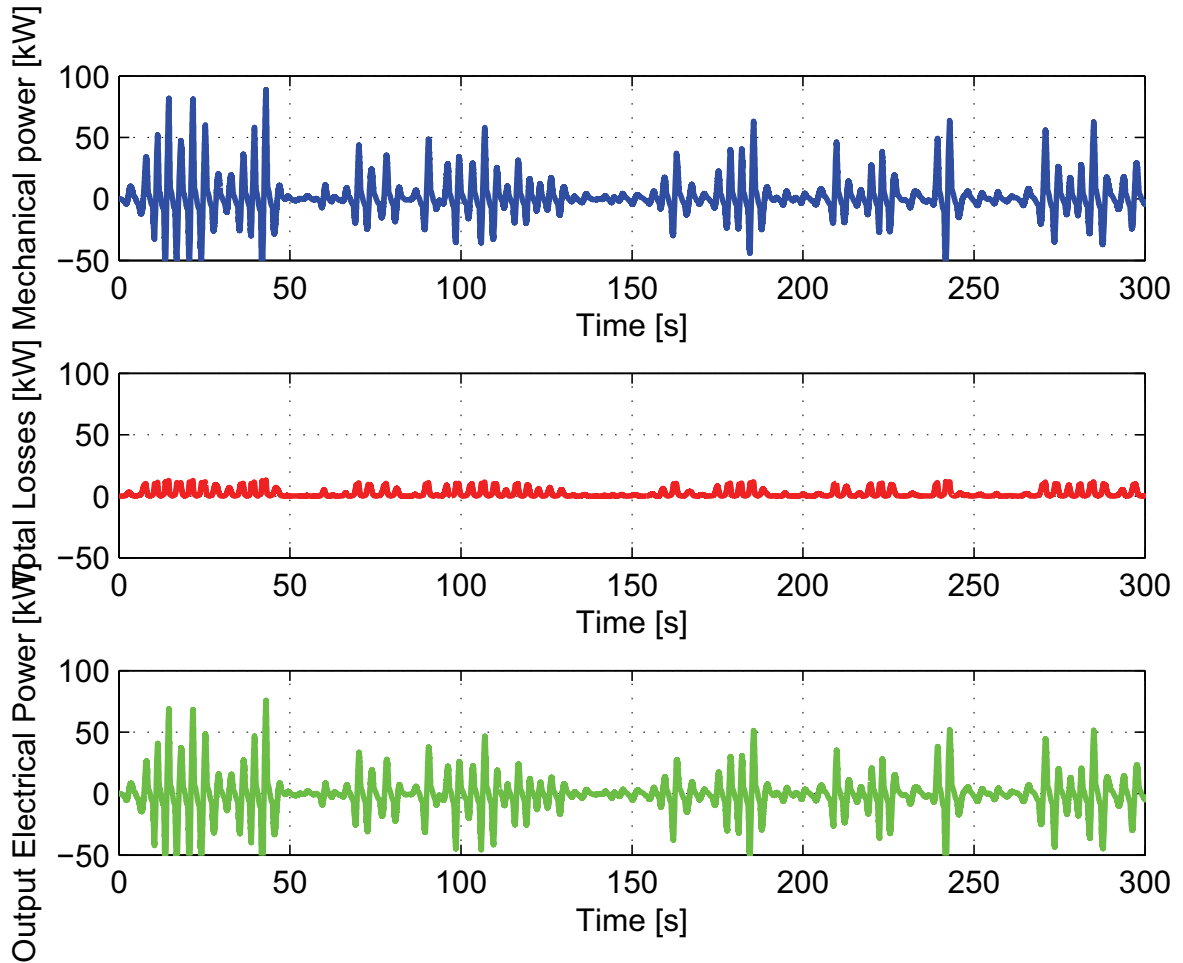
Figure 4.16: *Mechanical extracted power (top), generator losses (middle) and electrical output power (bottom). System is reactively controlled.*

a large loss-to-average ratio, and this also needs to be kept in mind when considering reactive control. This leads to the following conclusions

- Approximate complex conjugate control leads to increased mechanical power extraction.

- However, the generator efficiency becomes more important as the bi-directional power peaks both contribute to the average losses.

- As Bolt2 has an average generator efficiency of around 80 %, the losses can become very large.

- Due to this, approximate complex conjugate control does *not* give maximum electrical power output.

In the following sections an experimental approach for determining the optimal control parameters for a given sea state will be outlined.
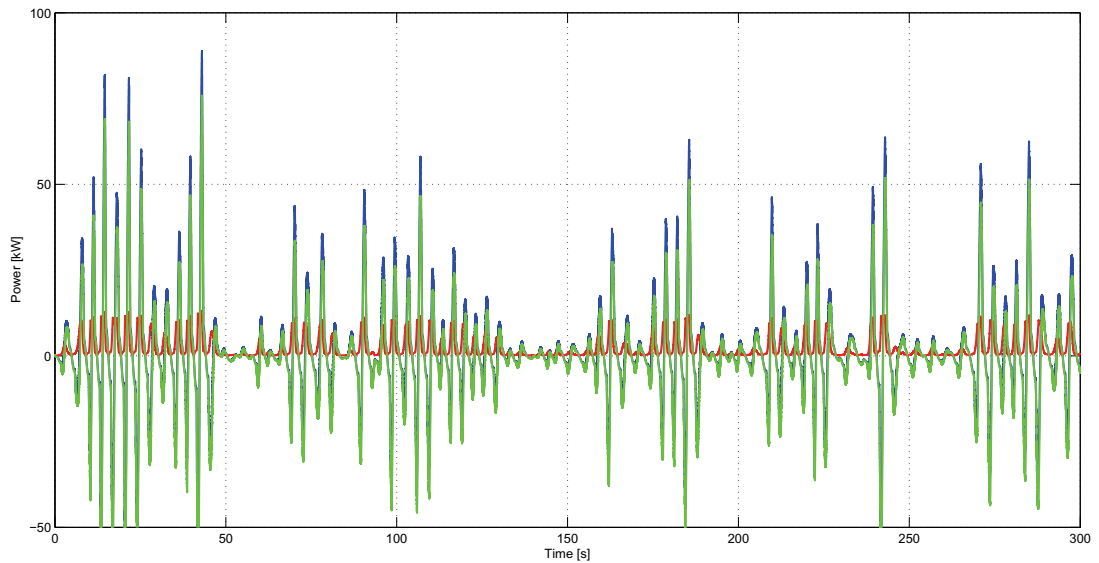
Figure 4.17: *Mechanical extracted power (blue), generator losses (red) and electrical output power (green). System is reactively controlled.*
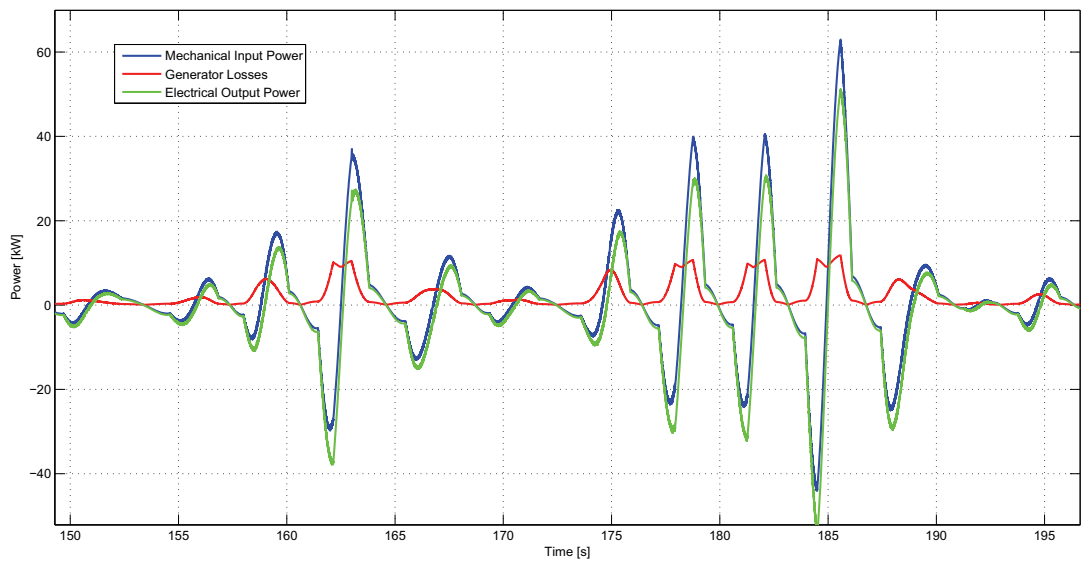
Figure 4.18: *Close-up of mechanical extracted power (blue), generator losses (red) and electrical output power (green). System is reactively controlled.*

4.6 Maximizing Electrical Output Power - Table of Optimal Operation Parameters

Optimal control of a wave energy converter is often though of as what gives maximum power extraction, or maximum energy absorbed from the sea. However, a practical def-

Table 4.4: *Proposed table of control parameters for a number of identified sea states.*

Peak Period / Significan Height							
	0,25	**0,5**	**1**	**1,5**	**2**	**2,5**	**3**	**5**
2,40	X	X	X	X	X	X	X	X
3,90	X	X	X	X	X	X	X	X
5,10	X	X	X	X	X	X	X	X
6,00	X	X	X	X	X	X	X	X
6,50	X	X	X	X	X	X	X	X
7,02	X	X	X	X	X	X	X	X
8,03	X	X	X	X	X	X	X	X
9,06	X	X	X	X	X	X	X	X
10,13	X	X	X	X	X	X	X	X
10,99	X	X	X	X	X	X	X	X

inition should be the set of control parameters which gives maximum electrical power delivered to the grid. From now on the term *Optimal Control* is used with this definition in mind. It has been shown that linear control theory is not a suitable approach to identify these optimal control parameters for irregular sea. Nevertheless, an analytical expression of the problem can be approximated from the average extracted power expression in equation (2.18) as well as the loss approximation expression in equation (4.1).

$$P_{opt,el}(R_l, L_L, \omega_{gen}) = max\left(P_M - |P_{loss}|\right) \qquad (4.2)$$

But this expression becomes non-trivial to solve as the generator losses is a 4th-order expression dependent on the control parameters as well as the generator speed. A simplified approach is therefore to run a number of simulations with different load parameters and identify optimal control for each sea state by trial and error. The goal if these simulations is to make a map of optimal control parameters for different sea states, as seen in Table 4.4

4.6.1   Example mapping of control parameters

The identification of optimal control parameters is achieved as follows:

- Added mass L_L is zet to zero, and simulations with different values of added damping R_L are performed. The interval for which R_L is chosen is between 5 to 10 kNs/m. Average extracted mechanical power, generator losses and output electric power is noted for these simulations.

- Once the damping which gives maximum average is power is decided for $L_L = 0$ the added mass is increased and the procedure is repeated for R_L

- Some intuitive search methods will of course be used in order to not evaluate all possible solutions.

- In the Tables where the results are shown only a few selected control parameters have been given a value while the rest are marked with 0. The powers for these control parameters are of course not zero, and the color of the plot indicate how the average power for those sea states compare to each other.

- Further simulations should be performed in order to thoroughly verify the results.

In the following paragraphs the results for a selected sea-states will be outlined. The results from these simulations are organized in tables where power in kW is expressed. These tables can also be considered a 'map', or a 3D plot in which the z-axis is the average extracted power. This is highlighted by colouring where green represents desirable and red represents undesirable.

Significant hight $H_s = 0.5$ and period $T_p = 6.5$

In Table 4.5 the average mechanical output power is shown for different control parameters. Notably the leftmost column represents when the system is passive loaded, or purely damped. Approximate complex conjugate control is typically represented to the 'upper right' in the map where there is a larger fraction of added mass, though as it will be shown complex conjugate control is outside the area of interest for these simulations.

The losses are seen in Table 4.6. Notably it is observed that maximum generator losses occur when the system is complex conjugately controlled. This is due to the accumulated

Table 4.5: *Table showing average mechanical extracted power [kW].*

Mechanical Power, Hs =0.5, Tp = 6.5 [kW]								
RL/LL	0	1,00E+04	2,00E+04	3,00E+04	4,00E+04	5,00E+04	6,00E+04	7,00E+04
2,00E+04								
3,50E+04								
4,00E+04								
4,50E+04								
5,00E+04								
5,90E+04								
7,00E+04					2,44			
7,74E+04								
8,00E+04								
9,00E+05	1,99							
1,00E+05	2,11			2,56				
1,10E+05								
1,20E+05	2,3			2,69	2,83			
1,40E+05	2,44				2,88			
1,80E+05								

Table 4.6: *Table showing average losses [kW].*

Generator Losses, Hs =0.5, Tp = 6.5 [kW]								
RL/LL	0	1,00E+04	2,00E+04	3,00E+04	4,00E+04	5,00E+04	6,00E+04	7,00E+04
2,00E+04								
3,50E+04								
4,00E+04								
4,50E+04								
5,00E+04								
5,90E+04								
7,00E+04					1			
7,74E+04								
8,00E+04								
9,00E+05	0,643							
1,00E+05	0,713			0,968				
1,10E+05								
1,20E+00	0,853			1,08	1,21			
1,40E+05	0,992				1,31			
1,80E+05								

average losses of the high bidirectional peaks in power. The losses are lowest for the upper left corner of the table, where the control parameters goes towards zero. This is natural for this corresponds to a no-load operation of the generator, and the losses are purely rotational losses and no stator copper losses.

Combining the two tables, the corresponding electric output table can be seen in Table 4.7. As is seen from this plot an optimal set of control parameters is identified for this sea state with a added damping $R_L = 120kNs/m$ and added mass of $L_L = 40$ tons. Notably, the average electric output power is increased by 11.9 % compared with the optimal passive loaded.

Table 4.7: *Table showing output electric power [kW].*

Electrical Power, Hs =0.5, Tp = 6.5 [kW]								
RL/LL	0	1,00E+04	2,00E+04	3,00E+04	4,00E+04	5,00E+04	6,00E+04	7,00E+04
2,00E+04	0	0	0	0	0	0	0	0
3,50E+04	0	0	0	0	0	0	0	0
4,00E+04	0	0	0	0	0	0	0	0
4,50E+04	0	0	0	0	0	0	0	0
5,00E+04	0	0	0	0	0	0	0	0
5,90E+04	0	0	0	0	0	0	0	0
7,00E+04	0	0	0	0	1,44	0	0	0
7,74E+04	0	0	0	0	0	0	0	0
8,00E+04	0	0	0	0	0	0	0	0
9,00E+05	1,347	0	0	0	0	0	0	0
1,00E+05	1,397	0	0	1,592	0	0	0	0
1,10E+05	0	0	0	0	0	0	0	0
1,20E+00	1,447	0	0	1,61	1,62	0	0	0
1,40E+05	1,448	0	0	0	1,57	0	0	0
1,80E+05	0	0	0	0	0	0	0	0

Significant hight $H_s = 1.75$ and period $T_p = 5.5$

The maps of average extracted mechanical power, generator losses and electrical output average power is seen in Tables 4.8 - 4.10. Notably, the operation point which gives the maximum extracted power has a very low factor of added mass, and the maximum mechanical power is reached close to the passive loading region of the map. This is however in accordance with the observations made in the specialization project [8] [5] that states the effect of reactive control becomes smaller when the significant height of the sea states increase. This is also observed in the power extraction, with an optimal average electric power extraction for this sea state is 19.29 kW. Compared to optimal electric power extraction for passive loading (19.03 kW) this is a 1.4 % increase, which is a significant reduction from the 11.9 % gain observed for the sea state of significant height of 0.5 meters.

Table 4.8: *Table showing average mechanical extracted power [kW]. $H_s = 1.5$ and $T_p = 7$*

Mechanical Power, Hs =1.75, Tp = 5.5 [kW]								
RL/LL	0	1,00E+04	2,00E+04	3,00E+04	4,00E+04	5,00E+04	6,00E+04	7,00E+04
2,00E+04								
3,50E+04								
4,00E+04								
4,50E+04								
5,00E+04								
5,90E+04								
7,00E+04								
7,74E+04								
8,00E+04	23,4							
9,00E+05	23,64							
1,00E+05	23,81	24,13	23,85					
1,10E+05	23,91	24,21	24,04	23,42				
1,20E+05								
1,40E+05								
1,80E+05								

Table 4.9: *Table showing average generator losses [kW]. $H_s = 1.5$ and $T_p = 7$*

Generator Losses, Hs =1.75, Tp = 5.5 [kW]								
RL/LL	0	1,00E+04	2,00E+04	3,00E+04	4,00E+04	5,00E+04	6,00E+04	7,00E+04
2,00E+04								
3,50E+04								
4,00E+04								
4,50E+04								
5,00E+04								
5,90E+04								
7,00E+04								
7,74E+04								
8,00E+04	4,49							
9,00E+05	4,65							
1,00E+05	4,77	4,84	4,94					
1,10E+05	4,88	4,92	5	5,13				
1,20E+00								
1,40E+05								
1,80E+05								

Table 4.10: *Table showing average electric output power [kW]. $H_s = 1.5$ and $T_p = 7$*

Electrical Power, Hs =1.75, Tp = 5.5 [kW]								
RL/LL	0	1,00E+04	2,00E+04	3,00E+04	4,00E+04	5,00E+04	6,00E+04	7,00E+04
2,00E+04	0	0	0	0	0	0	0	0
3,50E+04	0	0	0	0	0	0	0	0
4,00E+04	0	0	0	0	0	0	0	0
4,50E+04	0	0	0	0	0	0	0	0
5,00E+04	0	0	0	0	0	0	0	0
5,90E+04	0	0	0	0	0	0	0	0
7,00E+04	0	0	0	0	0	0	0	0
7,74E+04	0	0	0	0	0	0	0	0
8,00E+04	18,91	0	0	0	0	0	0	0
9,00E+05	18,99	0	0	0	0	0	0	0
1,00E+05	19,04	19,29	18,91	0	0	0	0	0
1,10E+05	19,03	19,29	19,04	18,29	0	0	0	0
1,20E+00	0	0	0	0	0	0	0	0
1,40E+05	0	0	0	0	0	0	0	0
1,80E+05	0	0	0	0	0	0	0	0

4.6.2   Wave-to-wire modelling for new optimal control parameters

It is now interesting to investigate how the device operates under the new optimal control parameters. Special focus will be on investigating how the generator torque is controlled.

Significant hight $H_s = 0.5$ and period $T_p = 6.5$

The input wave into the simulation is shown in figure 4.19. The corresponding generator speed is shown in figure 4.20. Notably, the generator operates in torque saturation mode for only two of the waves. The speed of the generator is significantly reduced compared to the simulations shown for the similar sea state and a approximately complex conjugately controlled system. In this sense it is more similar to the generator speed plot of the passive loaded system shown in figure 4.8.

The plots of mechanical power, generator losses and output electrical power in figure 4.22 show that the bidirectional power flow that is characteristic for a load force with a
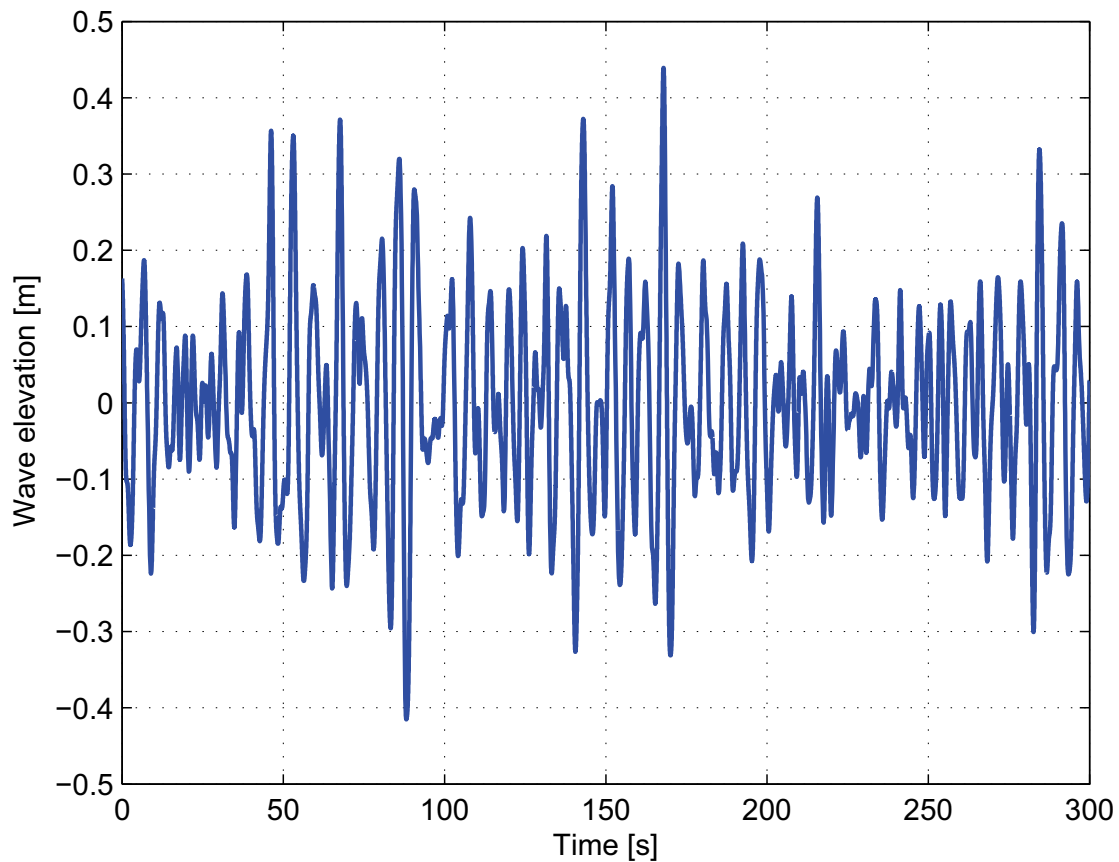
Figure 4.19: *Input wave elevation time series for of $H_s = 0.5$. System is optimized for optimal electrical power extraction.*
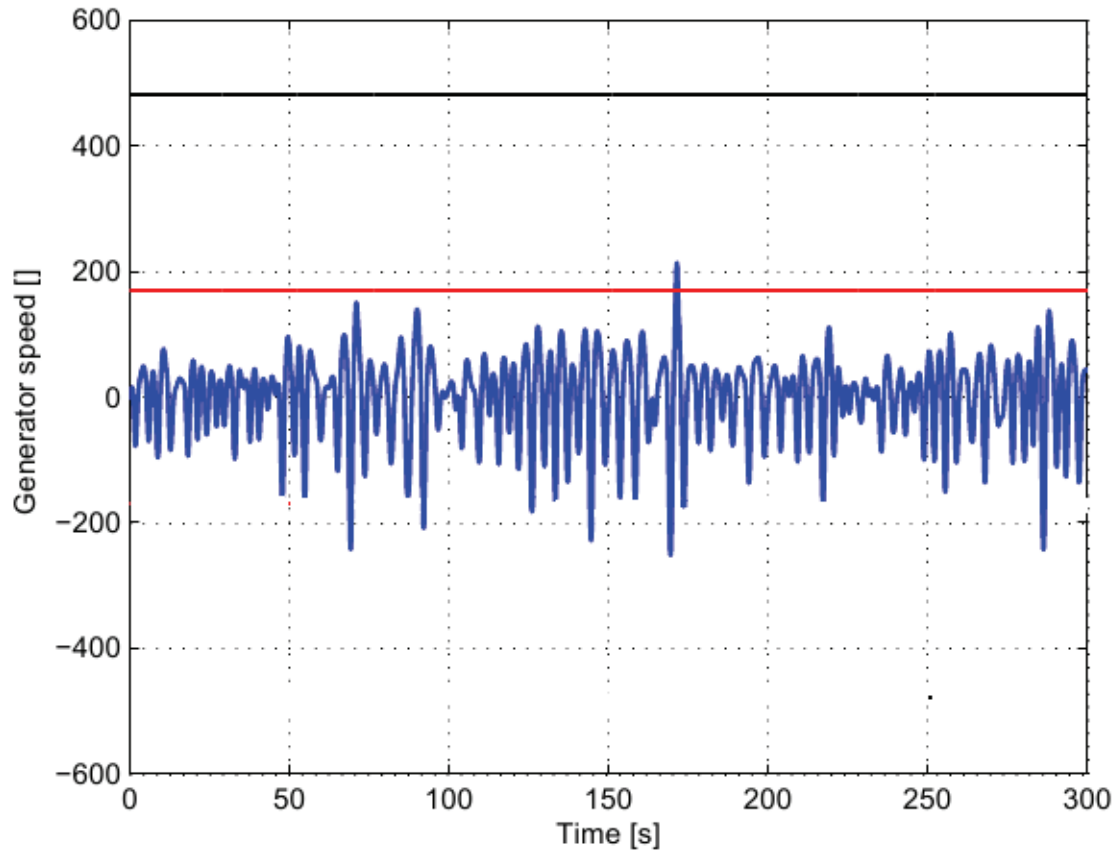
Figure 4.20: *Generator speed for input wave seen in figure 4.19. System is optimized for optimal electrical power extraction.*

reactive component, but the positive power-flow is much more dominant than the negative part of the oscillating cycle. One can also see that the electric output power is positive. Calculations show that for this particular simulation the average electrical output power is 1.62 kW.

Figure 4.23 show the speed and the generator torque have a significantly smaller phase difference than for the approximately complex conjugate control. There seems to be a difference of 0.5 seconds on average for this simulation, compared to a 0.75 seconds difference on average for approximate complex conjugate control. Figure 4.24 show the plot of normalized generator speed and excitation force plotted together. For a approximate complex conjugately controlled system these should be in phase, and there should therefore be a phase-offset between them for this simulation. But as the phase offset between these measurements seem to be to a large degree random, this measurement of optimality loose some of its value for irregular seas.
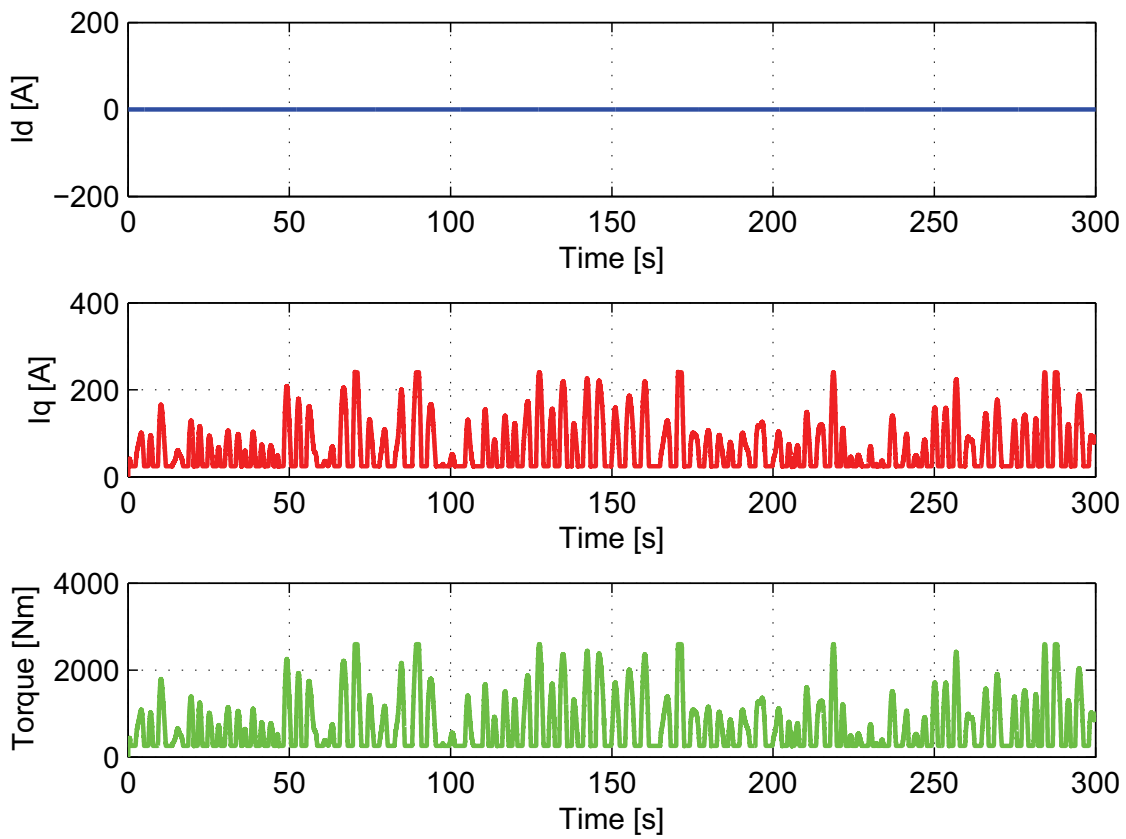
Figure 4.21: *D- and q-axis current and generator torque. System is optimized for optimal electrical power extraction.*
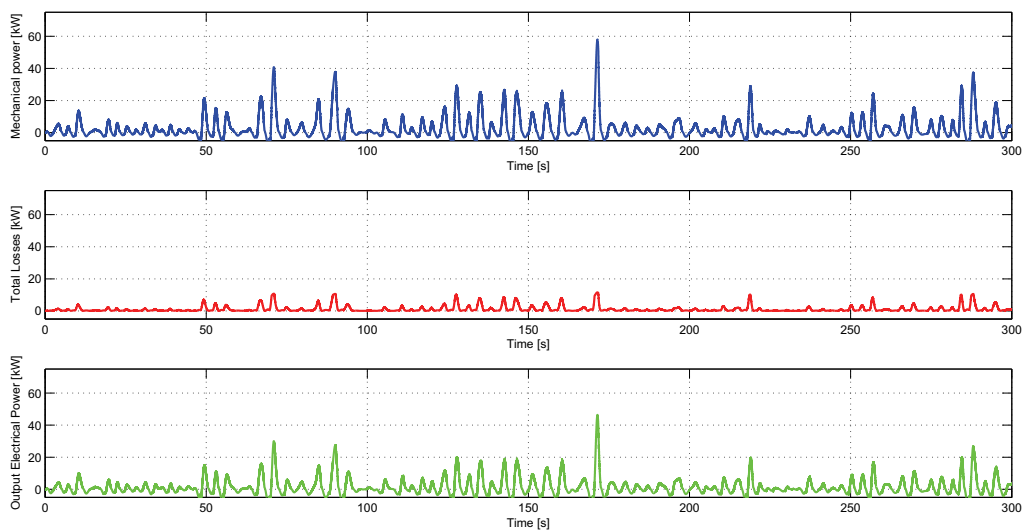
Figure 4.22: *Mechanical extracted power, generator losses and electrical output power. System is optimized for optimal electrical power extraction.*
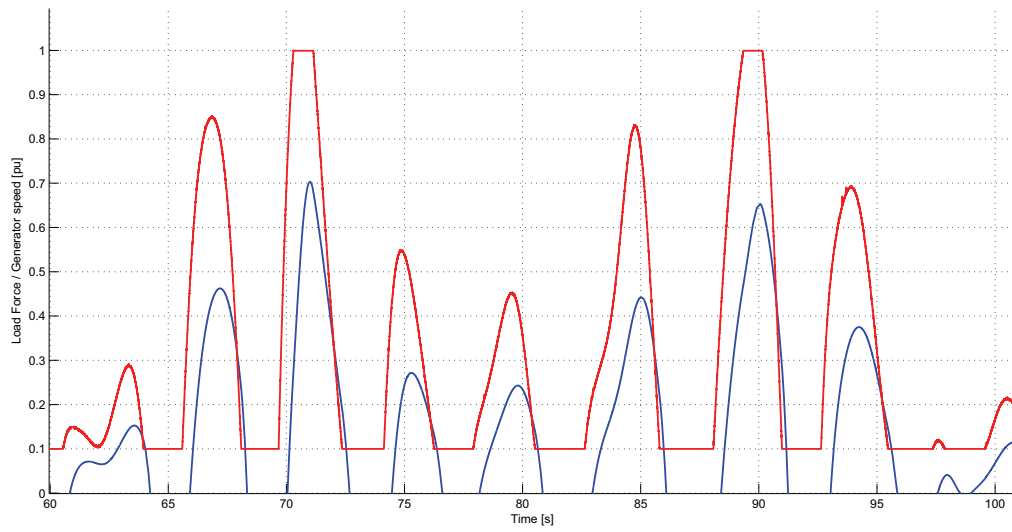
Figure 4.23: *Detailed plot of generator speed and torque. System is optimized for optimal electrical power extraction.*
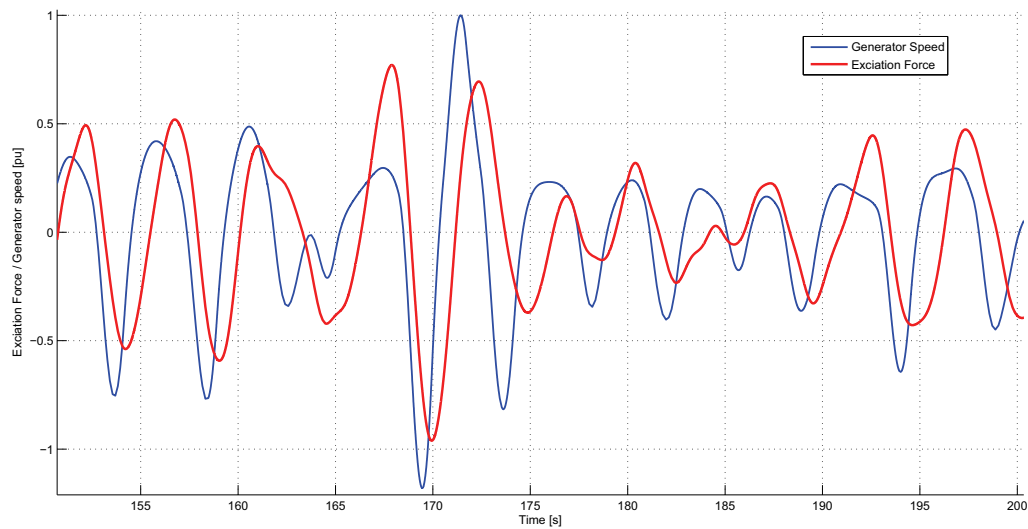
Figure 4.24: *Detailed plot of generator speed and exciation force. System is optimized for optimal electrical power extraction.*

4.6.3   Discussions regarding mapping of optimal control parameters

From the main simulations and results for the selected sea states, some general observations can be made about the mapping of optimal control parameters.

- Combining the maps of output mechanical power and generator losses, a map of optimal control parameters with respect to electrical output power is made.

- For sea states with low significant height the optimal control parameters have have a larger component of added mass and smaller component of added damping.

- For the sea states with low significant height, the average power is increased by a significant factor. (10 % for $H_s = 0.5$

- When the significant height increases, the optimal control parameters shift towards a larger factor of added damping.

- For the sea state with higher significant height, the increase in average power compared with the reference case of passive loading goes towards zero.

- For a sea state with lower peak periods, the optimal control parameters have a larger factor of added damping.

- For increasing peak periods, the optimal control parameters have larger fraction of added damping. This means the optimal control moves towards complex conjugate control.

- Average power extraction decreases with increasing peak period of the sea.

Summarized, a method to identify optimal control parameters for a given sea state has been demonstrated and general tendencies for these optimal control parameters has been commented on. This method of identifying optimal control parameters of the WEC can now be used in order to determine the maximum annual energy extraction of Bolt2 by comparing its performance with traditional passive loading.

4.7 Energy Calculations - Potential Increase in Annual Energy Production with Optimal Control

By using sea-state statistics, estimations of annual energy production can be made. Previous estimations have been made for the Bolt2 concept [25], and some preliminary investigation has also been performed into potential increase in annual energy production using reactive control [6]. However the latter paper does not take into account the generator force limitation or generator losses, and as it has been shown in section 4.5 these factors become very significant under reactive control in particular. This means that an investigation into increased energy production using reactive control with generator limitations is a very interesting and novel addition to the former research .

Identifying the optimal control parameters for all sea-states defined in Table 4.4 has not been performed, so only selected sea-states will used as a representation the whole spectra. From the wave scatter diagram i Table 4.11 one can define the following three sea states:

- $H_s = 0.75$ and $T_p = 4.5$ is the sea states which represents the low energy sea states.

- $H_s = 1.75$ and $T_p = 5.5$ represents the medium energy sea states.

- $H_s = 3.25$ and $T_p = 6.5$ represents the high energy sea states.

Defining the different sea states in Table 4.11 as one of these three and summing the total annual hours, one gets the results seen in Table 4.12.

Using the similar approach as seen in the previous section, Table 4.13 show the average power extraction for each of the three defined sea states for both optimal passive loading,

Table 4.11: *Wave scatter diagram for Wavehub location taken with permissions from [25]. Blue area represents low-energy sea-states, green represents medium energy sea-states, and ref represent high energy sea-states.*

Significant wave height hs [m]	Wave period Tz [sec]								
	3,5	4,5	5,5	6,5	7,5	8,5	9,5	10,5	11,5
0,25	20	79	44	18	0	0	0	0	0
0,75	499	832	491	140	18	0	0	0	0
1,25	184	1031	004	307	70	26	9	0	0
1,75	0	587	701	333	149	53	26	0	9
2,25	0	96	534	254	123	44	9	0	0
2,75	0	0	237	228	105	26	9	9	0
3,25	0	0	26	175	123	44	9	0	0
3,75	0	0	0	79	96	35	18	0	0
4,25	0	0	0	9	44	26	9	9	0
4,75	0	0	0	0	26	18	9	0	0
5,25	0	0	0	0	18	26	18	0	0
5,75	0	0	0	0	0	18	9	0	0
6,25	0	0	0	0	0	9	0	0	0

Table 4.12: *Annual hours of 3 types of sea states.*

	Low energy	Medium Energy	High Energy
Hours	2182	4371	2468

and optimal control parameters from an electrical output perspective. The results show that an annual energy production increase of 1 % is a fair estimation for Bolt2 if optimal reactive control is implemented.

Table 4.13: *Power calculations for the representing sea states*

	Low energy	Medium Energy	High Energy
Average Power Passive Loading [kW]	6.70	19.04	31.40
Average Power Optimal Control [kW]	7.02	19.24	31.47
Percentage increase [%]	4.78	1.4	0.22

Table 4.14: *Annual Energy calculations for the representing sea states*

	Low energy	Medium Energy	High Energy	Total
Energy Passive Loading [MWh]	14.62	83.22	77.53	175.37
Energy Optimal Control [MWh]	15.32	84.10	77.70	177.12
Percentage increase [%]	4.78	1.40	0.22	1.0

4.8   Evaluation of Reactive Control and Sensitivity Analysis of PTO Force Constraints

The 1% increase in annual energy production when applying optimal control as opposed to passive loading is a quite modest result compared to the 18% increase other estimations have resulted in [6]. The main reason for this is of course the force constraint of the system, which is limiting in two important ways.

- The maximum force constraint of 100 kN limits the use of control parameters near complex conjugate control, as these will even for small sea states require a applied force larger than this limit.

- The minimum force constraint of 10 kN disables the use of reactive control for half of the oscillation cycle, as this would require a negative applied force.

Especially the second point is important when explaining the low effect of optimal control. As explained by Falnes [4], reactive control is in fact controlling both amplitude and phase of the WEC motion. The amplitude of the WEC is controlled by the damping, while the phase is controlled by the added mass. Due to the restriction on negative force, one loses control control of the amplitude and phase of the WEC for half the cycle and this greatly diminished the effect of the control technique. The limitations of the PTO-systems enforces Bolt2 to be purely passive damped for over half of the time, and this means that the difference between passive and optimal control becomes minimal.

As it has been defined in this thesis, the Bolt2 concept has shown little potential for reactive control, but slightly different PTO-solutions might yield very different results. Next, a few of the limitations of the PTO and generator will be varied and results of wave-to-wire simulations for the different systems will be discussed.

4.8.1 Allowing Negative Applied Force

The minimum force of 10 kN is a system requirement in order to keep the tension in the rope. However, for the purpose of investigating the power take-off capabilities, a system with a stiff rope is considered. Such a system would not need a minimum force in order to keep tension, and could therefore implement reactive control for the whole oscillation cycle. In appendix C it is shown in detail how such an system behaves, and also a detailed optimization of control parameters is performed with corresponding annual energy production estimations. The key results can be summed up as follows:

- Control parameters that give maximum mechanical power extraction become much closer to complex conjugate control compared to simulations shown in section 4.6.

- For sea states with low significant height, a very significant increase in electrical output power is experienced with optimal control. An example sea state of $H_s = 0.5$ meters and $T_p = 6.5$ seconds show a gain of 32.2 %.

- Energy calculations shown that an annual 10 % increase of energy production can be achieved by applying optimal control compared to a case of passive loading.

These results prove that a full oscillatory amplitude and phase control is important in power extraction terms, and that such a system could provide a significant improvement in annual energy production.

4.8.2 Increasing the Generator Maximum Force Limitation

A rule of thumb for offshore energy extraction is to increase the PTO ratings as large as possible. A larger generator would allow a higher maximum force, and it is interesting to

evaluate how much of an increase in extracted power and annual generated energy one
would get by increasing this maximum force by a certain percentage. In Tables 4.15 and
4.16 the average power and annual energy calculations are performed in a similar manner
as in section 4.7, both for the reference case of a maximum force of 100 kN as well as an
maximum force of 120 kN.

Table 4.15: *Power calculations for increased maximum force*

	Low energy	Medium Energy	High Energy
Ref. Av. Power, $F_{L,max} = 100$ kN [kW]	6.71	19.04	31.40
Av. Power, $F_{L,max} = 120$ kN [kW]	6.76	20.27	33.24
Percentage increase [%]	0.72	6.45	5.85

Table 4.16: *Annual Energy calculations for increased maximum force*

	Low energy	Med. Energy	High Energy	Tot.
Ref. An. Energy [MWh], $F_{L,min} = 10$ kN	14.62	83.22	77.53	175.37
An. Energy [MWh], $F_{L,min} = 10$ kN	14.73	88.09	82.03	184.85
Percentage increase [%]	0.72	6.45	5.85	5.41

The main observations and results of this analysis is as follows:

- Increasing the maximum force limitation gives increased power extraction in the
  higher sea states where force-saturation is happening for most waves.

- The annual energy production is increased by approximately 5 % with a 20 %
  increase in maximum force. Such data can be used to evaluate the cost benefit of
  such an upgrade.

- Such an machine will increase the cost with about 15 000 NOK and annual energy
  productions with about 9500 kWh. This means that if the energy price pluss other
  economic intensives are closer to 2 NOK / kWh than such an upgrade in generator is
  interesting. It is of course also important to remember that if a increased generator
  rating is achieved than one could also invest in a larger buoy giving even higher
  power extraction.

- All in all, Bolt2 shows economic potential for increase in the the PTO ratings.
  But none of the limitations as for example the maximum rope force are considered.
  These factors are most probably the constraining elements at these stages in the
  concept development.

4.8.3 Decreasing the Generator Minimum Force Limitation

The minimum force limitation is important in order to maintain tension in the rope, and in the downward motion of the WEC this means that energy needs to be delivered to the device. By decreasing the minimum force, one will therefore also reduce the this 'negative' energy. Recognizing this, it is interesting to evaluate how the annual energy increase by decreasing the minimum force constraint. In the following calculations, the minimum force constraint is decreased from 10 kN to 8 kN, and an annual energy calculation is performed in a similar matter as previously shown. Also, a reference case where with the original minimum force value of 10 kN will be simulated with the same input. In Table 4.17 power calculations is performed for reference sea states. Table 4.18 shows the corresponding energy calculations.

Table 4.17: *Power calculations for reduced minimum force constraint*

	Low energy	Medium Energy	High Energy
Ref. Av. Power, $F_{L,min} = 10$ kN [kW]	6.711	19.04	31.40
Av. Power, $F_{L,min} = 8$ kN [kW]	6.874	19.474	32.38
Percentage increase [%]	2.45	2.28	3.13

Table 4.18: *Annual Energy calculations for reduced minimum force constraint*

	Low energy	Med. Energy	High Energy	Tot.
Ref. An. Energy [MWh],$F_{L,min} = 10$ kN	14.62	83.22	77.53	175.37
An. Energy [MWh], $F_{L,min} = 10$ kN	14.98	85.12	79.96	180.06
Percentage increase [%]	2.45	2.28	3.13	2.67

The results of these simulations are the following:

- In the example simulation is it is shown that by reducing the minimum force constraint 20 % from 10 kN to 8 kN, the annual energy production is increased by 2.67 %.

- The method for increasing power extraction is good for all sea states, and perhaps most useful in high energetic seas.

4.8.4 Summary

- It has been shown that by allowing for a symmetrical force to be applied gives great advantage to the power take off capability for the Bolt2 concept. This is in particular linked to the increased effect of reactive control.

- By reducing the minimum force constraint or by increasing the maximum force constraint it has been shown that the energy production can by increased. Preliminary cost analysis show that this is economically interesting, but there is reason to believe that other constraints that are not taken into account in this superficial analysis is greatly limiting for the system at the moment.

Chapter 5

Discussion

5.1 General

Most of the important results have already been discussed throughout the thesis. This section aims therefore to summarize the key findings and to discuss the implications of these results for the physical Bolt2 wave energy converter. This section also discusses the impact the work presented in this thesis has on the ongoing research in wave energy. Focus is on how the results in this thesis can be further verified and proposals for coming research topics both for Bolt2 and for wave energy as a general field.

5.2 Key Results

The main motivation of this thesis was to develop a full wave-to-wire model of the Bolt2 WEC, and use this model to investigate how to control the device in order to extract maximum power. Based on this, the key results found in this thesis are as follows:

- A full wave-to-wire model of a Bolt2 point absorber with all-electric power take off system has been made in Matlab and Simulink.

- The main characteristics of the Bolt2 generator and power take off system has been modelled using classical representation of a permanent magnet synchronous generator complete with field weakening operation, and a simplified model of the inverter and DC-link.

- A control method has been demonstrated which maintains the force, voltages and currents within the different rating constraints of the power take-off system, even for the sea states with high significant height.

- Wave-to-wire simulations show that Bolt2 has limited potential for increased power extraction using reactive control due to the force limitations of the generator. Analysis show that if the device is optimally controlled, only a 1 % increase in annual energy production can be expected compared to the reference case of passive loading.

- In comparison simulations on a device which allows for a symmetric load-force shows that a 10 % increase in annual energy production is realistic. This verifies that the force constraints of the Bolt2 PTO is what diminishes the effect of reactive control.

In the introduction it was pointed out that previous research indicated that Bolt2 showed promise for implementing reactive control and increased power extraction. The research presented in this thesis on the other hand show that the electric power take-off system has limitations that dramatically reduce effect of such control techniques.

5.3 Regarding Practical Implementation in Bolt2

Several wave-to-wire simulations has been performed, including many with reactive controlled load parameters. As Bolt2 is currently deployed in the ocean for an extensive testing period, the results observed in this thesis can also experimentally verified. There is naturally some degree of uncertainty regarding how realistic this model is of the real-life Bolt2 WEC. This is especially because to the following factors:

- Hydrodynamic model is based on data from Bolt and not Bolt2.

- How the generator efficiency is treated and combined with the PMSG block.

- The validity and preciseness of the simplified PSMG model used.

- The damping coefficients used by Bolt2 in the sea are not the same found to give optimal power extraction in the model.

With this in mind, it is still interesting to also in practice investigate the effect of reactive control. Very simplified one can suggest a control strategy for a preliminary test of Bolt2's response to reactive control based on the observations done in this thesis. As a rule of thumb, the results in this investigations find that optimal control of Bolt2 occurs with an added mass of approximately 10 % of the added damping. For Bolt2, which operates with an added damping of 300 kNs/m, this means by also having an added mass of approximately 30 tons. Should this approach give a positive result, it is advisable to identify more detailed sets of optimal control parameters similar to the 'map' seen in Table 4.4.

However, to undertake such an investigation might not be desirable if the theoretical maximum annual increase in energy is only 1 %. It is therefore important to analyse the initial test in detail in order to evaluate if the limited potential described in this paper seems to be valid also in practice. Regarding this, one need to be aware of an important difference between experimental measurements and model measurements: In the sea it is not possible to recreate previous conditions, meaning that it might be difficult to identify small increases in power take-off capabilities due to the randomness of the sea. This means longer simulations need to be performed in order to get average values.

5.4 Implications for the General Wave Energy Converter

There are several of the experiences in this project that are very useful for the general point absorber, and can thus be implemented in planing and research of future wave energy devices. First and foremost this is regarding how to develop a wave-to-wire model based on hydrodynamic measurement data of the device and on electric power take-off ratings. Perhaps most interesting is that such a wave-to-wire model can be used to investigate control techniques and decide on favourable power electronic and generator ratings at an early stage in concept development. In order to do this, all one would need is hydrodynamic parameters like the *Excitation Force Coefficient,Radiation Resistance* and the mass of the device for a range of different frequencies. These can either be obtained by (small-scale) testing of a prototype or by some software analysis.

Another important lesson learned in this paper is how the tuning frequency used in linear control techniques relates to the dominant frequency of the sea state and of the excitation force. The initial assumption that the dominant frequency of the excitation force can be used for tuning the control parameters for optimal power extraction has been shown to be wrong. This paper shows a practical approach where a number of simulations are performed to iteratively identify the optimal damping parameters. Based on this a table of tuning frequencies corresponding to the peak frequencies of sea states is made. However, an analytical expression or approach to determine the optimal tuning frequency of Bolt2 or a general wave energy device is not discussed in this paper. This could therefore be considered a interesting study for further work in this field.

Lastly the experiences from wave-to-wire simulations of Bolt2 is important to keep in mind when deciding on design of the power take-off systems of potential future WEC's. This is especially regarding the limited effect of reactive control for a device such as Bolt2, which does not have the possibility for a symmetrical load force. To be aware of these limitations, and also the potential for increased power extraction for more complex PTO-

solutions is important. In this thesis it has also been shown that wave-to-wire simulations can be used to predict annual energy production for wave energy converters, and that it is a powerful tool for performing sensitivity analysis regarding what ratings to be used for the different components.

5.5   Lessons learned and future research

The main result in this thesis is that by applying reactive control to the wave-to-wire model of Bolt2, the average energy extraction can be increase by 1 % annually. Based on this there are a number of different ways in which to continue the research on wave energy in general, and on the Bolt2 wave energy concept in particular. The following points is considered to be the most interesting areas for further work and research on Bolt2 wave-to-wire model.

- Compare performance of this model with similar simulations performed by Fred Olsen simulation software and models. In particular it is interesting to compare the performance using optimal control parameters.

- Implement optimal control with respect to electrical output power as suggested in this thesis on the physical Bolt2 WEC device under real sea conditions.

- Develop a hydrodynamic model of Bolt2 based on the hydrodynamic parameters for the Bolt2 buoy and also the complete toroid device.

- Also, mapping of optimal control parameters should be performed for more sea states and more exact energy estimations performed.

The results seen in this thesis highlights several questions for wave energy in general. Further research into the following problems would be interesting for the field of wave energy:

- Developing an improved method for determining optimal tuning frequency when applying linear control theory. Ideally an analytical expression for this should be developed as a function of wave peak period and device hydrodynamics.

- How optimal generator ratings change when optimal reactive control is realized compared to pure passive loading. Main focus should be on cost of equipment versus increased energy production.

- Research how a device which is able to apply a symmetrical load force could be realized, and make a detailed analysis into the drawbacks and benefit for such a solution.

- Investigate the possibility for implementing predictive control, and test this on a wave-to-wire model of a WEC in order to compare the power take-off capabilities of such a control strategy with the strategies suggested in this thesis.

Chapter 6

Conclusion

The motivation for this project was to develop a wave-to-wire model of the *Bolt2Wavehub* wave energy converter in order to investigate its potential for increased power extraction by the use of reactive control. Initial investigations showed promise for the device, with some estimations as large as 17 % increase in annual energy. The Bolt2 WEC has in this thesis been modelled in the Simulink environment and consists of the hydrodynamic model of the device, the electric PTO-system and the control system.

The hydrodynamic model used in this thesis is the same one as was developed for the Bolt wave energy concept in the authors specialization project *Wave-to-Wire Time Domain Model for the Wave Energy Convert Bolt.* The power take-off system, which consist of a permanent magnet synchronous generator, an inverter-bridge and a stiff DC-link, are modelled based on the characteristics of the equipment presently installed on Bolt2. These two models are combined together by linear scaling of the applied force on the rope by the generator.

The PMSG is modelled and controlled using the well established vector control scheme, or field oriented control, which uses the dq-reference frame analysis. The implemented control strategy allows the generator to operate under over-speed conditions by weakening the magnetic field set up by the permanent magnets by setting up a negative d-axis current. The whole control consists of an inner current control loop and an outer torque control loop. Simulations show that the model is successfully limiting the values of the generator electromagnetic torque as well as the current and voltage in the switchgear within the rated values for all evaluated sea states. The generator losses are externally approximated through an polynomial function supplied by Fred Olsen.

Wave-to-wire simulations show that implementing reactive control with load parameters close to approximate conjugate control does not give increased electrical output power. This is because the high peak-to-average power ratio of approximate complex conjugate control gives large accumulated average losses, and in the extreme examples these losses can be larger then the average extracted mechanical power, meaning electric

power is on average extracted from the grid. An intermediate control strategy based on a smaller component of added mass is found to be the optimal control strategy from an electrical output power point of view, and the optimal control parameters for a set of representative sea states is identified.

Annual energy production estimations are performed based on a set of representative sea states. Compared to the reference case of passive loading, the optimally controlled Bolt2 shows an annual increase in energy production of 1 %. This indicates that Bolt2 has low potential for increased power extraction using reactive control, and it is recognized that this is due to the non-negative minimum force restriction of the power take-off system. These results are compared to a similar WEC which has a PTO system which allows for a negative applied load force, and energy estimations show that such a device would have a 10 % annual energy increase if optimal control was performed. Such an device requires a more advanced PTO-solution, but could the increased annual energy production might justify the additional cost.

In conclusion, the limited effect of reactive control on Bolt2 has been demonstrated through a series of wave-to-wire simulations. This analysis of the power take-off capability of the Bolt2 WEC is nonetheless valuable, especially for future development of point absorber wave energy devices. In addition to demonstrating the development of a wave-to-wire model of a WEC, perhaps the most important contribution of this thesis is highlighting some of the major advantages, characteristics and drawbacks of the power take-off capability for the direct driven point absorber.

Bibliography

[1] T.W. Thorpe. 2010 Survey of Energy Resources. Technical report, World Energy Council, 2010.

[2] IEA. Electricity in the World, 2008. Technical report, International Energy Agency.

[3] www.wavehub.co.uk.

[4] J. Falnes. *Ocean Waves and Oscillating Systems, Linear Interaction including Wave-Energy Extraction.* Cambridge University Press, April 2002.

[5] C. Sandvik, M. Molinas, and J. Sjolte. Time Domain Modelling of the Wave-to-Wire Energy Convert Bolt. In *Proc. 7'th Int. Conference and Exh. on Ecological Vehicles and Renewable Energies, EVER12, Monaco*, 2012.

[6] J. Bedos, M. Molinas, and J. Sjolte. Analysis of the Power Exctraction Capability for the Wave Energy Converter BOLT. In *Technoport 2012*, 2012.

[7] J. Sjolte, G. Tjensvoll, and G. Molinas. All Electric Wave Energy Converter with Stand-alone 600VDC Power System and Ultracapacitor Bank. In *Proc. 7'th Int. Conference and Exh. on Ecological Vehicles and Renewable Energies, EVER12, Monaco*, 2012.

[8] C. Sandvik. *Wave-to-Wire Time Domain Model for the Wave Energy Convert Bolt.* Specialization project, Norwegian University of Science and Technology.

[9] W. H. Mitchell. Sea Spectra Revisited. In *Marine Technology*, volume 4, pages 211–227, 1999.

[10] R.G. Dean and R.A. Dalrymple. *Water wave mechanics for engineers and scientists*, volume 2. Prentice Hall, 1984.

[11] J. Hals. *Modelling and phase control of wave-energy converters.* diploma thesis, Norwegian University of Science and Technology.

[12] W. E Cummins. The impulse response functions and ship motions. *Schiffstechnik*, 1962.

[13] Reza Taghipour, Tristan Perez, and Torgeir Moan. Hybrid frequencyâĂŞtime domain models for dynamic response analysis of marine structures. *Ocean Engineering*, 35(7):685 – 705, 2008.

[14] S. Kung. A new identification and model reduction algorithm via singular value decompositions. In *Proc. of the 12th Aslilomar Conf. on Circuits, Systems and Computers*, pages 705–714, 1978.

[15] J. Falnes J. Hals, T. Bjarte-Larsson. Optimum Reactive Control and Control by Latching of a Wave-Absorbing Semisubmerged Heaving Sphere. In *Proc. of the 21th Int.l Conf. on Offshore Mechanics and Arctic Eng.*, volume 3, pages 343–350, 2002.

[16] E. Tedeschi and M. Molinas. Impact of control strategies on the rating of electric power take off for Wave Energy conversion. In *Industrial Electronics (ISIE), 2010 IEEE International Symposium on*, pages 2406 –2411, july 2010.

[17] E.Tedeschi and M. Molinas. Control Strategy of Wave Energy Converters Optimized Under Power Electronics Ratings Constraints. In *Proceedings of the International Conference on Ocean Energy*, volume 3, pages 343–350, 2010.

[18] N. Mohan. *Advanced Electric Drives Analysis, Control and Modeling using Simulink*. MNPERE Minneapolis, 2001.

[19] N. Mohan, T.M. Undeland, and W.P. Robbins. *Power Electronics Converters, Applications and Designs*, volume 3. John Wiley and Sons, Inc, 2003.

[20] N. Mohan. *Electric Drives an Integrative Approach*. MNPERE Minneapolis, 2001.

[21] J.W. Umland and M. Safiuddin. Magnitude and Symmetric Optimum Criterion for the Design of Linear Control Systems - What is it and Does it Compare with the Others? In *Industry Applications Society Annual Meeting, 1988., Conference Record of the 1988 IEEE*, pages 1796 –1802 vol.2, oct. 1988.

[22] S. Morimoto, Y. Takeda, T. Hirasa, and K. Taniguchi. Expansion of operating limits for permanent magnet motor by current vector control considering inverter capacity. *Industry Applications, IEEE Transactions on*, 26(5):866 –871, sep/oct 1990.

[23] Ching-Tsai Pan and Jenn-Horng Liaw. A robust field-weakening control strategy for surface-mounted permanent-magnet motor drives. *Energy Conversion, IEEE Transactions on*, 20(4):701 – 709, dec. 2005.

[24] Ida Kathrine Bjerke, Jonas Sjolte, and Gaute Tjensvoll. Experiences from Field Testing with the BOLT Wave Energy Converter. In *Proc. of the 9th European Wave and Tidal Energy Conf.*, 2011.

[25] J. Sjolte, I. Bjerke, A. Crozier, G. Tjensvoll, and G. Molinas. All Electric Wave Energy Power Take Off System with Improved Power Quality at the Grid Connection Point. In *2012 IEEE Power and Energy Society Transmission and Distribution Conf. and Exposition.*

Appendix A

Simulink Model
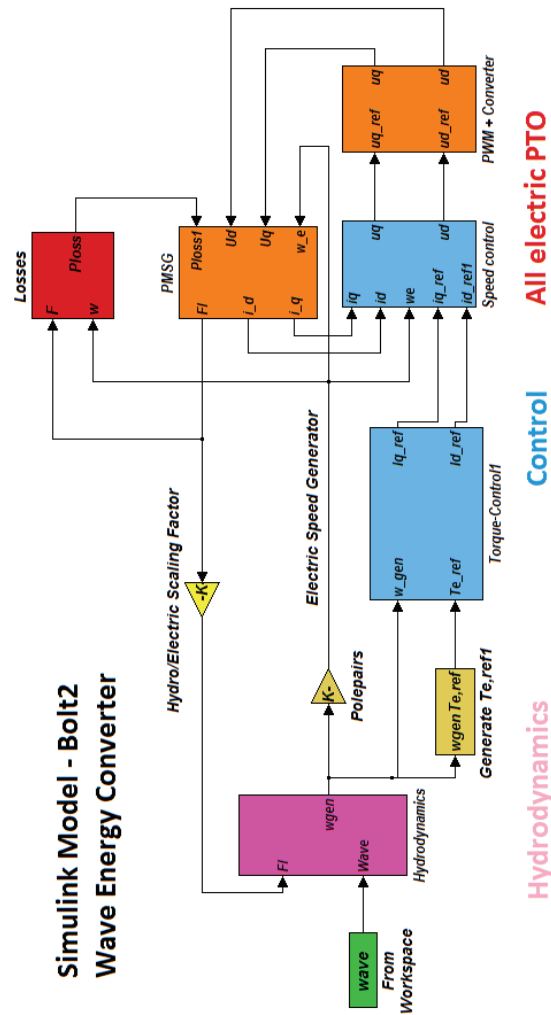
Figure A.1: *Simulink wave-to-wire model of Bolt2.*
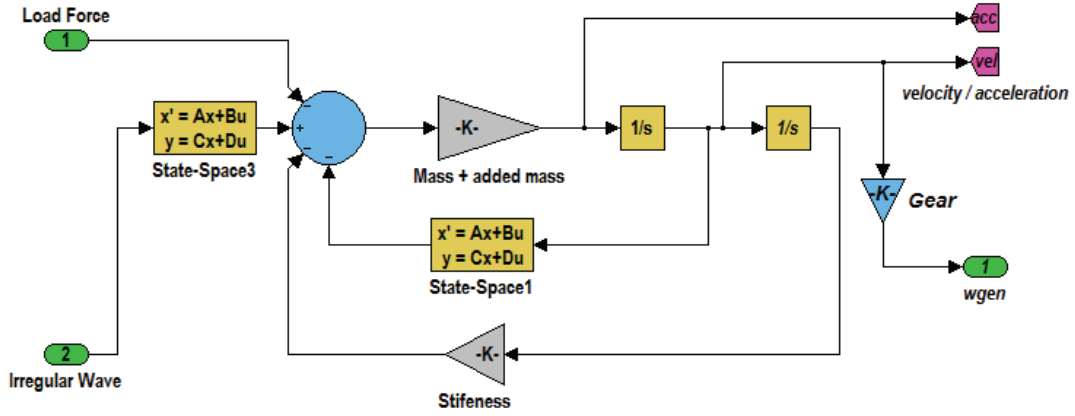
Figure A.2: *Simulink Model of hydrodynamics*
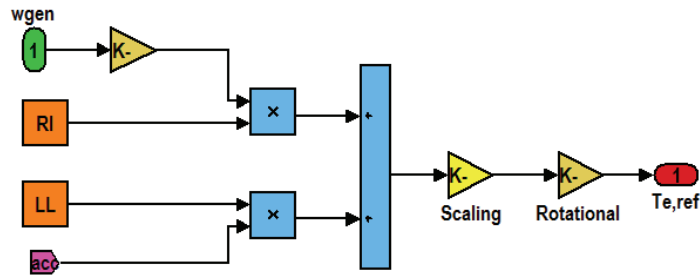
Figure A.3: *Simulink Block showing how the reference torque is determined*
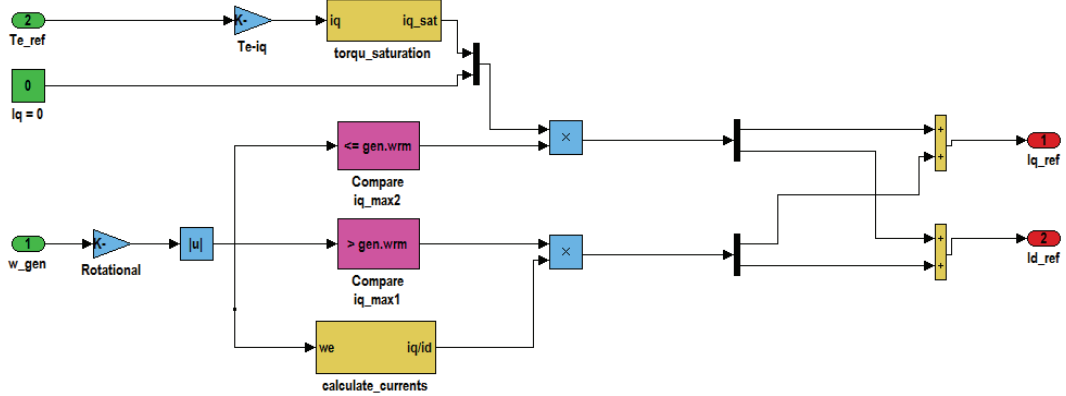
Figure A.4: *Simulink block showing the torque control.*
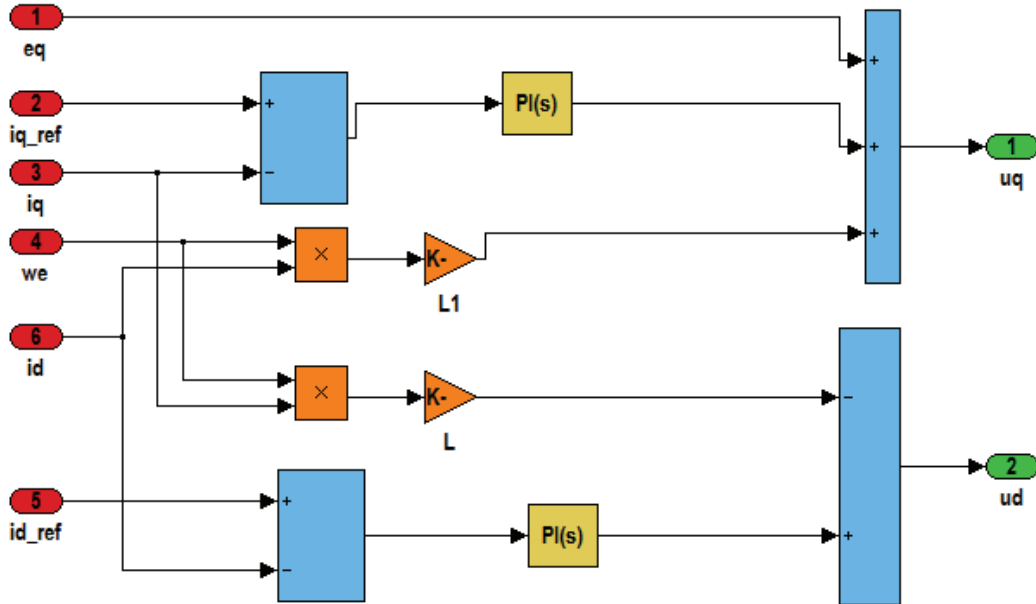
Figure A.5: *Simulink block showing the speed control.*
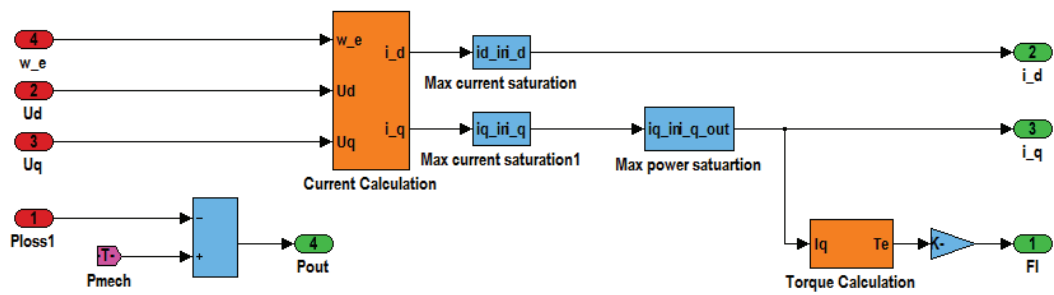
Figure A.6: *Figure showing the Permanent Magnet Synchronous Generator Simulink Block.*
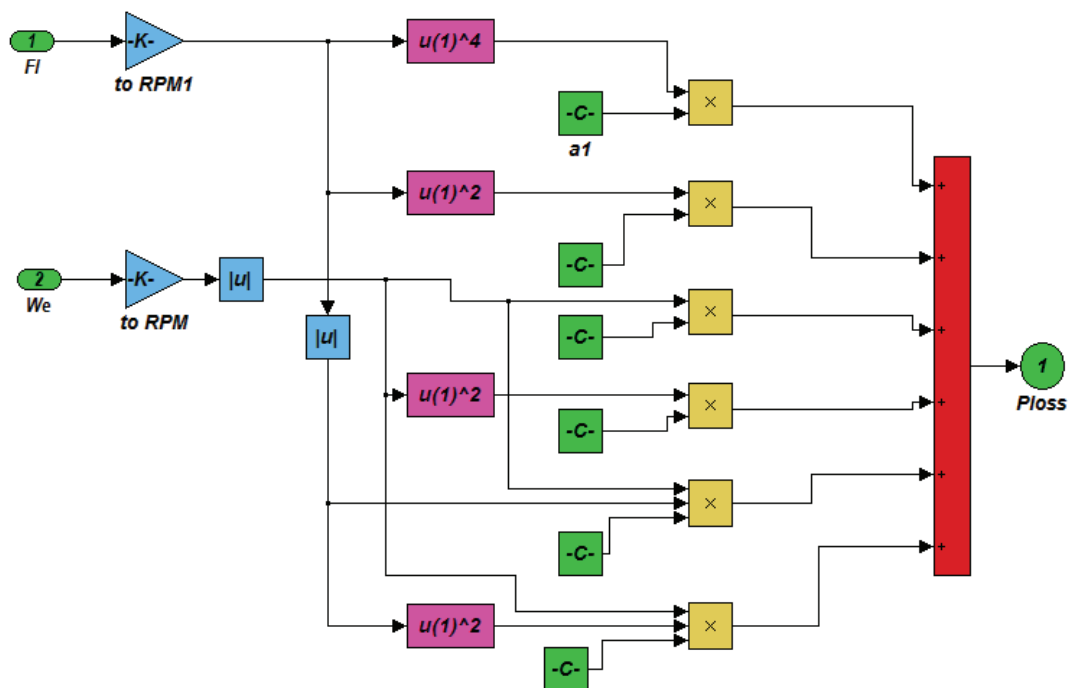
Figure A.7: *Simulink Block showing the calculation of Generator Losses .*

Appendix B

Basic Principles and Equations of PWM

A carrier based Pulse-Width Modulation is a common switching scheme used on voltage source converters as is used on the Bolt2 concept. The principle behind the PWM switching scheme is a carrier signal v_{tri} is switched at high frequency, called the switching frequency f_s, which is compared to the control signal $v_{control}$. The output voltage v_{A0} can then be generated by on- and off-pulses giving either value 0 or V_d as seen in figure B.1. The midpoint of signal is often shifted giving $v_{A0} = \pm\frac{1}{2}V_d$. This is expressed [19] in the following equations

$$v_{control} > v_{tri}, \quad v_{A0} = \frac{1}{2}V_d \tag{B.1}$$

$$v_{control} < v_{tri}, \quad v_{A0} = -\frac{1}{2}V_d \tag{B.2}$$

where v_d is the amplitude dc-link voltage. The ration between the on-time and the off-time is described by the duty-cycle D, and is expressed in percent of the time where a 100 % means that the output signal is equal to V_d.

It is of course important that the switching frequency be significantly higher than the input signal in order to get a good modulation of a sinusoidal signal. Also as higher order frequency harmonics will be present, a high switching frequency lets these be filtered with relative ease [19]. With modern devices as IGBT's one can achieve switching frequencies in the range of 20 kHz and more, but are due to switching losses often kept lower than this [19].
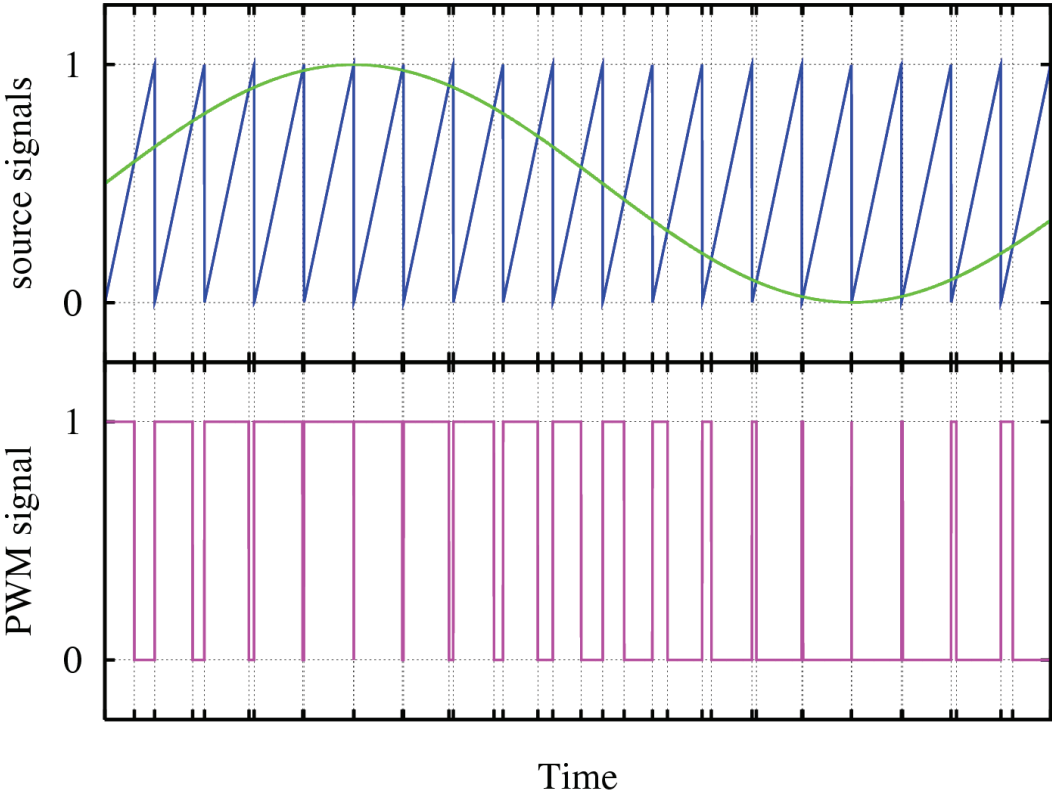
Figure B.1: *Pulse-Width Modulation. Green plot shows the control voltage $v_{control}$, blue plot shows the carrier signal v_{tri} and the lower pink plot shows the output voltage v_{Ao}*

Appendix C

Wave-to-Wire Modelling With Symmetric Force

This appendix aims to highlight the potential for increase in average extracted power and annual energy production for a power take off system which allows for bi-directional generator torque. This means that reactive control can be implemented for the whole oscillation cycle, as the force is not saturated a minimum value. To achieve this a slight change is made in the control system, but other than this the model is identical to the one defined in section 4 in the thesis.

In order to investigate the devices potential under such circumstances, a simplified approach is used where a number of simulations of with different load parameters is run and optimal control for each sea state is identified by trial and error. The goal if these simulations is to make a map of optimal control parameters for different sea states, as seen in Table 4.4 in section 4

C.1   Example mapping of control parameters

The approach used to determine optimal operation parameters are similar to the method explained in section 4. Next follows the measurements for a few selected sea states.

Significant hight $H_s = 0.5$ and period $T_p = 6.5$

In Table C.1 the average mechanical output power is shown for different control parameters. Notably the leftmost column represents when the system is passive loaded, or purely damped. The top-right corner represent where the load parameters move towards complex conjugate control, though the parameters that correspond to complex conjugate control are not defined in this table as this set of control parameters are outside the area of interest. It is sufficient to note that the average power increases when one moves towards

these control parameters in the top right.

The losses are seen in Table C.2. Notably it is observed that maximum generator losses occur when the system is complex conjugately controlled. This is due to the accumulated average losses of the high bidirectional peaks in power. The losses are lowest for the upper left corner of the table, where the control parameters goes towards zero. This is natural for this corresponds to a no-load operation of the generator, and the losses are purely rotational losses and no stator copper losses.

Combining the two tables, the corresponding electric output table can be seen in Table

Table C.1: *Table showing average mechanical extracted power [kW].*

Mechanical Power, Hs = 0.5, Tp = 6.5 [kW]						
RL/LL	0	1,00E+04	2,00E+04	3,00E+04	4,00E+04	5,00E+04
3,50E+04						
4,00E+04				3,651	4,115	
4,46E+04	2,156			3,649	4,088	4,372
5,00E+04	2,2455	2,665		3,637	4,057	4,344
6,20E+04	2,335	2,74		3,552	3,904	4,176
7,00E+04	2,3715	2,752		3,475		
7,74E+04	2,408	2,745		3,394		
8,00E+04	2,412	2,74				
9,00E+05	2,418					
1,00E+05	2,403					
1,40E+05	2,193					
1,80E+05	2,035					

Table C.2: *Table showing average losses [kW].*

Power Loss, Hs = 0.5, Tp = 6.5 [kW]						
RL/LL	0	1,00E+04	2,00E+04	3,00E+04	4,00E+04	5,00E+04
3,50E+04						
4,00E+04				0,796	1,177	
4,46E+04	0,296			0,771	1,104	1,451
5,00E+04	0,328	0,388		0,762	1,072	1,399
6,20E+04	0,36	0,436		0,75	0,997	1,266
7,00E+04	0,392	0,468		0,725		
7,74E+04	0,424	0,496		0,758		
8,00E+04	0,435	0,506				
9,00E+05	0,474					
1,00E+05	0,511					
1,40E+05	0,657					
1,80E+05	0,7175					
Max	1					

Table C.3: *Table showing output electric power [kW].*

Mechanical Power, Hs = 0.5, Tp = 6.5 [kW]						
RL/LL	0	1,00E+04	2,00E+04	3,00E+04	4,00E+04	5,00E+04
2,00E+04						
3,00E+04						
3,50E+04				0	0	0
4,00E+04				2,855	2,938	0
4,46E+04	1,86		0	2,878	2,984	2,921
5,00E+04	1,9175	2,277	0	2,875	2,985	2,945
6,20E+04	1,975	2,304	0	2,802	2,907	2,91
7,00E+04	1,9795	2,284		2,75	0	0
7,74E+04	1,984	2,249		2,636	0	0
8,00E+04	1,977	2,234				0
9,00E+05	1,944	0				
1,00E+05	1,892	0	0	0		
1,40E+05	1,536	0	0	0	0	
1,80E+05	1,3175	0	0	0	0	0

C.3. As is seen from this plot an optimal set of control parameters is identified for this sea state with a added damping $R_L = 50kNs/m$ and added mass of $L_L = 40$ tons. Notably, the average electric output power is increased by 50 % compared with the optimal passive loaded.

Table C.4: *Table showing average mechanical extracted power [kW]. $H_s = 1.5$ and $T_p = 7$*

RL/LL	Mechanical Power, Hs =1.5, Tp = 7 [kW]					
	0	1,00E+04	2,00E+04	3,00E+04	4,00E+04	5,00E+04
2,00E+04						
3,50E+04						
4,00E+04						
4,46E+04				23,02		
5,00E+04				23,57	22,9	
6,20E+04	19,96			24,05		
7,00E+04	20,3		23,65	24,21	24,15	
7,74E+04	20,51			24,24	24,25	
8,00E+04	20,57			24,25	24,25	
9,00E+05	20,75					
1,00E+05						
1,40E+05						
1,80E+05						

Significant hight $H_s = 1.5$ and period $T_p = 7$

The maps of average extracted mechanical power, generator losses and electrical output average power is seen in Tables C.4 - C.6. Notably, the operation point which gives the maximum extracted power is not in the complex conjugate control area (top right), but in the 'middle' of the map. This is however in accordance with the observations made in the specialization project [8] [5] that states the effect of reactive control becomes smaller when the significant height of the sea states increase. This is also observed in the power extraction, with an optimal average electric power extraction for this sea state is 20.03 kW. Compared to optimal electric power extraction for passive loading (17.29 kW) this is a 15.2 % increase, which is a significant reduction to the 50 % gain observed for the sea state of significant height of 0.5 meters.

Table C.5: *Table showing average generator losses [kW]. $H_s = 1.5$ and $T_p = 7$*

RL/LL	0	1,00E+04	2,00E+04	3,00E+04	4,00E+04	5,00E+04
3,50E+04						
4,00E+04						
4,46E+04				4,165		
5,00E+04				4,151	4,7	
6,20E+04	2,811			4,15		
7,00E+04	3,041		3,774	4,18	4,56	
7,74E+04	3,222			4,207	4,54	
8,00E+04	3,28			4,218	4,536	
9,00E+05	3,48					
1,00E+05						
1,40E+05						
1,80E+05						

Power Loss, Hs = 1.5, Tp = 7 [kW]

Table C.6: *Table showing average electric output power [kW]. $H_s = 1.5$ and $T_p = 7$*

RL/LL	0	1,00E+04	2,00E+04	3,00E+04	4,00E+04	5,00E+04
2,00E+04						
3,00E+04						
3,50E+04						
4,00E+04				0	0	
4,46E+04	0	0	0	18,855	0	0
5,00E+04	0	0	0	19,419	18,2	0
6,20E+04	17,149	0	0	19,9	0	0
7,00E+04	17,259	0	19,876	20,03	19,59	0
7,74E+04	17,288	0	0	20,033	19,8	0
8,00E+04	17,29	0	0	20,032	19,874	0
9,00E+05	17,27	0	0	0	0	0
1,00E+05	0	0	0	0	0	0
1,40E+05	0	0	0	0	0	0
1,80E+05	0	0	0	0	0	0

Mechanical Power, Hs = 1.5, Tp = 6.5 [kW]

Significant hight $H_s = 0.5$ and period $T_p = 10$

For a sea state with increased peak period, Tables C.7 - C.9 show the mechanical extracted power, generator losses and electrical output power.

Table C.7: *Table showing average mechanical extracted power [kW]. $H_s = 0.5$ and $T_p = 10$*

Mechanical Power, Hs =0.5, Tp = 10 [kW]									
RL/LL	0	1,00E+04	2,00E+04	3,00E+04	4,00E+04	5,00E+04	8,00E+04	1,00E+05	1,10E+05
2,00E+04									
3,50E+04									
4,00E+04	0,521				1,01	1,14	1,248	1,332	
4,46E+04									
5,00E+04	0,575				1,02	1,13	1,22		
6,20E+04			0,817		1,01	1,1	1,18	1,238	
7,00E+04	0,644		0,825		1	1,08	1,148	1,201	
7,74E+04					0,982				
8,00E+04			0,827		0,982	1,05			
9,00E+05					0,96				
1,00E+05	0,684		0,816		0,937				
1,10E+05	0,687				0,913				1,03
1,30E+05					0,865				
1,50E+05					0,818				
1,80E+05					0,754				

Table C.8: *Table showing average generator losses [kW]. $H_s = 0.5$ and $T_p = 10$*

Generator Losses, Hs =0.5, Tp = 10 [kW]									
RL/LL	0	1,00E+04	2,00E+04	3,00E+04	4,00E+04	5,00E+04	8,00E+04	1,00E+05	1,10E+05
2,00E+04									
3,50E+04						0,534			
4,00E+04	0,104				0,296	0,534	0,534	0,686	
4,46E+04									
5,00E+04	0,112				0,274	0,357	0,457		
6,20E+04			0,169		0,26	0,325	0,4	0,488	
7,00E+04	0,13		0,174		0,256	0,313	0,378	0,453	
7,74E+04					0,253				
8,00E+04			0,181		0,253	0,302			
9,00E+05					0,253				
1,00E+05	0,159		0,196		0,254				
1,10E+05	0,168				0,257				0,543
1,30E+05					0,262				
1,50E+05					0,27				
1,80E+05					0,281				

Table C.9: *Table showing average electric output power [kW]. $H_s = 0.5$ and $T_p = 10$*

Electrical Power, Hs =0.5, Tp = 10 [kW]									
RL/LL	0	1,00E+04	2,00E+04	3,00E+04	4,00E+04	5,00E+04	6,00E+04	7,00E+04	1,10E+05
2,00E+04									
3,50E+04									
4,00E+04	0,417	0	0	0	0,714	0,606	0,714	0,646	0
4,46E+04	0	0	0	0	0	0	0	0	0
5,00E+04	0,463	0	0	0	0,746	0,773	0,763	0	0
6,20E+04	0	0	0,648	0	0,75	0,775	0,78	0,75	0
7,00E+04	0,514	0	0,651	0	0,744	0,767	0,77	0,748	0
7,74E+04	0	0	0	0	0,729	0	0	0	0
8,00E+04	0	0	0,646	0	0,729	0,748	0	0	0
9,00E+05	0	0	0	0	0,707	0	0	0	0
1,00E+05	0,525	0	0,62	0	0,683	0	0	0	0
1,10E+05	0,519	0	0	0	0,656	0	0	0	0,487
1,30E+05	0	0	0	0	0,603	0	0	0	0
1,50E+05	0	0	0	0	0,548	0	0	0	0
1,80E+05	0	0	0	0	0,473	0	0	0	0

C.2   Wave-to-wire modelling for new optimal control parameters

It is now interesting to investigate how the device operates under the new optimal control parameters. Special focus will be on investigating how the generator torque is controlled.

Significant hight $H_s = 0.5$ and period $T_p = 6.5$

The input wave into the simulation is shown in figure C.1. The corresponding generator speed is shown in figure C.2. Notably, the generator operates in torque saturation mode for only two of the waves. The speed of the generator is significantly reduced compared to the simulations shown for the similar sea state and a approximately complex conjugately controlled system. In this sense it is more similar to the generator speed plot loaded system shown in figure 4.8.

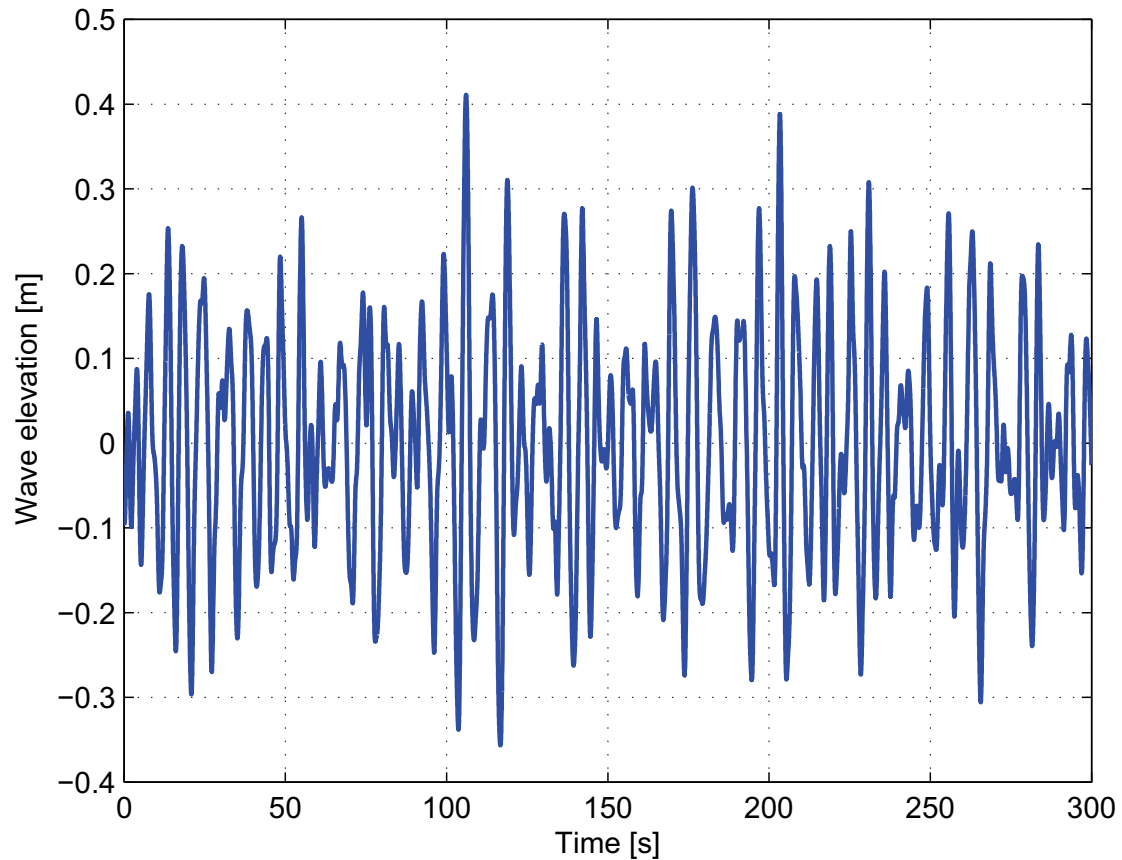The plots of mechanical power, generator losses and output electrical power in figure

Figure C.1: *Input wave elevation time series for of $H_s = 0.5$. System is optimized for optimal electrical power extraction.*
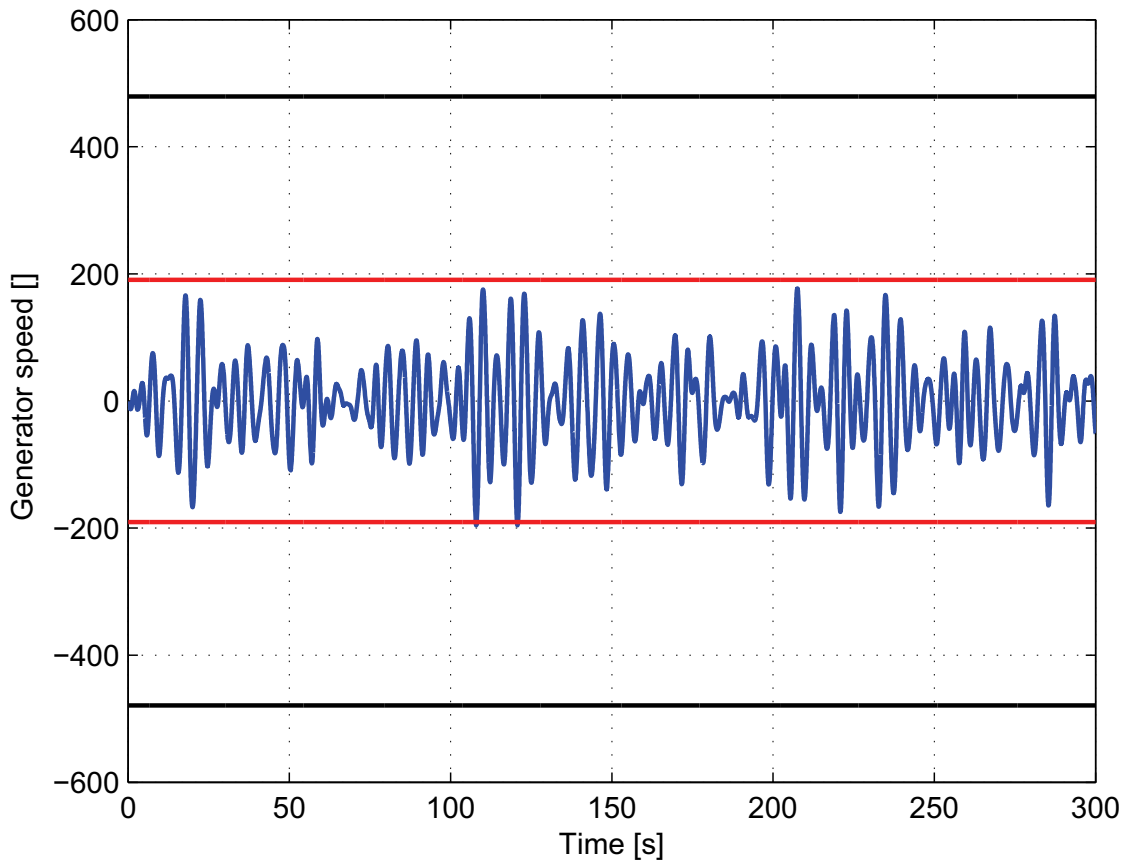
Figure C.2: *Generator speed for input wave seen in figure C.1. System is optimized for optimal electrical power extraction.*

C.4 show that the bidirectional power flow that is characteristic for a load force with a reactive component, but the positive power-flow is much more dominant than the negative part of the oscillating cycle. One can also see that the electric output power positive. Calculations show that for this particular simulation the average electrical output power is 2.98 kW.

Figure C.5 show the speed and the generator torque have a significantly smaller phase difference than for the approximately complex conjugate control. There seems to be a difference of 0.5 seconds on average for this simulation, compared to a 0.75 seconds difference on average for approximate complex conjugate control. Plot C.6 show the normalized generator speed and excitation force plotted together. For a approximate complex conjugately controlled system these should be in phase, and there should therefore be a phase-offset between them for this simulation. But as the phase offset between these measurements seem to be to a large degree random, this measurement of optimality loose some of its value for irregular seas.
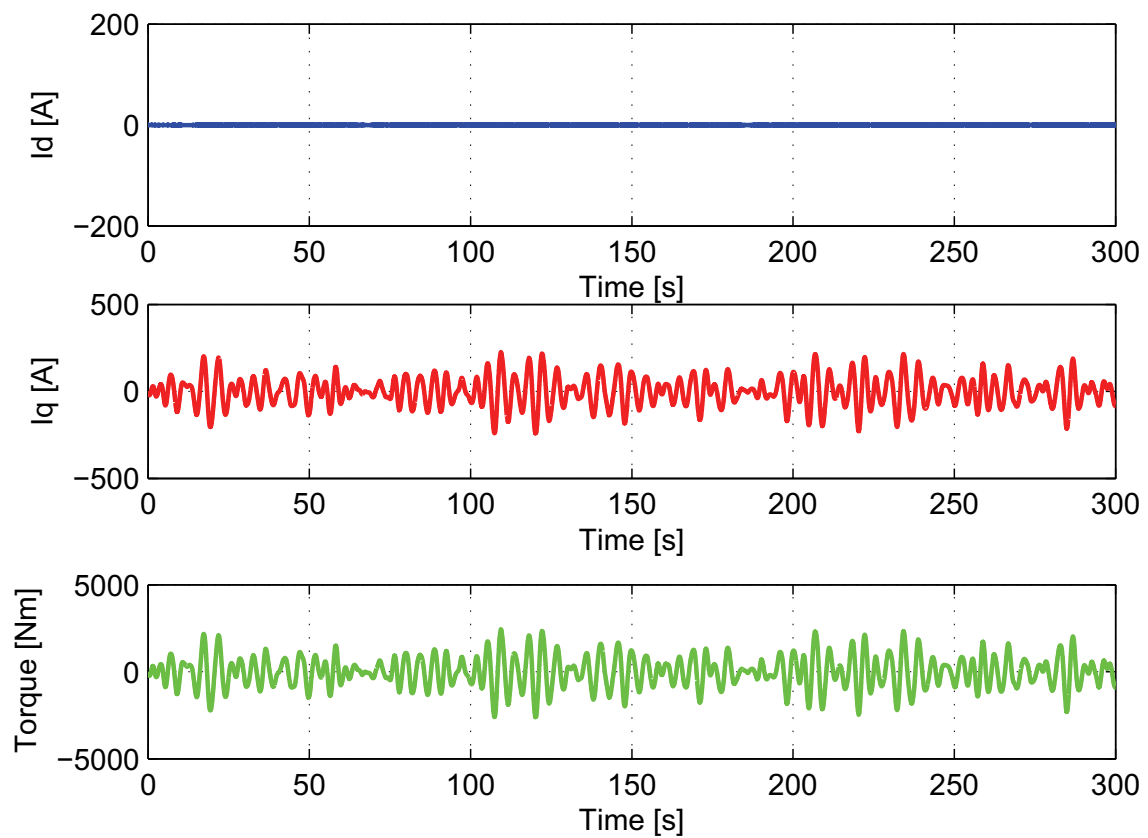
Figure C.3: *D- and q-axis current and generator torque. System is optimized for optimal electrical power extraction.*

Figure C.4: *Mechanical extracted power, generator losses and electrical output power. System is optimized for optimal electrical power extraction.*
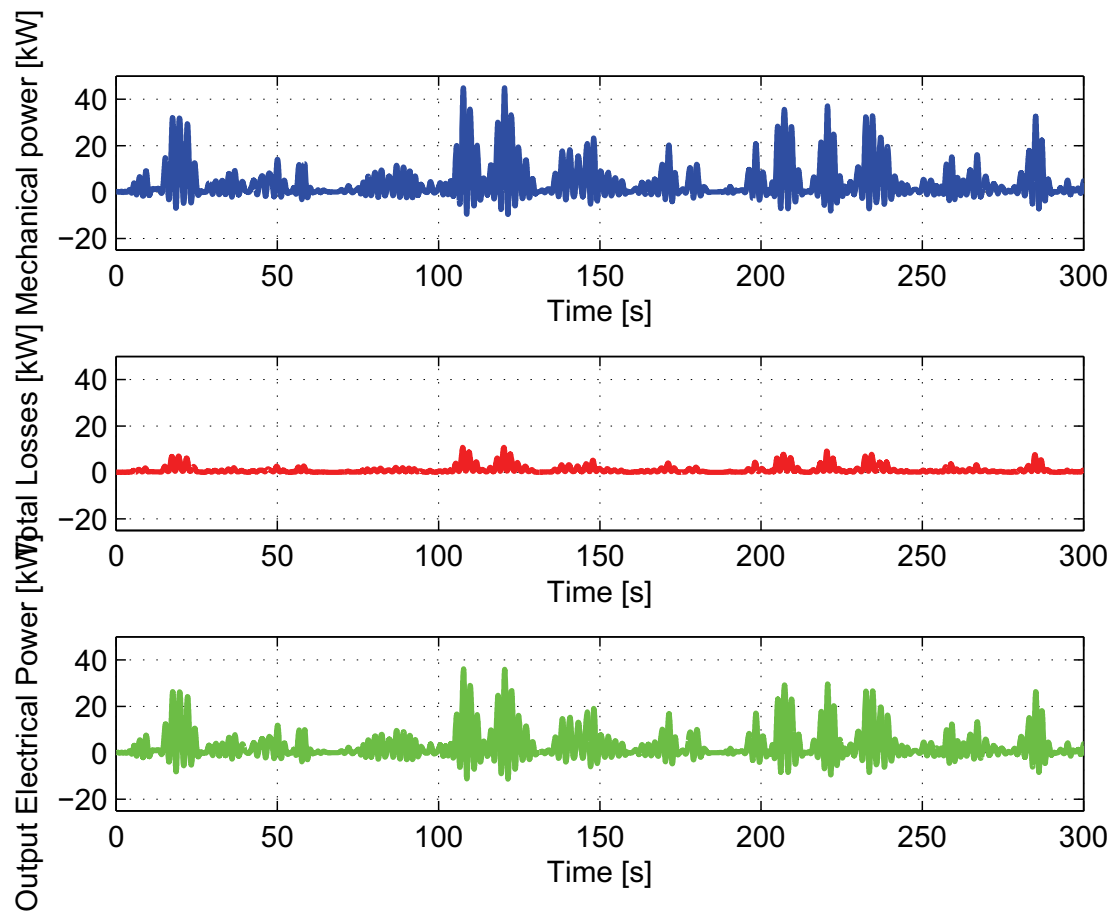
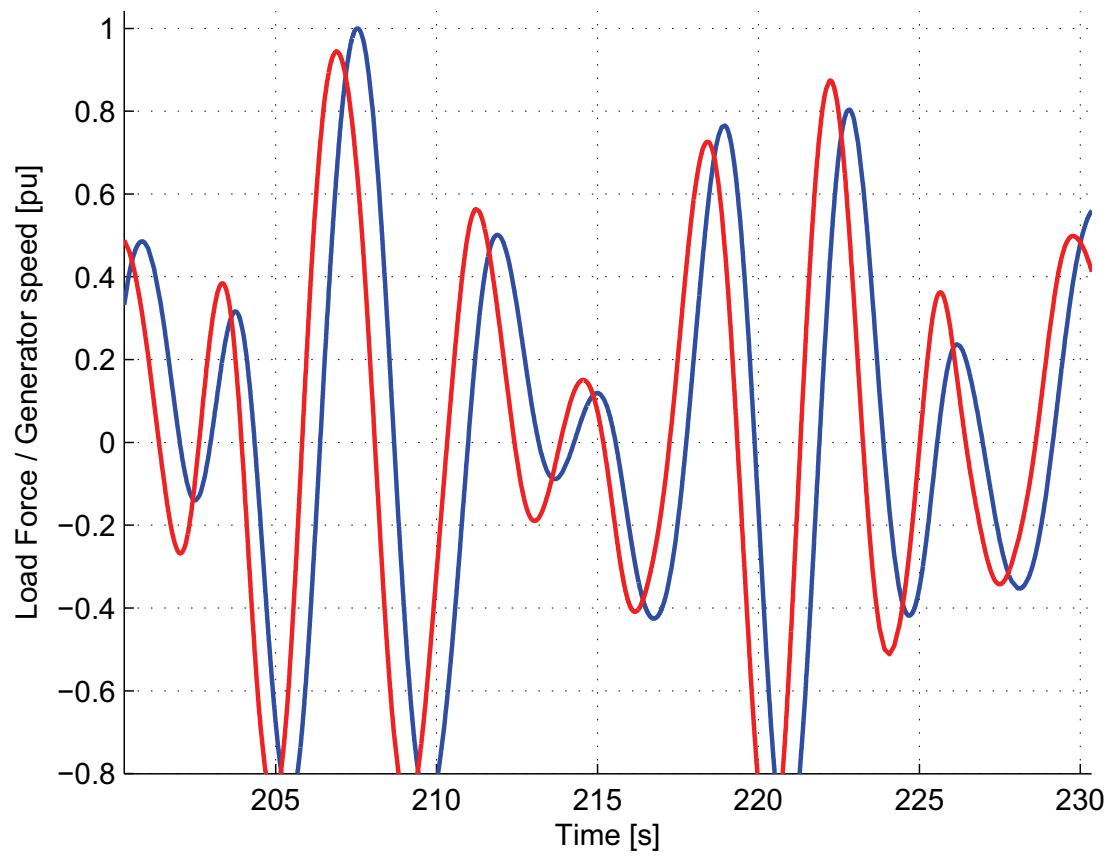**Figure C.5:** *Detailed plot of generator speed and torque. System is optimized for optimal electrical power extraction.*
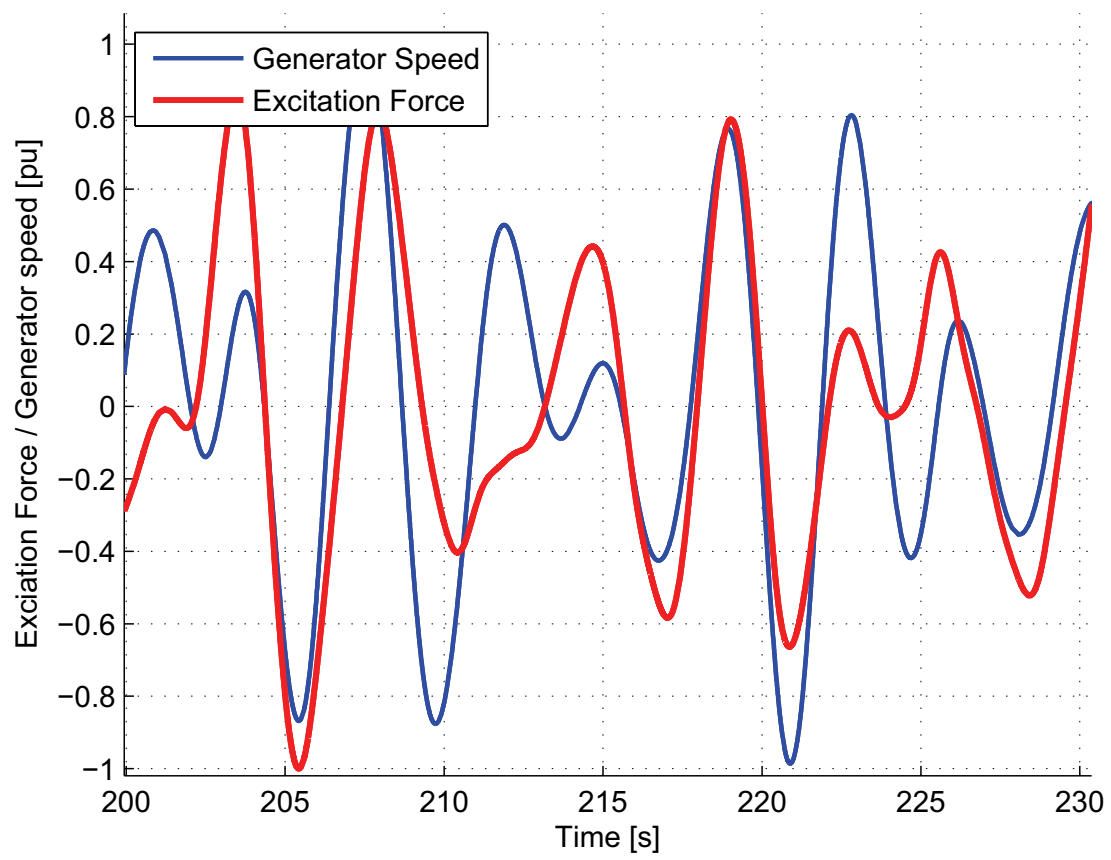
Figure C.6: *Detailed plot of generator speed and exciation force. System is optimized for optimal electrical power extraction.*

C.3   Discussions regarding mapping of optimal control parameters

From the main simulations and results for the selected sea states, some general observations can be made about the mapping of optimal control parameters.

- Combining the maps of output mechanical power and generator losses, a map of optimal control parameters with respect to electrical output power is made.

- For sea states with low significant height the optimal control parameters have have a larger component of added mass and smaller component of added damping.

- For the sea states with low significant height, the average power is increased by a significant factor. (50 % for $H_s = 0.5$

- When the significant height increases, the optimal control parameters shift towards a larger factor of added damping.

- For the sea state with higher significant height, the increase in average power compared with the reference case of passive loading goes towards zero.

- For a sea state with lower peak periods, the optimal control parameters have a larger factor of added damping.

- For increasing peak periods, the optimal control parameters have larger fraction of added damping. This means the optimal control moves towards complex conjugate control.

- Average power extraction decreases with increasing peak period of the sea.

In figure C.7 it is indicated how the optimal operation point (green area) changes with increasing significant height. Similarly, for increasing peak period of the sea state, figure
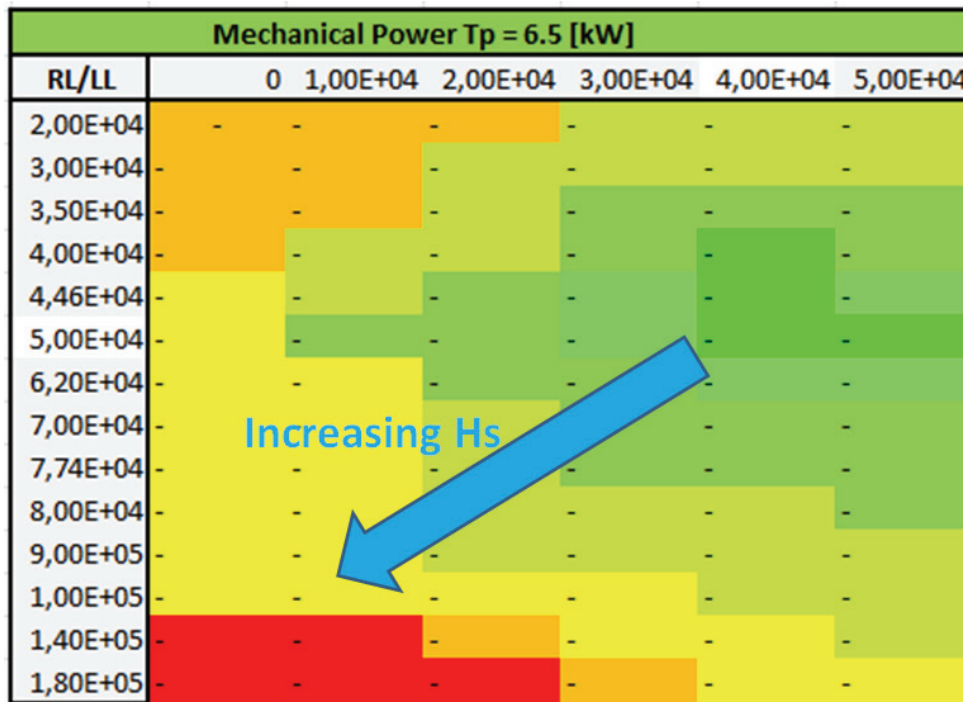
Mechanical Power Tp = 6.5 [kW]						
RL/LL	0	1,00E+04	2,00E+04	3,00E+04	4,00E+04	5,00E+04
2,00E+04	-	-	-	-	-	-
3,00E+04	-	-	-	-	-	-
3,50E+04	-	-	-	-	-	-
4,00E+04	-	-	-	-	-	-
4,46E+04	-	-	-	-	-	-
5,00E+04	-	-	-	-	-	-
6,20E+04	-	-	-	-	-	-
7,00E+04	-	-	-	-	-	-
7,74E+04	-	-	-	-	-	-
8,00E+04	-	-	-	-	-	-
9,00E+05	-	-	-	-	-	-
1,00E+05	-	-	-	-	-	-
1,40E+05	-	-	-	-	-	-
1,80E+05	-	-	-	-	-	-

Increasing Hs

Figure C.7: *Map of optimal control parameters with trajectory of increasing H_s.*

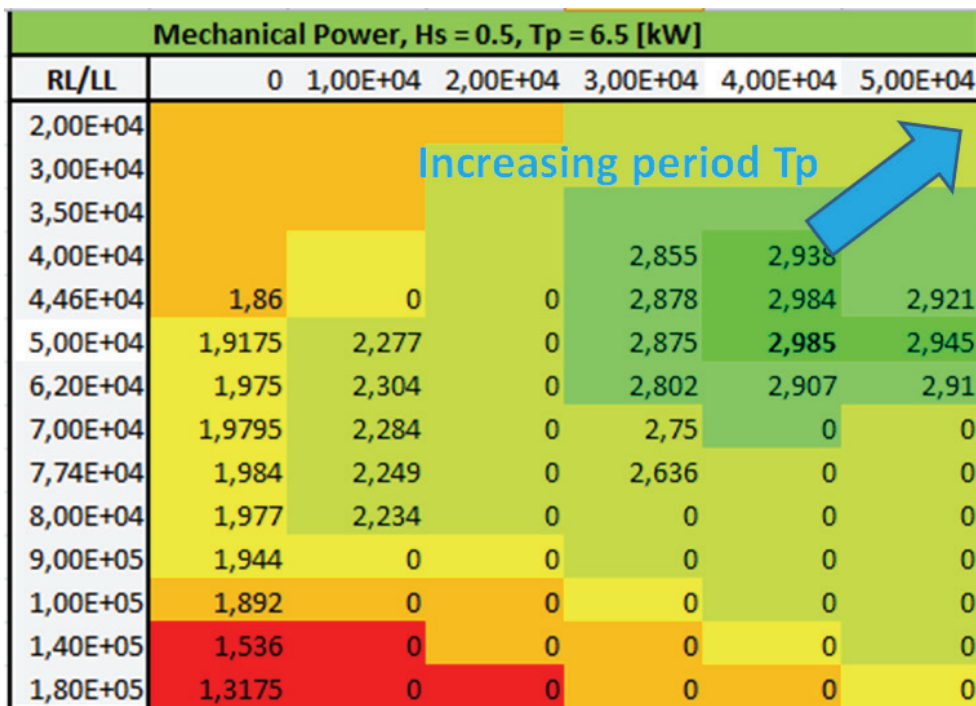| Mechanical Power, Hs = 0.5, Tp = 6.5 [kW]						
RL/LL	0	1,00E+04	2,00E+04	3,00E+04	4,00E+04	5,00E+04
2,00E+04						
3,00E+04						
3,50E+04						
4,00E+04				2,855	2,938	
4,46E+04	1,86	0	0	2,878	2,984	2,921
5,00E+04	1,9175	2,277	0	2,875	**2,985**	2,945
6,20E+04	1,975	2,304	0	2,802	2,907	2,91
7,00E+04	1,9795	2,284	0	2,75	0	0
7,74E+04	1,984	2,249	0	2,636	0	0
8,00E+04	1,977	2,234	0	0	0	0
9,00E+05	1,944	0	0	0	0	0
1,00E+05	1,892	0	0	0	0	0
1,40E+05	1,536	0	0	0	0	0
1,80E+05	1,3175	0	0	0	0	0

Increasing period Tp

Figure C.8: *Map of optimal control parameters with trajectory of increasing T_p.*

C.4 Energy calculations - Potential increase in annual energy production with optimal control

Energy calculations are performed in the same manner as seen in section 4, and the same representative sea states are used. Table C.10 show the average power for the different

control strategies, while Table C.11 shows the annual energy production. These results show that when applying bi-directional force, the annual energy gain of optimal control is increased by 10 %.

Table C.10: *Power calculations for the representing sea states*

	Low energy	Medium Energy	High Energy
Average Power Passive Loading [kW]	8.47	28.69	55.85
Average Power Optimal Control [kW]	11.2	33.02	56.83
Percentage increase [%]	32.23	15.0	1.75

Table C.11: *Annual Energy calculations for the representing sea states*

	Low energy	Medium Energy	High Energy	Total
Energy Passive Loading [MWh]	18.48	125.4	137.84	281.72
Energy Optimal Control [MWh]	24.44	144.3	140.26	309.0
Percentage increase [%]	32.23	15.0	1.75	9.68

Appendix D

State-space parameters in hydrodynamic model

D.1   Radiation Force State-Space Parameters

The radiation force is approximated through the following state-space expression:

$$F_r(t) = \mathbf{C}_k \mathbf{z}(t) + \mathbf{D}_k \dot{\eta}(t)$$

$$\dot{\mathbf{z}}(t) = \mathbf{A}_k \mathbf{z}(t) + \mathbf{B}_k \dot{\eta}(t)$$

The parameters are given as follows:

$$A = \begin{bmatrix} -3.812 & 3.647 & 3.490 & 0.3548 & -0.452 \\ -3.647 & -0.005 & -0.090 & -0.016 & 0.017 \\ -3.499 & -0.090 & -3.467 & -3.560 & 1.682 \\ 0.355 & 0.0162 & 3.560 & -0.108 & 0.323 \\ -0.452 & -0.012 & -1.682 & 0.323 & -2.563 \end{bmatrix}$$

$$B = \begin{bmatrix} -79.63 \\ -2.673 \\ -30.461 \\ 4.113 \\ -4.756 \end{bmatrix}$$

$$C = \begin{bmatrix} -1.593 & 53.45 & 609.2 & 82.27 & -95.20 \end{bmatrix}$$

$$D = \begin{bmatrix} 2502.0 \end{bmatrix}$$

D.2   Excitation Force State Space Model

The excitation force is approximated through the following state-space expression:

$$F_e(t) = \mathbf{C}\mathbf{z}(t) + \mathbf{D}\zeta(t)$$

$$\dot{\mathbf{z}}(t) = \mathbf{A}\mathbf{z}(t) + \mathbf{B}_k\zeta(t)$$

$$A = \begin{bmatrix} -0.848 & -0.501 & -0.394 & 0.405 & -0.408 & -0.511 \\ -0.501 & -0.360 & -1.270 & 0.328 & -0.607 & -0.580 \\ 0.394 & 1.270 & -0.070 & 0.734 & -0.107 & -0.208 \\ 0.405 & 0.328 & -0.734 & -0.332 & 2.754 & 0.950 \\ 0.408 & 0.607 & -0.107 & -2.730 & -0.190 & -0.450 \\ 0.5113 & 0.580 & -0.208 & -0.950 & -0.445 & -2.1930 \end{bmatrix}$$

$$B = \begin{bmatrix} -90.74 \\ -37.71 \\ 14.36 \\ 26.28 \\ 17.96 \\ 25.73 \end{bmatrix}$$

$$C = \begin{bmatrix} -1815 & -754.2 & -287.2 & 526.6 & -359.2 & -514.6 \end{bmatrix}$$

$$D = \begin{bmatrix} 4560.0 \end{bmatrix}$$

Appendix E

Hydrodynamic Parameters

Hydrodynamic Stiffness

$$S = 197400 \qquad\qquad (E.1)$$

Excitation Force Coefficient

The excitation force coefficient is represented by the plot seen in figure E.1.

Radiation Resistance

The radiation resistance coefficient is represented by the plot seen in figure E.2
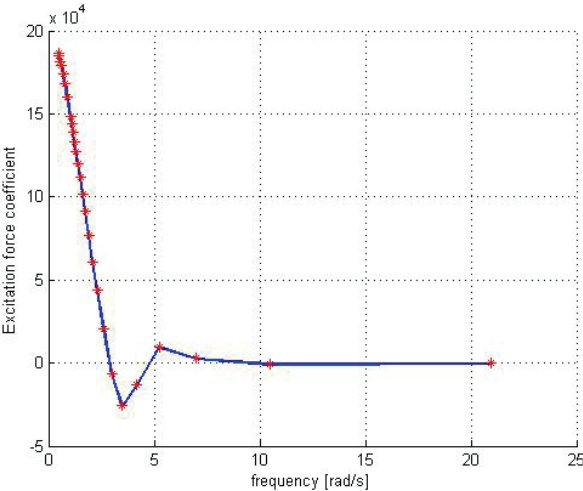

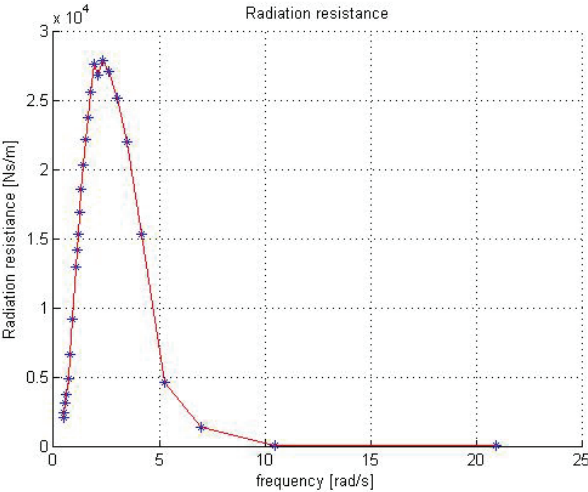**Figure E.1:** *Plot of excitation force coefficient of Bolt*

Figure E.2: *Plot of excitation force coefficient of Bolt*

Appendix F

Conference Proceedings

Time Domain Modelling of the Wave-to-Wire Wave Energy Converter Bolt

Christian McLisky Sandvik

Department of Electrical Power Engineering
Norwegian University of Science and Technology, O. S. Bragstads plass 2E, N-7034 Trondheim
E-mail: chrsan@stud.ntnu.no

Marta Molinas

Department of Electrical Power Engineering
Norwegian University of Science and Technology, O. S. Bragstads plass 2E, N-7034 Trondheim
E-mail: Marta.Molinas@ntnu.no

Jonas Sjolte

Fred Olsen / Norwegian University of Science and Technology
Fred. Olsens Gate 2, 0152
E-mail: Jonas.Sjolte@fredolsen.no / Jonas.Sjolte@ntnu.no

Abstract: *The aim of this paper is develop a wave-to-wire model of the wave energy converter (WEC) Bolt® in the time domain. For that purpose the first step is to model the hydrodynamic forces acting on the WEC under real sea conditions. A methodology for representing the excitation and radiation forces through a state-space model approximation based on frequency dependent hydrodynamic parameters is demonstrated, while the irregular wave elevation time-series input is developed based on the Bretschneider spectra. Three well established control strategies are investigated and compared by simulating a complete wave-to-wire model in which the Power Take Off (PTO) system is represented by an applied force which is obtained from the electric equivalent circuit of the WEC in frequency domain. From the results of the simulations it is observed that Bolt® has potential for an increase in power extraction in seas with limited significant height.*

Keywords: Wave Energy, Control Strategies, Power Take Off, Hydrodynamic Model, Irregular Waves.

1. Introduction

The world has an increasing demand for renewable energy, and wave energy has the potential to become a significant contribution to a diverse energy production. It is estimated that today's technology will be able to commercially exploit around $140 - 750\,TWh$ when fully matured [1], though theoretically the resource is many times higher. There are some great advantages with wave energy. It is predictable and constant over a longer period of time compared to other renewable energies as solar and wind power. It also has a higher energy density which can allow for smaller components giving potential lower costs.

Nevertheless, wave energy is an immature technology, and there is still no clear candidate of what is going to prove to be the most successful topology [2]. Typically, young technologies are subjected to high fixed costs. This is true for wave energy devices seen today which have high generation costs attributed to them due to acquisition of permits, surveys and grid connection. However, as later installations will benefit from existing knowledge and infrastructure, future expenses can be expected to be greatly reduced. Collaboration with for example offshore wind power and research projects as WaveHub also help to reduce initial investment costs.

As wave energy is still very much at the be-

ginning of its evolution, one has the opportunity to implement control strategies at an early stage for optimizing power take off capabilities. There are widely known and well analysed linear control strategies as passive loading and optimal control (see for example [3]), but these have mostly been studied under the assumption of sinusoidal waves. If the input wave is to be considered irregular, this will greatly influence the effect of such control strategies [4]. In order to demonstrate how the WEC will behave in a real ocean it is therefore crucial to be able to accurately model the force excited on the device by an irregular sea.

2. Presentation of the device

The wave energy converter analysed in this paper in the Fred Olsen concept Bolt®. The WEC is a cylinder shaped point absorber with key data as seen in table 1

Table 1: Key characteristics of Bolt®

Diameter	[m]	5.15
Height	[m]	1.5
Weight	[kg]	5000
Peak Power	[kW]	130
Maximum generator speed	[rpm]	4500

The first prototype Bolt® has been through a thorough test phase outside Risør in Norway [5], and hydrodynamic parameters and measurement data are available and provided by Fred Olsen.

The power take off system (PTO) for Bolt® consists of a rope wound around a winch. The heaving motion of the buoy is transformed into a rotational motion and generated into electricity by an induction generator [5]. Bolt® has an hydraulic motor in the PTO which keeps tension in the rope and also functions as a energy storage system. During the upwards heaving motion, the excitation force is used drive the

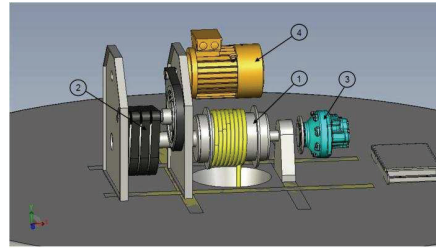**Figure 1:** Bolt® 1 in the sea

Figure 2: Conceptual sketch of the Bolt® hybrid power take-off system. The main components are the tensioned rope winch (1), a high capacity belt gear (2), a hydraulic spring (3) and the electric generator (4). [5]

generator as well as pressurizing the hydraulic accumulator. On the downwards motion the accumulator is de-pressurized and the force from this is used to drive the generator and to keep tension in the rope. Figure 2 shows a sketch of the PTO taken from [5]

3. Modelling of the sea

A simplified way of modelling the sea is to imagine a high, but finite number of sinusoidal waves of different height and frequencies propagating along a plane. The total energy must necessarily be the sum of the energy in all the waves the sea state is made up of. By modelling the sea as energy density as a function of frequency, one can obtain the distribution of energy contribution by different parameter waves. There are various mathematical models that are used for defining the sea spectra [6]. Depending on the conditions such as wind strength, fetch, depth and how fully developed the sea-state can be considered, the different models have their advantages and limitations.

The most widely known energy spectrum for ocean waves is the two parameter Brettschneider spectrum developed in 1959. Its preferred analytical form is as given in the following equation [6]:

$$S_{(\omega)} = \frac{5}{16} \ H_s^2 \ \frac{\omega_0^4}{\omega^5} \ e^{-\frac{5\omega_0^4}{4\omega^4}} \qquad (1)$$

Where H_s is the significant wave height and ω_0 is the peak frequency. Figures 3 and 4 show the Bretschneider spectra for varying values of significant height and peak frequencies.

The wave spectrum can be used to decompose the sea into waves of different frequencies. The elevation due to each wave can be shown [7] to be written as:
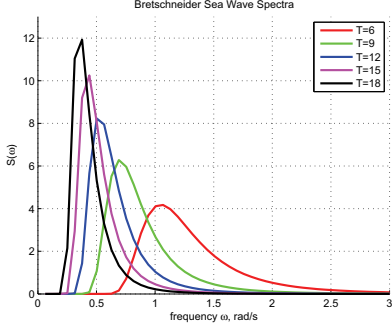
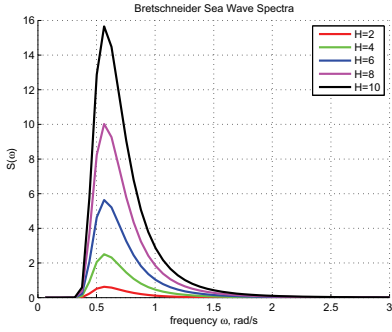**Figure 3:** Bretschneider spectra for different values of peak period T_p

Figure 4: Bretschneider spectra for different values of the significant height H_s

$$\zeta_n(t) = \sqrt{2S(\omega_n)d\omega} \sin\left(\omega_n t + \phi_n\right) \quad (2)$$

Where $d\omega$ is defined as

$$d\omega = \frac{2\pi}{T_{ser}} \quad (3)$$

and T_{ser} is the period of the time series that are being analysed.

The elevation of the sea is determined by summing all the different waves. These waves of different frequencies need to have random offset in the phase [7], illustrated in equation (2) by the angle ϕ. The equation for the elevation η can therefore be written as a sum:

$$\zeta(t) = \sum_{n=1}^{N} \sqrt{2S(\omega_n)d\omega} \sin\left(\omega_n t + \phi_n\right) \quad (4)$$

Where ϕ_n is randomly generated for each n.

For a time series of 90 seconds, with a significant wave height of 7 meters and a peak period of 11 seconds, figure (5) is an example time-series.

4. Forces acting upon the system

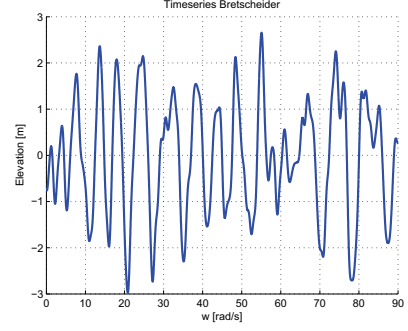A body submerged in water is considered to have six degrees of motion. These are along each of the x-, y- and z- axis, and rotational movement around these axis. These movements are called surge, sway, heave (along axis) and roll, pitch, yaw (rotational) [8]. However, as the device is defined to only move in a heaving motion it is considered a one degree of freedom system.

The force balance of such a point absorber system can be expressed as

$$M\ddot{\eta} = f_e(t) + f_s(t) + f_r(t) + f_m(t) + f_v(t) + f_l(t) + f_o(t) \quad (5)$$

where η is the device position and M is the equivalent mass of the system corresponding to the mass of the WEC and added mass due the inertia of the power take off system. Here f_e is the excitation force, f_m is the machinery force, or the force related to the power take off system. f_s represents the net hydrostatic stiffness, or hydrostatic force. The radiation force f_r is explained in section 4.2. The mooring force f_l, the viscous force f_v and the environmental force f_o will not be analysed in this paper.

4.1 Hydrostatic force

The hydrostatic force can be understood as the lack of equilibrium between the gravitational forces and the forces acting upon the point absorber due to displaced water. These forces are therefore a function of the displacement, η, from its equilibrium position. A usual expression for the hydrostatic force can be written as

$$f_s = S\eta \quad (6)$$

where S represents the hydrostatic matrix. Commonly this can be considered constant, and is regarded as the hydrodynamic stiffness of the device.

Figure 5: Timerseries of a Bretschneider spectrum $H_s = 7$ and $T_p = 11s$

4.2 Radiation Force

When the device oscillates in a sea, it creates a wave. The resulting pressure forces on the body due to this diffraction wave are referred to as the radiation force. This force normally expressed as

$$\hat{F}_R(\omega) = m_r(\omega)\ddot{\eta} + R_r(\omega)\dot{\eta} \qquad (7)$$

where m_r represents the added mass due water moving with the oscillating body. R_r is the radiation resistance. In time domain [9], this function can be written as (8)

$$F_r(t) = m_r(\infty)\ddot{\eta} + \int_0^t k(t-\tau)\dot{\eta}(\tau)d\tau \qquad (8)$$

Here $m_r(\infty)$ is the added mass at the limit of infinite frequency and is a constant value. $\dot{\eta}$ is the heaving velocity of the device, and $\ddot{\eta}$ is the acceleration. The convolution term $k(t)$ can be understood as the impulse response function of the radiation force. Equation 8 can become complex for polychromatic sea states, as is the case for the real irregular sea. However, given a few conditions reasonable simplification can be made. As discussed by J. Hals [8] a good representation of the radiation force is by replacing the convolution term in equation (8) by state-space models. It can be summed up by the representation

$$F_r(t) = \mathbf{C}_k \mathbf{z}(t) + \mathbf{D}_k \dot{\eta}(t) \qquad (9)$$

where the state vector z is given by

$$\dot{\mathbf{z}}(t) = \mathbf{A}_k \mathbf{z}(t) + \mathbf{B}_k \dot{\eta}(t) \qquad (10)$$

There are various methods in which to identify the state-space parameters $\mathbf{A}_k$, $\mathbf{B}_k$, $\mathbf{C}_k$ and $\mathbf{D}_k$. Taghipoura, Pereza and Moan [10] describe three approaches used in wave energy.

1. Regression in the frequency domain

2. Impulse response curve fitting

3. Realization theory

Realization Theory has been shown to be especially suitable for devices with discrete time system [10] as is the case for the measurement data acquired for Bolt®. Another great advantage of this approach is that if the data manipulated correctly, the Matlab function *imp2ss* can be used directly to identify the state-space system.

4.2.1 Determining Bolt radiation force state-space parameters using Realization Theory

The convolution kernel integral seen in equation (8) is defined as the inverse Fourier transform of $k(\omega)$ [8] as shown in equation (12).

$$k(t) = \mathcal{F}^{-1}\{k(\omega)\} \qquad (11)$$

$$k(t) = \mathcal{F}^{-1}\{i\omega\{m_r(\omega) - m_r(\infty)\delta(\omega)\} + R_r(\omega)\} \qquad (12)$$

This equation for $k(t)$ can be used directly, but better is to realize that the the even series expansion of (12) can be extracted and the radiation force impulse response $k(t)$ can be written as purely a function of the radiation resistance

$$k(t) = \frac{2}{\pi}\int_0^\infty R_r(\omega)\cos(\omega t)d\omega \qquad (13)$$

As one does not have a continuous function of the radiation resistance, but rather some values for a span of frequencies, a function in the discrete time domain is needed.

$$k(t) = \frac{2}{\pi}\sum_{k=1}^n R_r(\omega_k)\cos(\omega_k t)d\omega \qquad (14)$$

Fred Olsen has provided frequency dependant parameters of the coefficients in equation (12), but since the inverse discrete Fourier transform does not converge towards zero unless sufficiently small values of $d\omega$ is used, linear interpolation is used to make the discrete vector $R_r(\omega)$ large enough. For determining the state space model for Bolt® this paper uses a methodology based on the Matlab Robust Toolbox function *imp2ss*. The function realizes the system based on the Hankel singular value decomposition proposed by Kung [11]. With a discrete system in the time domain as an input, a state-space representation of the equivalent continuous system is the output. Another important attribute of the Kung method is order reduction of the state space parameters. As a typical input vector will give an a matrix in the order of $100's$, being able to reduce the order while keeping the accuracy of the impulse acceptable is of great value.

As figure 6 implies, a state-space model of order 5 gives a very good description of the radiation force impulse response. The state-space parameters corresponding to this impulse are shown in the following matrices.
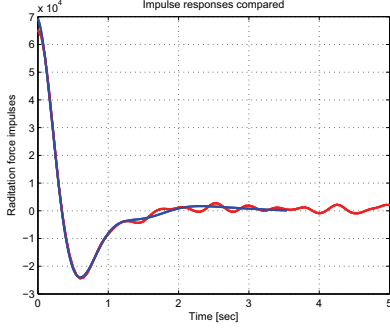
Figure 6: Comparison of the radiation force impulse reponse between the discrete timeseries (red) and the reduced state space model (blue) of order 5
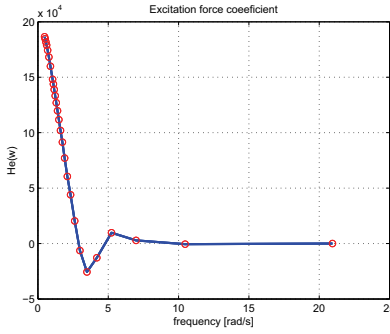

Figure 7: Excitation force coefficient $\hat{H}_{F\zeta}(\omega)$ data of Bolt[®]

4.3 Excitation Force

When an undisturbed incident wave interacts with the fixed body, a force acts on the device. This is called the excitation force, and is given by the wave elevation ζ and what is known as the excitation force coefficient, $\hat{H}_{F\zeta}$. In time domain the excitation force $F_{e,c}(t)$ is expressed by $h_{F\zeta}$ as shown in (15)

$$F_{e,c}(t) = h_{F,\zeta}(t) * \zeta_{e,c}(t) \qquad (15)$$

One can calculate the excitation force directly from wave elevation using state-space approximation for the convolution seen in the following equation:

$$F_{e,c}(t) = \int_0^t h_{F\zeta}(t-\tau)\zeta(\tau)d\tau \qquad (16)$$

This is obtained in similar manner as for the radiation force, making a discrete inverse Fourier transform of the frequency dependent excitation force coefficient $\hat{H}_{F\zeta}$. A set of measurement data for this coefficient are known for Bolt[®] and is plotted in figure 7

In time domain, the impulse response $h_{F\zeta}(t)$ can be approximated as shown by equation (17)
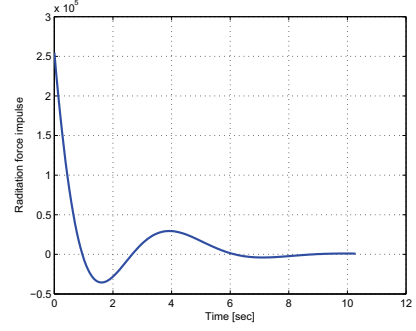

Figure 8: Impulse response from excitation force state space system

$$h_{F\zeta}(t) = \frac{2}{\pi} \sum_{k=1}^n H_{F\zeta}(\omega_k) \cos \omega_K t d\omega \qquad (17)$$

Using the same approach as applied when determining the radiation force state-space parameters, the discrete system impulse response is identified. Applying the Matlab function *imp2ss* with a appropriate order reduction a sixth order state space model is chosen for representing the excitation force.

5. Wave-to-wire modelling of the wave energy system

Disregarding the viscous, mooring and environmental forces equation (5) simplifies to

$$\mathbf{M}\ddot{\eta}(t) = \mathbf{f}_e(t) + \mathbf{f}_r(t) + \mathbf{f}_s(t) + \mathbf{f}_m(t) \qquad (18)$$

Using equation (8) for the time domain model of the radiation force $\mathbf{f}_r$, and assuming a constant hydrostatic coefficient, (18) can be expressed as

$$(M + m_r(\infty))\ddot{\eta} + \int_0^t k(t-\tau)\dot{\eta}(\tau)d\tau + S\eta$$
$$= \int_0^t h_{F\zeta}(t-\tau)\zeta(\tau)d\tau + F_L(t) \qquad (19)$$

Where $F_L(t)$ represents the machinery forces. Graphically, this is illustrated in the Simulink model in figure 9. Here the convolution term for excitation force and radiation force is replaced by the state-space models. As seen in table 1 Bolt[®] has a mass of 5000 kg and an hydrodynamic stiffness of $197,4kN/m$. When exposed a 90 second irregular wave time series, Simulink gives the device response as shown in figure 10

When operating at no-load it is expected that the device should follow the elevation of the device. In figure 11 this can be observed to be the case. This indicated that the hydrodynamical representation of the device is correct. When applying a load the peaks in both device velocity and position will be dampened, but is nevertheless recognized that some control methods will be necessary.

5.1 Linear Control Strategies

Linear control strategies are well established for wave energy converters [3] [12]. These are based on the frequency domain electrical equivalent [13] of the hydrodynamical model as described by equation (19).

The relation between the mechanical and the electrical domain is summed up in table 2

Passive loading is to consider the power take off system as purely damped, or in the electrical domain purely resistive with $X_L = 0$. From the basic electrical circuit one get maximum power output by keeping the velocity (current) in phase with the power take off force (load voltage). This is done by tuning R_L according to
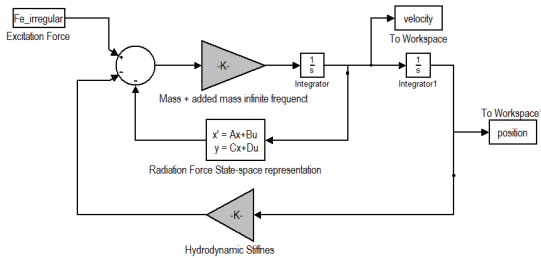

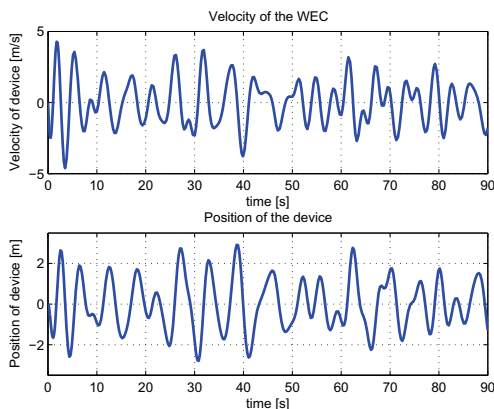**Figure 9:** Time domain model WEC response to irregular excitation force

Figure 10: Velocity and position response of Bolt$^{\circledR}$ for an irregular excitation force time series. $T_p = 7$ and $H_s = 5$

Table 2: Mechanical to electrical domain equivalents

Mechanical Domain	Electrical Domain
Excitation force, F_e	Source Voltage, V_S
PTO Force, F_L	Load voltage, V_L
Velocity, $dot\eta$	Electric current, i
Position, η	Electric charge, q
Damping, $B(\omega)$	Resistance, R
Mass, M + $a(\omega)$	Inductance, L
Stiffness, K	Inverse Capacitance, C^{-1}
Added damping, B_L	Load resistance, R_L
Added Mass, M_L	Load reactance, X_L

equation (20)

$$R_L(\omega) = \sqrt{R^2 + (\omega L - 1/\omega C)^2} \qquad (20)$$

By applying reactive control one maximizes the average power take off, one has to keep the reactive term of the total system impedance zero.

$$X_L = -(\omega L - 1/\omega C) \qquad (21)$$

$$R_L = R \qquad (22)$$

This means that the velocity is in phase with the excitation force, resulting in bidirectional power flow. However, the biggest challenge from the electrical point of view is the large peak-to-average ratio experienced [12] calling for a large overrating of the electrical and power-electronic equipment. It has been shown that by applying control methods based on a
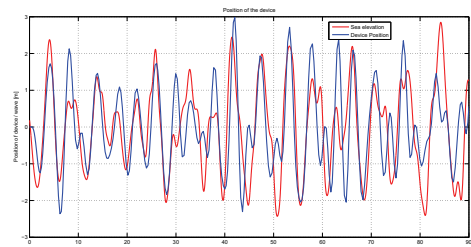

Figure 11: Position of the device (blue) and the wave elevation (red) when using a state space representation of the excitation force. $T_p = 7$ and $H_s = 5$
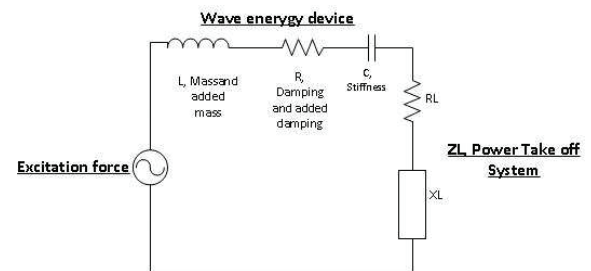

Figure 12: Electrical equivalent of the point absorber WEC

peak power constraint [4] this ratio can be largely reduced without considerably degrading the average power take off.

5.2 Intermediate Control Strategy

A more dynamic control strategy needs to be implemented, and fulfil the following criteria.

1. Peak instantaneous power below maximum rating (130 kW)

2. Device velocity below maximum rating (5 m/s)

3. Maximize average power

At this stage of the wave to wire model, only a simple control strategy has been implemented which assumes that if 1 is respected, so is 2. The implemented strategy is summed up as seen in figure 13

The wave energy converter or a measuring device registers a peak in incident wave, and measures the height of the wave at that moment. It is assumed here that the peak frequency is known through real-time measurements. Using these three inputs, a set of control parameters will be calculated. In figure 14 an input wave elevation time series is shown, with wave peaks and time of control parameter triggering marked.

There are several methods in which to optimize the control parameters for maximum power take off under a peak power constraint. This paper uses an approach proposed by E. Tedeschi and M. Molinas [4]. The average power $\bar{P}$ in the electrical circuit in figure 12 is given as
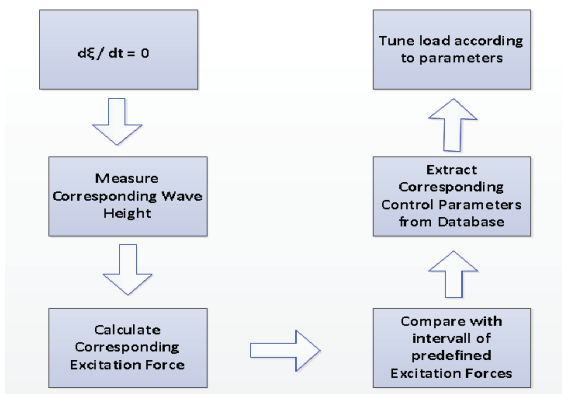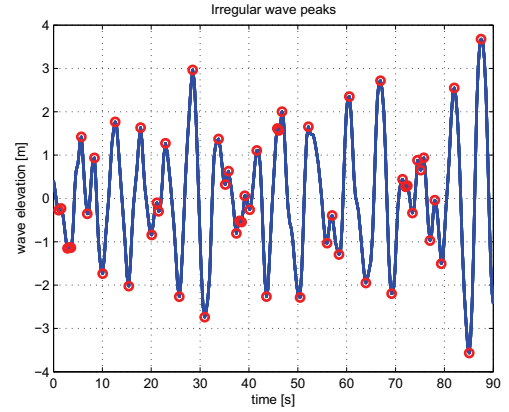

Figure 13: Flowchart of control strategy.

Figure 14: Wave elevation time series. Peaks of all waves are marked with red. The control method calculates the excitation force corresponding to a wave height of twice the registered displacement. $T_p = 7$ and $H_s = 5$

$$\bar{P} = \frac{E^2 R_L}{(R + R_L)^2 + (\omega L - \frac{1}{\omega C} \pm \frac{R_L \sqrt{1 - \cos^2 \phi_L}}{\cos \phi_L})^2} \quad (23)$$

where the electric parameters are as defined in table 2. The load factor ϕ_L gives the ratio between average power and peak power $\hat{P}$.

$$\hat{P} = \bar{P}(1 + \frac{1}{\cos \phi_L}) \quad (24)$$

The idea of the optimization algorithm is solving for real solutions of the second order equation for R_L derived from the two equations (23) and (24). A code for this has been implemented in Matlab, and a plot of how the control parameters should change with varying incoming wave heights is shown in figure 15. Notably, the border between passive loading and intermediate control can be seen at approximately 1.4 meter wave amplitude for the frequency that is being used ($T_p = 7$ sec).

Applying an irregular wave elevation time series, the response of the device is as seen in figure 16.

In figures 17 and 18 one can see how the control strategy is implemented through triggering changes in the added mass and added damping at the PTO.

5.3 Comparing performance of the control strategy with a passive loading

In order to evaluate the power take off performance of the proposed control strategy, a series of longer time domain simulations needs to be performed. As a reference, a passive loaded

power take off system is synchronously simulated with the same wave elevation input. Figure 19 shows how the WEC can be modelled when the load parameters are controlled. For the passive loaded system, the load parameters can be modelled as a static gain representing the added damping R_L.

From these models the power time series is calculated from device velocity and power take off force, F_L.

$$P_L = F_L \dot{\eta} \qquad (25)$$

A 300 seconds simulation is performed with a significant wave height of 1.5 meters and a peak period of 7 seconds. In figure 20 and 21 the instantaneous power for these two control methods is showed for such an example wave elevation time series.

Similar analysis is performed for different wave heights, and the results are summarized in table 3. For seas with significant wave heights
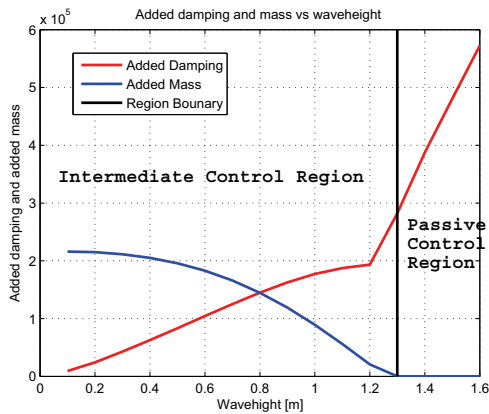

Figure 15: Plot showing how the control parameters added damping (red) and added mass (blue) should change for different wave heights and with a constant $T_p = 7$ seconds with a peak power constraint of 130 kW.
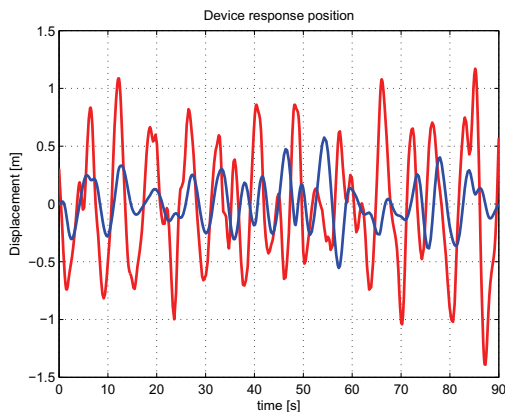

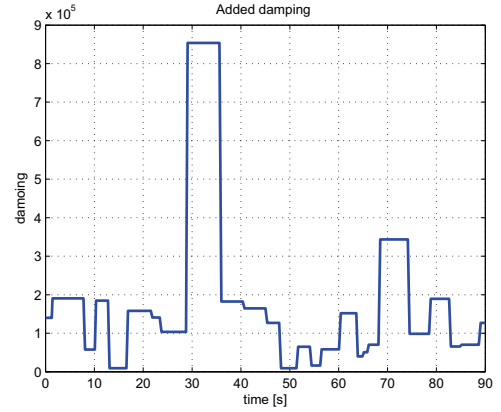Figure 16: Wave elevation and WEC position when applying intermediate control

Figure 17: Plot showing the load added damping is varying for the time domain simulation, when applying the proposed control strategy.
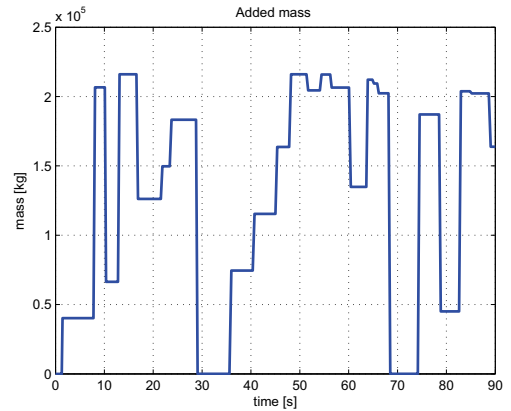

Figure 18: Plot showing the load added mass is varying for the time domain simulation, when applying the proposed control strategy.

between $1 - 1.5$ meters the average power extraction can be increased by approximately 10%. Then the gain decreases for larger significant wave heights. There seems to be no increased power extraction in seas of significant wave heights above 2.8 meters. This corresponds to the boundary where the control algo-
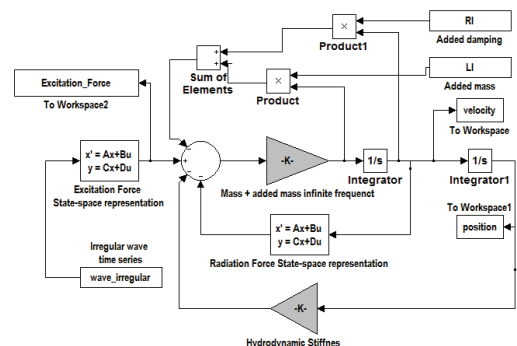

Figure 19: Simulink model used in the simulation with control parameter obtained through intermediate control algorithm

rithm goes into passive loading as seen in figure 15.

Table 3: Extracted average power for Bolt using passive control and intermediate reactive control for different significant wave heights. Peak period is 7 seconds.

H_s	Pass. load	Int. Cont.	Gain
1.0 m	2.38 kW	2.66 kW	11.8 %
1.5 m	5.83 kW	6.46 kW	10.8 %
2.0 m	10.15 kW	10.79 kW	6.3 %
2.5 m	15.11 kW	15.94 kW	5.5 %
2.8 m	18.7 kW	18.9 kW	1.07 %

6. Discussion

These simulations have shown that the average power extraction can be increased by a significant factor when applying intermediate conjugate control. But as it is shown from table 3, this is only for waves of lower significant height and thus lower energy. The increase in average power for a sea of significant height of 1 meter is a mere 0.25 kW, which corresponds only 1.5% of the average power of a sea with $H_S = 2$ meters. In order to fully evaluate the impact of implementing a intermediate reactive control, statistical data of the sea state at the sight of WaveHub is needed. In this way one can estimate the increase in annual delivered energy, which is a better indicator of the impact of intermediate control.

Further work will be on developing a model for an all-electric power take-off system, as well as improving the control strategy where focus should be on implementing a constraint on PTO-force.
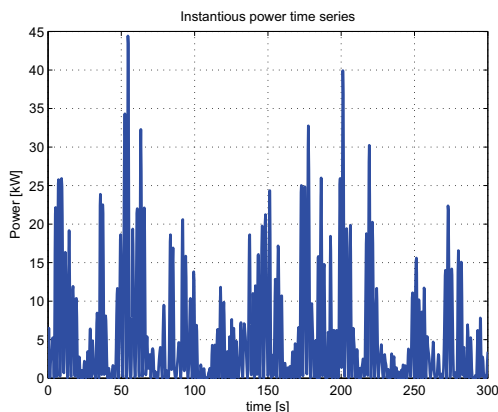
Figure 20: Instantaneous power when passive loaded with $R_l = 200\ 000$. Significant wave height 1.5 meters and peak period of 7 seconds.
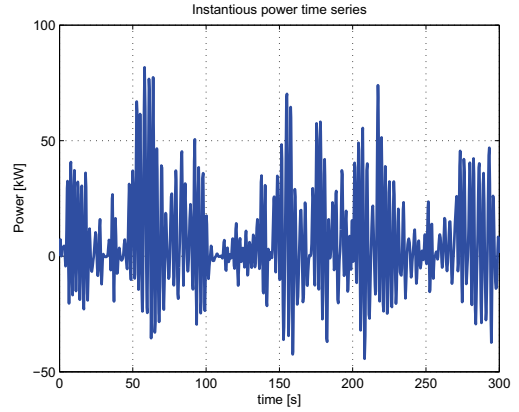
Figure 21: Instantaneous power with load parameters realized through the proposed control strategy. Significant wave height 1.5 meters and peak period of 7 seconds.
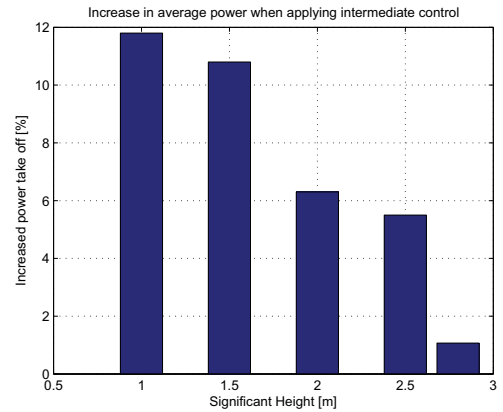
Figure 22: Percentage increase in average extracted power as a function of significant wave height.

7. Conclusion

In this paper a wave-to-wire time domain model of the wave energy converter Bolt® has been developed. A detailed hydrodynamical model of the WEC has been developed, based on frequency domain hydrodynamic data obtained through real-sea testing.

Three methods for modelling the frequency dependent wave spectrum of the sea has been reviewed, and the Bretschneider spectra is chosen for further analysis. A methodology for generating a wave elevation time series is implemented in order to model a real sea in the time domain.

In order to dynamically approximate the excitation force as a function of the wave elevation, a state-space representation is used. The radiation force is also realized through a state-space approximation, and the impulse responses of the approximations are thoroughly analysed. No-load time domain simulation confirm that the hydrodynamic model behaves as

expected, as the device position is a slightly damped and delayed version of the incoming wave elevation.

Finally, time domain simulations are performed with an irregular wave elevation time series as input. In order to represent the power take off system it is applied a force determined by the electric equivalent of the WEC in frequency domain. A control algorithm for intermediate control is suggested, and is shown to restrict the peak power within the maximum power constrain while increasing average power extraction. A series of simulations for different significant wave heights are performed, and it is shown that the average power take off can for waves of significant wave height between 1 - 2 meters can be increased with around 10%.

References

[1] T.W. Thorpe. 2010 survey of energy resources. Technical report, World Energy Council, 2010.

[2] A. Babarit, J. Hals, M.J. Muliawan, A. Kurniawan, T. Moan, and J. Krokstad. Numerical benchmarking study of a selection of wave energy converters. *Renewable Energy*, (0):–, 2011.

[3] J. Falnes J. Hals, T. Bjarte-Larsson. Optimum reactive control and control by latching of a wave-absorbing semisubmerged heaving sphere. In *Proc. of the 21th Int.l Conf. on Offshore Mechanics and Arctic Eng.*, volume 3, pages 343–350, 2002.

[4] E.Tedeschi and M. Molinas. Control strategy of wave energy converters optimized under power electronics ratings constraints. In *Proceedings of the International Conference on Ocean Energy*, volume 3, pages 343–350, 2010.

[5] Ida Kathrine Bjerke, Jonas Sjolte, and Gaute Tjensvoll. Experiences from field testing with the bolt wave energy converter. In .

[6] W. H. Mitchell. Sea spectra revisited. In *Marine Technology*, volume 4, pages 211–227, 1999.

[7] R.G. Dean and R.A. Dalrymple. *Water wave mechanics for engineers and scientists*, volume 2. Prentice Hall, 1984.

[8] J. Hals. *Modelling and phase control of wave-energy converters.* diploma thesis, Norwegian University of Science and Technology.

[9] W. E Cummins. The impulse response functions and ship motions. *Schiffstechnik*, 1962.

[10] Reza Taghipour, Tristan Perez, and Torgeir Moan. Hybrid frequencytime domain models for dynamic response analysis of marine structures. *Ocean Engineering*, 35(7):685 – 705, 2008.

[11] S. Kung. A new identification and model reduction algorithm via singular value decompositions. In *Proc. of the 12th Aslilomar Conf. on Circuits, Systems and Computers*, pages 705–714, 1978.

[12] E. Tedeschi and M. Molinas. Impact of control strategies on the rating of electric power take off for wave energy conversion. In *Industrial Electronics (ISIE), 2010 IEEE International Symposium on*, pages 2406 –2411, july 2010.

[13] J. Falnes. *Ocean Waves and Oscillating Systems.* April 2002.